POLITECNICO DI MILANO
Doctoral School (Ph.D.) in Mathematical Engineering
– XXVII cycle –

Discontinuous Finite Element approximation of Cahn-Hilliard problems

Presented to Dipartimento di Matematica "F. Brioschi"
POLITECNICO DI MILANO

by

Simone STANGALINO

Graduated in Mathematics, Università di Pavia

Advisor
Dr. Marco VERANI
Co-advisor
Dr. Paola F. ANTONIETTI
Politecnico di Milano

Ph.D. Coordinator: Prof. Roberto LUCCHETTI

Milan, December 2014

Table of Contents

1 Introduction **1**
- 1.1 Phase separation process . . . 1
- 1.2 The Cahn-Hilliard equation . . . 2
- 1.3 Boundary conditions . . . 5
- 1.4 DG methods . . . 6
- 1.5 Notations . . . 7

2 High order DG methods for elliptic problems on surfaces **9**
- 2.1 Model problem . . . 9
- 2.2 High order DG approximation . . . 10
  - 2.2.1 Primal formulation . . . 12
  - 2.2.2 Examples of surface DG methods . . . 14
- 2.3 Technical tools . . . 19
  - 2.3.1 Surface lifting . . . 19
  - 2.3.2 Geometric estimates . . . 20
  - 2.3.3 Boundedness and stability . . . 23
- 2.4 Convergence . . . 30
- 2.5 Numerical experiments . . . 35

3 DG approximation of parabolic problems with dynamic bcs **37**
- 3.1 Basic notation . . . 37
- 3.2 The stationary problem . . . 38
  - 3.2.1 Discontinuous Galerkin space discretization . . . 39
- 3.3 The parabolic problem and its fully-discretization . . . 45

3.4 Stability and error estimates . . . 51
3.5 Numerical experiments . . . 54
3.5.1 Example 1 . . . 54
3.5.2 Example 2 . . . 55
3.5.3 Example 3 . . . 56

4 Fast solution techniques for the Cahn-Hilliard problem 59
4.1 Problem discretization . . . 59
4.1.1 Space-time discretization of the Cahn-Hilliard equation . . . 60
4.1.2 Numerical examples . . . 63
4.2 Multigrid-based solution algorithms . . . 66
4.3 FAS algorithm . . . 66
4.4 Newton-Multigrid solver . . . 70

5 Collective block Gauss-Seidel smoothers 73
5.1 Motivation . . . 73
5.2 Definition of the smoother for linear problem . . . 74
5.3 Definition of the smoothers for the CH problem . . . 77
5.4 LFA approach . . . 79
5.4.1 Fourier analysis for a block-Toeplitz matrix A_h . . . 80
5.4.2 Spectral analysis . . . 82
5.5 Two-level analysis . . . 93
5.5.1 Example 1 . . . 94
5.5.2 Example 2 . . . 96
5.5.3 Example 3 . . . 96
5.5.4 Damping parameter . . . 99
5.6 Numerical results . . . 103
5.6.1 Test case 1 . . . 104
5.6.2 Test case 2 . . . 104

6 DG discretization of the CH problem with dynamic bcs 113
6.1 Continuous problem . . . 113
6.2 DG discretization . . . 114
6.3 Numerical experiments . . . 116
6.3.1 Example 1 . . . 116
6.3.2 Example 2 . . . 116
6.3.3 Example 3 . . . 117

A Appendix 119
A.1 Newton method . . . 119
A.2 Multigrid schemes . . . 120

Bibliography 129

1

Introduction

Multiphase flows are ubiquitous in science and applications. For this reason, the study of reliable mathematical models and the design of accurate numerical solutions for their approximations are crucial challenges.

In this chapter we briefly introduce the phase-separation problem and its modelization with the Cahn-Hilliard (CH) equation. In particular, we will focus our attention on the role of boundary conditions, discussing the so called dynamic boundary conditions that take into account the interactions of the two mixtures with the wall of the box containing the two-phase fluid. Finally, we discuss the choice of employing discontinuous Galerkin (DG) discretization for the Cahn-Hilliard problem.

1.1 Phase separation process

Let us consider a melted binary alloy. If the temperature is still above the critical threshold T_c of the alloy, there exists only a mixed phase and the configuration is stable. When the alloy is cooled down to $T < T_c$, there happens a partial nucleation: the initial homogeneous mixture is rapidly split into small growing subregions rich of a single component (cf. Figure 1.1). This process is known as spinodal decomposition. At the same time of the development of the subregions, it takes place the coarsening phenomena: the current shaped structures slowly aggregate themselves in bubble-like regions and grow.

According to the theoretical point of view, the stationary state, if it exists, is often composed by few big regions of pure components. The final pattern depends on the mean of the concentration of the phases, their initial patterns and the type of boundary condition imposed. With the aid of the phase diagram

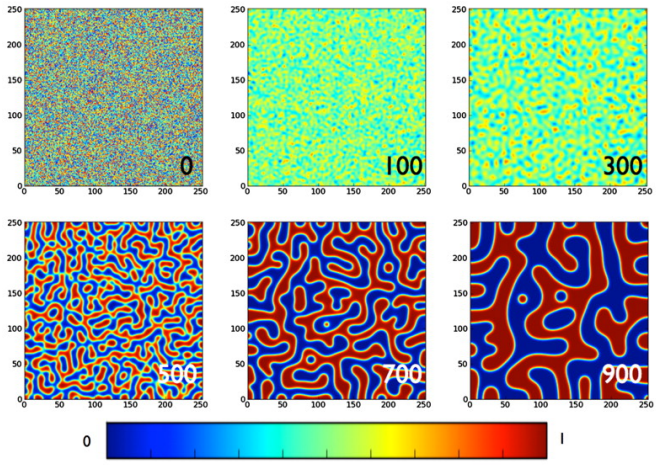

Figure 1.1: Snapshots of phase separation process taken. In the figure is represented the concentration of a phase of a chemical compound at some time-step of Cahn-Hilliard problem (taken from [24]).

in Figure 1.2 we can more formally summarize what happens when the alloy is cooled down [15]. Above the coexistence (blue) curve, the two phases form a stable homogeneous composite. Otherwise, in the zone below, there are allowed heterogeneous distributions. On the other hand, the spinodal (red) curve divides the unstable configuration (below) from the stable mixtures with respect to small perturbation, called metastable configuration (above).

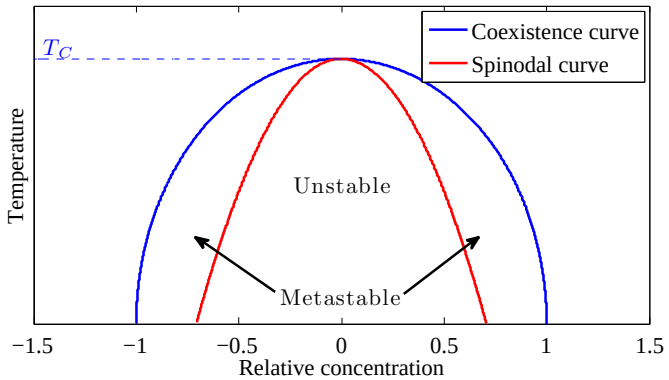

Figure 1.2: The different phase status in function of the temperature.

1.2 The Cahn-Hilliard equation

One of the most utilized model for phase separations is the Cahn-Hilliard equation introduced by Cahn and Hilliard in 1958 [46] where it is assumed that there exists a tiny diffused interface (separating the different phases) where the phases can

coexist. The Cahn-Hilliard equation is a time dependent non-linear equation of the fourth order. One of its simplified version reads as

$$\partial_t u + \Delta(\gamma^2 \Delta u - \phi(u)) = 0, \tag{1.1}$$

where $\gamma > 0$ is a given constant known as the interface parameter related to the thickness of the interface and $\phi(\cdot)$ is the derivative of a suitable potential $\Phi(\cdot)$.

More frequently, the Cahn-Hilliard equation is stated making explicit the chemical potential $w = \phi(u) - \gamma^2 \Delta u$:

$$\begin{cases} \partial_t u - \Delta w = 0, \\ w = \phi(u) - \gamma^2 \Delta u. \end{cases} \tag{1.2}$$

The solution u, also called order-parameter, is defined such that $u(x,t) \approx 1$ if and only if, at time t, phase 1 is present at the point $x \in \Omega$, and, respectively, $u(x,t) \approx -1$ if and only if phase 2 is present at the point $x \in \Omega$ at time t.

An important role in (1.2) is played by the choice of the potential Φ. A common choice for Φ is represented by the Helmholtz free energy density which takes into account the different phase status in function of the temperature T and the critical threshold T_c and reads as follows

$$\Phi(s) = \frac{N k_B T_c}{2}(1-s^2) + \frac{N k_B T}{2}[(1-s)\ln(\frac{1-s}{2}) + (1+s)\ln(\frac{1+s}{2})],\ 0 < T < T_c, \tag{1.3}$$

for $s \in (-1,1)$, being k_B the Boltzmann constant and N the molecular density.

This type of free energy forces the solution u to belong to the interval $I = (-1,1)$ (cf. Figure 1.3). However, this potential is very difficult to handle, especially in numerical simulation, due to its singularities in ± 1. For this reason it is commonly replaced by the smooth polynomial free energy

$$\Phi(s) = \frac{1}{4}(s^2-1)^2,\ s \in \mathbb{R}.$$

In the following we will always consider the smooth polynomial free energy. This approximation of the physical potential does not guarantee that u belongs to I, but it keeps the double-well behaviour.

The equation (1.1) can be easily derived from the minimization over the time of the following energy functional

$$\mathbb{E}(u) = \int_\Omega \left(\frac{\gamma^2}{2} |\nabla u|^2 + \Phi(u) \right), \tag{1.4}$$

where Ω is a smooth enough domain of the problem. In fact, minimizing the energy $\mathbb{E}(\cdot)$ over the time yields the mass balance law

$$\partial_t u + \nabla \cdot J = 0 \text{ in } \Omega.$$

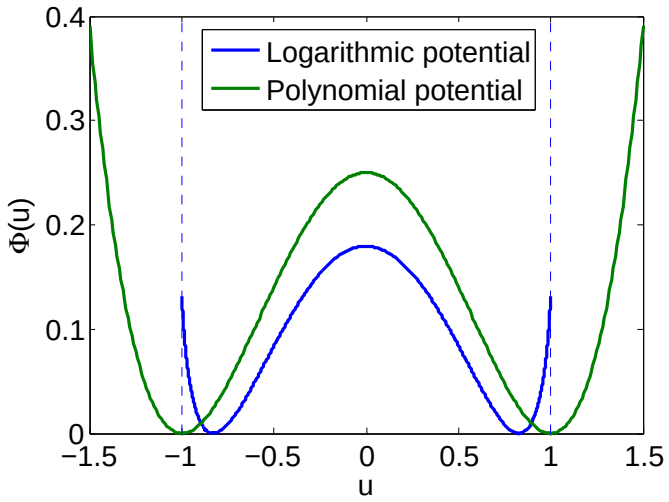

Figure 1.3: Comparison between the logarithmic potential (with $T_c = 10/7$ and $T = 1$) and the polynomial potential.

The Cahn-Hilliard equation is obtained by defining the flux J as

$$J = -\nabla\left(\frac{\delta E(u)}{\delta u}\right) = \nabla\left(\phi(u) - \gamma^2\Delta u\right).$$

The interface parameter γ is usually taken in the range of $10^{-3} - 10^{-2}$.
This number plays an important role because it is proportional to the maximum thickness in which the two phases coexists (cf. Figure 1.4): the interface thickness δ is about 7.5γ (see, e.g., [49]).
In numerical simulations, small values of γ requires higher spatial resolution: typically at least 8-10 elements are needed across the interfacial region (see, e.g., [33]).

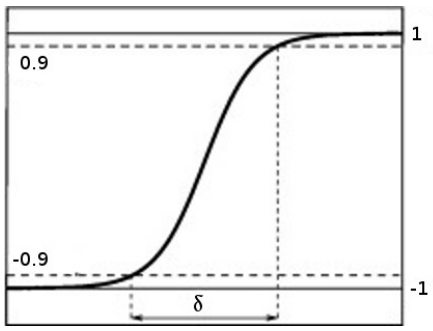

Figure 1.4: Example of tiny layer in which the two phases coexists and its thickness δ.

As discussed above when we described the phase separation process, the Cahn-Hilliard problem exhibits two characteristic time lengths: the former is related

to the early aggregation of the spinodal decomposition and the latter to the long time behaviour of the solution. Those time lengths are very different (cf. Figure 1.1) and it is very difficult to precisely capture the behaviour of the solution with a fixed choice of the time-step. Explicit numerical discretizations require severe time-step restrictions of the form $\Delta t \sim h^4$. Recently, adaptive time schemes has been proposed to deal with this restriction (see, e.g., [42]).

We conclude this brief overview mentioning that the Cahn-Hilliard equation is not only used to model phase-separation processes, but, suitable modifications have been applied in several fields like: liquid-liquid interface [55], solidification processes [20, 58], dendritic flow [47, 51], microstructure evolution in solids [39], thin films [64], irregular structure of Saturn's rings [66]. More recent applications are model foams [38], biofilms [52], inpainting in binary images [14, 19], wound healing and tumor growth [50] and the study of spatial distribution of mussels [54].

1.3 Boundary conditions

As it is typical in modelling physical phenomena with PDEs, the choice of appropriate boundary conditions plays a crucial role. A common choice for the Cahn-Hilliard problem is to impose homogeneous Neumann condition for the chemical potential w. This can be justified by a physical point of view; in fact, if we integrate the first equation of (1.2) over Ω and we apply the divergence theorem we obtain

$$\frac{d}{dt}\int_\Omega u = 0,$$

and, consequently, the conservation of the mean concentration of u.

As far as the boundary condition for u, homogeneous Neumann condition is typically employed. This choice forces the gradient of u to be parallel with respect to $\Gamma = \partial\Omega$. However, since this is a strong assumption that in real application it is not always satisfied, physicist have recently introduced a new type of boundary condition that takes into account the interaction of the mixture with the walls of the box containing the fluid. Those conditions are called *dynamic* since they are characterized by the explicit presence of the time derivative $\partial_t u$. In the sequel, we briefly sketch the derivation of the dynamic boundary conditions. Following [21], we introduce the new total free energy as

$$\mathbb{E}(u) = \int_\Omega \left(\frac{\gamma^2}{2}|\nabla u|^2 + \Phi(u)\right) dx + \int_\Gamma \left(\frac{\sigma_s}{2}|\nabla_\Gamma u|^2 + \frac{\lambda_s}{2}|u|^2 + \Psi(u)\right) ds, \quad (1.5)$$

where $\sigma_s,\ \lambda_s > 0$ and Ψ is the antiderivative of a regular enough function ψ. The first integral in (1.5) represents the bulk energy (like in (1.4)), while the second

is related to the surface energy. Evaluating the first variation of the total energy $\mathbb{E}(u)$ with respect to u and testing it with a smooth enough function v we obtain

$$\left\langle \frac{\delta \mathbb{E}(u)}{\delta u}, v \right\rangle = \int_\Omega \left(-\gamma^2 \Delta u + \phi(u)\right) v \, dx + \int_\Gamma \left(-\sigma_s \Delta_\Gamma u + \lambda_s u + \gamma^2 \partial_n u + \psi(u)\right) z \, ds.$$

Assuming that on Γ the density relaxes proportionally to the part of the flux belonging to the border, the dynamic boundary condition reads as

$$\lambda \partial_t u = \frac{\sigma_s}{\gamma^2} \Delta_\Gamma u - \partial_n u - \frac{\lambda_s}{\gamma^2} u - \frac{1}{\gamma^2} \psi(u) \text{ on } \Gamma,$$

with $\lambda > 0$.

1.4 DG methods

The design of efficient and reliable numerical schemes for the discretization of the Cahn-Hilliard equation is the object of an intensive research activity (see, e.g. [34, 35, 40, 65] and [57] where dynamic boundary condition are employed). However, due to the fact that the solution of the Cahn-Hilliard equation exhibits large variation in its gradient, discontinuous Galerkin methods have been recently proposed as a numerical strategy to obtain accurate simulations (see [49, 68]). The discontinuous Galerkin method are a non-conforming technique for solving differential equations introduced for the first time in 1973 by Reed and Hill for hyperbolic equations [60]. They combine features of the finite element and the finite volume framework, approximating the discrete solution with discontinuous basis functions. The communication between the basis functions of different elements takes place by the introduction of suitable penalization terms on the jumps (i.e., the difference of the function values defined from adjacent elements on the common interface). Recently, those methods became largely utilized and they also extended to elliptic and parabolic problems. They are also applied to a very wide variety of problems. The DG methods have several advantages like

- They can be easily designed for any order of accuracy: the basis functions can be locally built on each element.
- They work on complicated geometry and boundary conditions. They can also allow hanging nodes in the triangulation.
- They exhibit at least $(k + \frac{1}{2})-$th order of accuracy (and often $k + 1-$th) in L^2 norm of the error, where k is the maximum degree of the piecewise polynomial functions used. That order is independent of the structure of the meshes.
- They are suitable for $hp-$adaptivity.

- They are local in data communications: every element needs to communicate only with their neighbours. This implies that the methods have high performances with parallel computing.

The major drawback of DG approach is that, since we work with discontinuous functions, we globally have more degrees of freedom and the size of the problem to be solved becomes larger. Despite this fact, $hp-$adaptivity is a powerful feature that has the chance to reduce the computational cost making the DG methods competitive with classical finite element methods.

1.5 Notations

Throughout the entire thesis, we write $x \lesssim y$ to signify $x < Cy$, where C is a generic positive constant whose value, possibly different at any occurrence, does not depend on the discretization parameters. Moreover, we use $x \sim y$ to state the equivalence between x and y, i.e., $C_1 y \leq x \leq C_2 y$, for $C_1,\ C_2$ independent on the discretization parameters.

This thesis is devoted to the design of a new DG approximation of CH equation with dynamic boundary conditions. To achieve this goal we focus on a set of subproblems that represent crucial steps towards the achievement of the final goal. In particular, Chapter 2 is devoted to the introduction of discontinuous Galerkin on elliptic surface problems in which we present the surface high-order discretization for the principal discontinuous methods present in literature. In Chapter 3 we present and analyze a parabolic problem with dynamic boundary conditions in symmetric interior penalty (SIPG) framework. In Chapter 4 we explore several classical multigrid techniques to improve the efficiency of the solution of the algebraic problems stemming from the DG approximation of the Cahn-Hilliard equation. In Chapter 5 we introduce a new set of smoothers and we analyze their performances using local Fourier analysis (LFA). Chapter 6 is devoted to the DG approximation of the Cahn-Hilliard problem with dynamic boundary conditions. Finally, Appendix A contains well-known multigrid schemes and useful results to solve non-linear problems.

2

High order discontinuous Galerkin methods for elliptic problems on surfaces

In this chapter we present and analyze a unified framework for high order DG methods on surfaces following the approach taken in [27]. The results contained in this chapter have been already presented in [2].

2.1 Model problem

The notation in this section closely follows the one used in [31]. Let Γ be a compact, oriented, C^∞, two-dimensional surface without boundary which is embedded in $\mathbb{R}^3$, and let $d(\cdot)$ denote the signed distance function to Γ which we assume to be well-defined in a sufficiently thin open tube U around Γ. The orientation of Γ is set by taking the normal ν of Γ to be in the direction of increasing $d(\cdot)$, i.e.,

$$\nu(\xi) = \nabla d(\xi),\ \xi \in \Gamma.$$

We denote by $\pi(\cdot)$ the projection onto Γ, i.e., $\pi : U \to \Gamma$ is given by

$$\pi(x) = x - d(x)\nu(x) \quad \text{where } \nu(x) = \nu(\pi(x)). \tag{2.1}$$

In the following, we assume that there is a one-to-one relation between points $x \in U$ and points $\xi = \pi(x) \in \Gamma$. In particular, (2.1) is invertible in U. We denote by

$$P(\xi) = I - \nu(\xi) \otimes \nu(\xi),\ \xi \in \Gamma,$$

the projection onto the tangent space $T_\xi\Gamma$ on Γ at a point $\xi \in \Gamma$, where $\otimes$ denotes the usual tensor product.

Remark 2.1 *It is easy to see that*

$$\nabla\pi = P - dH, \tag{2.2}$$

where $H = \nabla^2 d$ *[31, Lemma 3].*

For any function η defined in an open subset of U containing Γ we define its *tangential gradient* on Γ by

$$\nabla_\Gamma \eta = \nabla\eta - (\nabla\eta \cdot \nu)\,\nu = P\nabla\eta,$$

and the *Laplace-Beltrami* operator by

$$\Delta_\Gamma \eta = \nabla_\Gamma \cdot (\nabla_\Gamma \eta).$$

For an integer $m \geq 0$, we define the surface Sobolev space

$$H^m(\Gamma) = \{u \ \in \ L^2(\Gamma) \ : \ D^\alpha u \in L^2(\Gamma) \ \forall \ |\alpha| \leq m\}.$$

We endow the Sobolev space with the standard seminorm and norm

$$|u|_{H^m(\Gamma)} = \left(\sum_{|\alpha|=m} \|D^\alpha u\|^2_{L^2(\Gamma)} \right)^{1/2}, \quad \|u\|_{H^m(\Gamma)} = \left(\sum_{k=0}^{m} |u|^2_{H^k(\Gamma)} \right)^{1/2},$$

respectively, cf. [69].

Let $f \in L^2(\Gamma)$ be a given function, we consider the following model problem: *Find* $u \in H^1(\Gamma)$ *such that*

$$\int_\Gamma \nabla_\Gamma u \cdot \nabla_\Gamma v + uv \ \mathrm{dA} = \int_\Gamma fv \ \mathrm{dA} \qquad \forall v \in H^1(\Gamma). \tag{2.3}$$

We denote by respectively dA and ds the two and one dimensional surface measures over Γ. Throughout the chapter, we assume that $u \in H^s(\Gamma)$, $s \geq 2$. Existence, uniqueness and regularity of such a solution are shown in [8].

2.2 High order DG approximation

We now follow the high order surface approximation framework introduced in [28]. We begin by approximating the smooth surface Γ by a polyhedral surface $\Gamma_h \subset U$ composed of planar triangles $\widetilde{K}_h$ whose vertices lie on Γ, and denote by $\widetilde{\mathcal{T}}_h$ the associated regular, conforming triangulation of Γ_h, i.e., $\Gamma_h = \bigcup_{\widetilde{K}_h \in \widetilde{\mathcal{T}}_h} \widetilde{K}_h$.

We next describe a family Γ_h^k of polynomial approximations to Γ of degree $k \geq 1$ (with the convention that $\Gamma_h^1 = \Gamma_h$). For a given element $\widetilde{K}_h \in \widetilde{\mathcal{T}}_h$, let

$\{\phi_i^k\}_{1\le i\le n_k}$ be the Lagrange basis functions of degree k defined on $\widetilde{K}_h$ corresponding to a set nodal points $x_1, ..., x_{n_k}$. For $x \in \widetilde{K}_h$, we define the discrete projection $\pi_k : \Gamma_h \to U$ as

$$\pi_k(x) = \sum_{j=1}^{n_k} \pi(x_j)\phi_j^k(x).$$

By constructing π_k elementwise we obtain a continuous piecewise polynomial map on Γ_h. We then define the corresponding discrete surface $\Gamma_h^k = \{\pi_k(x) : x \in \Gamma_h\}$ and the corresponding regular, conforming triangulation $\widehat{\mathcal{T}}_h = \{\pi_k(\widetilde{K}_h)\}_{\widetilde{K}_h\in\widetilde{\mathcal{T}}_h}$. We denote by $\widehat{\mathcal{E}}_h$ the set of all (codimension one) intersections $\widehat{e}_h$ of elements in $\widehat{\mathcal{T}}_h$, i.e., $\widehat{e}_h = \widehat{K}_h^+ \cap \widehat{K}_h^-$, for some elements $\widehat{K}_h^\pm \in \widehat{\mathcal{T}}_h$. Furthermore, we denote by $h_{\widehat{e}_h}$ the length of the edge $\widehat{e}_h \in \widehat{\mathcal{E}}_h$. For any $\widehat{e}_h \in \widehat{\mathcal{E}}_h$, the conormal n_h^+ to a point $x \in \widehat{e}_h$ is the unique unit vector that belongs to $T_x\widehat{K}_h^+$ and that satisfies

$$n_h^+(x) \cdot (x - y) \ge 0 \quad \forall y \in \widehat{K}_h^+ \cap B_\epsilon(x),$$

where $B_\epsilon(x)$ is the ball centered in x with (small enough) radius $\epsilon > 0$. Analogously, one can define the conormal n_h^- on $\widehat{e}_h$ by exchanging $\widehat{K}_h^+$ with $\widehat{K}_h^-$. It is important to notice that, with the above definition,

$$n_h^+ \neq -n_h^-$$

in general and independently of the surface approximation k (see Figure 2.1). Finally, we denote by ν_h the outward unit normal to Γ_h^k and define for each $\widehat{K}_h \in \widehat{\mathcal{T}}_h$ the discrete projection P_h onto the tangential space of Γ_h^k by

$$P_h(x) = I - \nu_h(x) \otimes \nu_h(x),\ x \in \widehat{K}_h,$$

so that, for v_h defined on Γ_h^k,

$$\nabla_{\Gamma_h^k} v_h = P_h \nabla v_h.$$

Let $K \subset \mathbb{R}^2$ be the (flat) reference element and let $F_{\widehat{K}_h} = \pi_k \circ F_{\widetilde{K}_h} : K \to \widehat{K}_h \subset \mathbb{R}^3$ for $\widehat{K}_h \in \widehat{\mathcal{T}}_h$, where $F_{\widetilde{K}_h} : K \to \widetilde{K}_h$ is the classical affine map from the reference element K to $\widetilde{K}_h$. We define the isoparametric DG space associated to Γ_h^k by

$$\widehat{S}_{hk} = \{\widehat{\chi} \in L^2(\Gamma_h^k)\ :\ \widehat{\chi}|_{\widehat{K}_h} = \chi \circ F_{\widehat{K}_h}^{-1} \text{ for some } \chi \in \mathbb{P}^k(K) \quad \forall \widehat{K}_h \in \widehat{\mathcal{T}}_h\}.$$

For $v_h \in \widehat{S}_{hk}$ we adopt the convention that $v_h^\pm$ is the trace of v_h on $\widehat{e}_h = \widehat{K}_h^+ \cap \widehat{K}_h^-$ taken within the interior of $\widehat{K}_h^\pm$, respectively. In addition, we define the vector-valued function space

$$\widehat{\Sigma}_{hk} = \{\widehat{\tau} \in [L^2(\Gamma_h^k)]^3\ :\ \widehat{\tau}|_{\widehat{K}_h} = \nabla F_{\widehat{K}_h}^{-T} \left(\tau \circ F_{\widehat{K}_h}^{-1}\right) \text{ for some } \tau \in [\mathbb{P}^k(K)]^2\ \ \forall \widehat{K}_h \in \widehat{\mathcal{T}}_h\}.$$

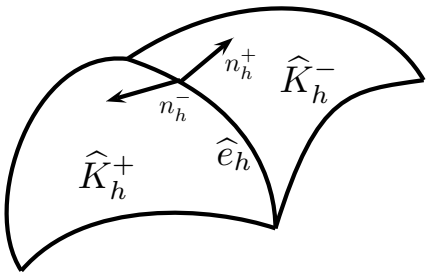

Figure 2.1: Example of two elements in $\widehat{\mathcal{T}}_h$ and their respective conormals on the common edge $\widehat{e}_h$.

Here, $\nabla F_{\widehat{K}_h}^{-1}$ refers to the (left) *pseudo-inverse* of $\nabla F_{\widehat{K}_h}$, i.e.,

$$\nabla F_{\widehat{K}_h}^{-1} = \left(\nabla F_{\widehat{K}_h}^T \nabla F_{\widehat{K}_h}\right)^{-1} \nabla F_{\widehat{K}_h}^T.$$

Note that $P_h \nabla F_{\widehat{K}_h}^{-T} = \nabla F_{\widehat{K}_h}^{-T}$, i.e., $\widehat{\tau} \in \widehat{\Sigma}_{hk} \Rightarrow \widehat{\tau} \in T_x \Gamma_h^k$ almost everywhere. This result straightforwardly implies that $\eta \in \widehat{S}_{hk} \Rightarrow \nabla_{\Gamma_h^k} \eta \in \widehat{\Sigma}_{hk}$. Indeed, by definition of $\widehat{S}_{hk}$ there exists $\chi \in \mathbb{P}^k(K)$ such that $\eta = \chi \circ F_{\widehat{K}_h}^{-1}$ and it holds

$$\nabla_{\Gamma_h^k} \eta = P_h \nabla(\chi \circ F_{\widehat{K}_h}^{-1}) = P_h \nabla F_{\widehat{K}_h}^{-T} (\nabla \chi \circ F_{\widehat{K}_h}^{-1}) = \nabla F_{\widehat{K}_h}^{-T} (\nabla \chi \circ F_{\widehat{K}_h}^{-1}). \tag{2.4}$$

Then, the result follows by taking $\tau = \nabla \chi$ in (2.4).

2.2.1 Primal formulation

Rewriting (2.3) as a first order system of equations and following the lines of [7], we wish to find $(u_h, \sigma_h) \in \widehat{S}_{hk} \times \widehat{\Sigma}_{hk}$ such that

$$\begin{aligned}
\int_{\widehat{K}_h} \sigma_h \cdot w_h \, \mathrm{dA_{hk}} &= -\int_{\widehat{K}_h} u_h \nabla_{\Gamma_h^k} \cdot w_h \, \mathrm{dA_{hk}} + \int_{\partial \widehat{K}_h} \widehat{u} \, w_h \cdot n_{\widehat{K}_h} \, \mathrm{ds_{hk}}, \\
\int_{\widehat{K}_h} \sigma_h \cdot \nabla_{\Gamma_h^k} v_h + u_h v_h \, \mathrm{dA_{hk}} &= \int_{\widehat{K}_h} f_h v_h \, \mathrm{dA_{hk}} + \int_{\partial \widehat{K}_h} \widehat{\sigma} \cdot n_{\widehat{K}_h} \, v_h \, \mathrm{ds_{hk}},
\end{aligned}$$

for all $w_h \in \widehat{\Sigma}_{hk}$, $v_h \in \widehat{S}_{hk}$, where $\mathrm{dA_{hk}}$ and $\mathrm{ds_{hk}}$ denote the two and one dimensional surface measures over Γ_h^k, respectively, and the discrete right-hand side $f_h \in L^2(\Gamma_h^k)$ will be related to f in Section 2.3.1. Here $\widehat{u} = \widehat{u}(u_h)$ and $\widehat{\sigma} = \widehat{\sigma}(u_h, \sigma_h(u_h))$ are the so called numerical fluxes which determine the inter-element behaviour of the solution and will be prescribed later on. In order to deal with these terms, we need to introduce the following discrete surface trace operators:

Definition 2.1 *Suppose there is an element numbering for all* $\widehat{K}_h \in \widehat{\mathcal{T}}_h$. *For* $q \in \Pi_{\widehat{K}_h \in \widehat{\mathcal{T}}_h} L^2(\partial \widehat{K}_h)$, $\{q\}$ *and* $[q]$ *are given by*

$$\{q\} = \frac{1}{2}(q^+ + q^-), \ [q] = q^+ - q^- \ \text{on } \widehat{e}_h \in \widehat{\mathcal{E}}_h.$$

For $\phi, \tilde{n} \in [\Pi_{\widehat{K}_h \in \widehat{\mathcal{T}}_h} L^2(\partial \widehat{K}_h)]^3$, $\{\phi; \tilde{n}\}$ *and* $[\phi; \tilde{n}]$ *are given by*

$$\{\phi; \tilde{n}\} = \frac{1}{2}(\phi^+ \cdot \tilde{n}^+ - \phi^- \cdot \tilde{n}^-), \quad [\phi; \tilde{n}] = \phi^+ \cdot \tilde{n}^+ + \phi^- \cdot \tilde{n}^- \quad \text{on } \widehat{e}_h \in \widehat{\mathcal{E}}_h. \quad (2.5)$$

We now state a useful formula which holds for functions in

$$H^1(\widehat{\mathcal{T}}_h) = \{v|_{\widehat{K}_h} \in H^1(\widehat{K}_h) \ : \ \forall \widehat{K}_h \in \widehat{\mathcal{T}}_h\}.$$

Its proof is straighforward and therefore is omitted.

Lemma 2.1 *Let* $\phi \in [H^1(\widehat{\mathcal{T}}_h)]^3$ *and* $\psi \in H^1(\widehat{\mathcal{T}}_h)$. *Then we have that*

$$\sum_{\widehat{K}_h \in \widehat{\mathcal{T}}_h} \int_{\partial \widehat{K}_h} \psi \phi \cdot n_{\widehat{K}_h} \ ds_{hk} = \sum_{\widehat{e}_h \in \widehat{\mathcal{E}}_h} \int_{\widehat{e}_h} [\phi; n_h]\{\psi\} + \{\phi; n_h\}[\psi] \ ds_{hk}.$$

We then prooced as in [7] and integrate again by parts the first equation, sum over all elements, and apply Lemma 2.1. We then obtain

$$\begin{aligned} \sum_{\widehat{K}_h \in \widehat{\mathcal{T}}_h} \int_{\widehat{K}_h} \sigma_h \cdot w_h \ \mathrm{dA_{hk}} = &\sum_{\widehat{K}_h \in \widehat{\mathcal{T}}_h} \int_{\widehat{K}_h} \nabla_{\Gamma_h^k} u_h \cdot w_h \ \mathrm{dA_{hk}} \\ &+ \sum_{\widehat{e}_h \in \widehat{\mathcal{E}}_h} \int_{\widehat{e}_h} [\widehat{u} - u_h]\{w_h; n_h\} + \{\widehat{u} - u_h\}[w_h; n_h] \ \mathrm{ds_{hk}}, \end{aligned} \quad (2.6)$$

$$\begin{aligned} \sum_{\widehat{K}_h \in \widehat{\mathcal{T}}_h} \int_{\widehat{K}_h} \sigma_h \cdot \nabla_{\Gamma_h^k} v_h + u_h v_h \ \mathrm{dA_{hk}} = &\sum_{\widehat{K}_h \in \widehat{\mathcal{T}}_h} \int_{\widehat{K}_h} f_h v_h \ \mathrm{dA_{hk}} \\ &+ \sum_{\widehat{e}_h \in \widehat{\mathcal{E}}_h} \int_{\widehat{e}_h} \Big(\{\widehat{\sigma}; n_h\}[v_h] + [\widehat{\sigma}; n_h]\{v_h\} \Big) \ \mathrm{ds_{hk}}, \end{aligned} \quad (2.7)$$

for every $w_h \in \widehat{\Sigma}_{hk}$ and $v_h \in \widehat{S}_{hk}$.

We now introduce the local DG lifting operators $r_{\widehat{e}_h} : L^2(\widehat{e}_h) \to \widehat{\Sigma}_{hk}$ and $l_{\widehat{e}_h} : L^2(\widehat{e}_h) \to \widehat{\Sigma}_{hk}$ which satisfy

$$\int_{\Gamma_h^k} r_{\widehat{e}_h}(\phi) \cdot \tau_h \ \mathrm{dA_{hk}} = - \int_{\widehat{e}_h} \phi\{\tau_h; n_h\} \ \mathrm{ds_{hk}} \quad \forall \tau_h \in \widehat{\Sigma}_{hk},$$

$$\int_{\Gamma_h^k} l_{\widehat{e}_h}(q)\cdot\tau_h \,\mathrm{dA_{hk}} = -\int_{\widehat{e}_h} q[\tau_h;n_h]\,\mathrm{ds_{hk}} \quad \forall \tau_h \in \widehat{\Sigma}_{hk}.$$

The existence of such operators follows from standard arguments. Moreover, notice that for any edge $\widehat{e}_h$, the support of the operators $r_{\widehat{e}_h}(\cdot)$ and $l_{\widehat{e}_h}(\cdot)$ is confined to the two neighboring elements sharing the edge $\widehat{e}_h$. We then set $r_h : L^2(\widehat{\mathcal{E}}_h) \to \widehat{\Sigma}_{hk}$ and $l_h : L^2(\widehat{\mathcal{E}}_h) \to \widehat{\Sigma}_{hk}$, given by

$$r_h(\phi) = \sum_{\widehat{e}_h\in\widehat{\mathcal{E}}_h} r_{\widehat{e}_h}(\phi), \qquad l_h(\phi) = \sum_{\widehat{e}_h\in\widehat{\mathcal{E}}_h} l_{\widehat{e}_h}(\phi).$$

Using these, we can write σ_h solely in terms of u_h. Indeed, on each element $\widehat{K}_h \in \widehat{\mathcal{T}}_h$ we obtain from (2.6) that

$$\sigma_h = \sigma_h(u_h) = \nabla_{\Gamma_h^k} u_h - r_h([\widehat{u}(u_h) - u_h]) - l_h(\{\widehat{u}(u_h) - u_h\}). \tag{2.8}$$

Note that (2.8) does in fact imply that $\sigma_h \in \widehat{\Sigma}_{hk}$ as $\nabla_{\Gamma_h^k} u_h \in \widehat{\Sigma}_{hk}$ and $r_h, l_h \in \widehat{\Sigma}_{hk}$ by construction. Taking $w_h = \nabla_{\Gamma_h^k} v_h$ in (2.6), substituting the resulting expression into (2.7) and using (2.8), we obtain the primal formulation: *Find* $(u_h,\sigma_h) \in \widehat{S}_{hk}\times\widehat{\Sigma}_{hk}$ *such that*

$$\mathcal{A}_h^k(u_h,v_h) = \sum_{\widehat{K}_h\in\widehat{\mathcal{T}}_h}\int_{\widehat{K}_h} f_h v_h \,\mathrm{dA_{hk}} \quad \forall v_h \in \widehat{S}_{hk}, \tag{2.9}$$

where

$$\begin{aligned}\mathcal{A}_h^k(u_h,v_h) = &\sum_{\widehat{K}_h\in\widehat{\mathcal{T}}_h}\int_{\widehat{K}_h} \nabla_{\Gamma_h^k}u_h\cdot\nabla_{\Gamma_h^k}v_h + u_h v_h \;\mathrm{dA_{hk}}\\ &+\sum_{\widehat{e}_h\in\widehat{\mathcal{E}}_h}\int_{\widehat{e}_h}([\widehat{u}-u_h]\{\nabla_{\Gamma_h^k}v_h;n_h\} - \{\widehat{\sigma};n_h\}[v_h]) \;\mathrm{ds_{hk}}\\ &+\sum_{\widehat{e}_h\in\widehat{\mathcal{E}}_h}\int_{\widehat{e}_h}(\{\widehat{u}-u_h\}[\nabla_{\Gamma_h^k}v_h;n_h] - [\widehat{\sigma};n_h]\{v_h\}) \;\mathrm{ds_{hk}}.\end{aligned} \tag{2.10}$$

2.2.2 Examples of surface DG methods

For the following methods we introduce the penalization coefficients $\eta_{\widehat{e}_h}$ and $\beta_{\widehat{e}_h}$ defined as

$$\eta_{\widehat{e}_h} = \alpha, \quad \beta_{\widehat{e}_h} = \alpha k^2 h_{\widehat{e}_h}^{-1}, \tag{2.11}$$

where $\alpha > 0$ is a parameter at our disposal.

2.2.2.1 Surface Bassi-Rebay method

To derive the surface Bassi-Rebay method, based on [10], we choose

$$\begin{aligned} \widehat{u}^+ &= \{u_h\}, & \widehat{u}^- &= \{u_h\}, \\ \widehat{\sigma}^+ &= \{\sigma_h; n_h\} n_h^+, & \widehat{\sigma}^- &= -\{\sigma_h; n_h\} n_h^-. \end{aligned}$$

By (2.8) we obtain $\sigma_h = \nabla_{\Gamma_h^k} u_h + r_h([u_h])$. From the definition (2.5) we have

$$\{\widehat{\sigma}; n_h\} = \{\sigma_h; n_h\} = \{\nabla_{\Gamma_h^k} u_h; n_h\} + \{r_h([u_h]); n_h\},$$

which implies

$$\begin{aligned} &\sum_{\widehat{e}_h \in \widehat{\mathcal{E}}_h} \int_{\widehat{e}_h} \{\widehat{\sigma}; n_h\}[v_h] \, \mathrm{ds_{hk}} \\ &\qquad = \sum_{\widehat{e}_h \in \widehat{\mathcal{E}}_h} \int_{\widehat{e}_h} \{\nabla_{\Gamma_h^k} u_h; n_h\}[v_h] \, \mathrm{ds_{hk}} + \sum_{\widehat{e}_h \in \widehat{\mathcal{E}}_h} \int_{\widehat{e}_h} \{r_h([u_h]); n_h\}[v_h] \, \mathrm{ds_{hk}} \\ &\qquad = \sum_{\widehat{e}_h \in \widehat{\mathcal{E}}_h} \int_{\widehat{e}_h} \{\nabla_{\Gamma_h^k} u_h; n_h\}[v_h] \, \mathrm{ds_{hk}} - \sum_{\widehat{K}_h \in \widehat{\mathcal{T}}_h} \int_{\widehat{K}_h} r_h([u_h]) \cdot r_h([v_h]) \, \mathrm{dA_{hk}}. \end{aligned}$$

Therefore, making use of the fact that $\{\widehat{u} - u_h\} = 0$, $[\widehat{u} - u_h] = [u_h]$ and $[\widehat{\sigma}; n_h] = 0$, we have that

$$\begin{aligned} \mathcal{A}_h^k(u_h, v_h) = &\sum_{\widehat{K}_h \in \widehat{\mathcal{T}}_h} \int_{\widehat{K}_h} \left(\nabla_{\Gamma_h^k} u_h \cdot \nabla_{\Gamma_h^k} v_h + u_h v_h + r_h([u_h]) \cdot r_h([v_h]) \right) \mathrm{dA_{hk}} \\ &- \sum_{\widehat{e}_h \in \widehat{\mathcal{E}}_h} \int_{\widehat{e}_h} \left(\{\nabla_{\Gamma_h^k} u_h; n_h\}[v_h] + \{\nabla_{\Gamma_h^k} v_h; n_h\}[u_h] \right) \mathrm{ds_{hk}}. \end{aligned} \tag{2.12}$$

2.2.2.2 Surface Brezzi et al. method

For the surface Brezzi et al. method, based on [18], we choose

$$\begin{aligned} \widehat{u}^+ &= \{u_h\}, & \widehat{u}^- &= \{u_h\}, \\ \widehat{\sigma}^+ &= \{\sigma_h + \eta_{\widehat{e}_h} r_{\widehat{e}_h}([u_h]); n_h\} n_h^+, & \widehat{\sigma}^- &= -\{\sigma_h + \eta_{\widehat{e}_h} r_{\widehat{e}_h}([u_h]); n_h\} n_h^-, \end{aligned}$$

The method is similar to that of Bassi-Rebay, but with an additional term. Indeed,

$$
\begin{aligned}
&\sum_{\widehat{e}_h\in\widehat{\mathcal{E}}_h}\int_{\widehat{e}_h}\{\widehat{\sigma};n_h\}[v_h]\ \mathrm{ds_{hk}}\\
&\quad=\sum_{\widehat{e}_h\in\widehat{\mathcal{E}}_h}\int_{\widehat{e}_h}\{\sigma_h+\eta_{\widehat{e}_h}r_{\widehat{e}_h}([u_h]);n_h\}[v_h]\ \mathrm{ds_{hk}}\\
&\quad=\sum_{\widehat{e}_h\in\widehat{\mathcal{E}}_h}\int_{\widehat{e}_h}\{\nabla_{\Gamma_h^k}u_h;n_h\}[v_h]\ \mathrm{ds_{hk}}+\sum_{\widehat{e}_h\in\widehat{\mathcal{E}}_h}\int_{\widehat{e}_h}\{r_h([u_h])+\eta_{\widehat{e}_h}r_{\widehat{e}_h}([u_h]);n_h\}[v_h]\ \mathrm{ds_{hk}}\\
&\quad=\sum_{\widehat{e}_h\in\widehat{\mathcal{E}}_h}\int_{\widehat{e}_h}\{\nabla_{\Gamma_h^k}u_h;n_h\}[v_h]\ \mathrm{ds_{hk}}-\sum_{\widehat{K}_h\in\widehat{\mathcal{T}}_h}\int_{\widehat{K}_h}r_h([u_h])\cdot r_h([v_h])\ \mathrm{dA_{hk}}\\
&\qquad-\sum_{\widehat{K}_h\in\widehat{\mathcal{T}}_h}\int_{\widehat{K}_h}\eta_{\widehat{e}_h}r_{\widehat{e}_h}([u_h])\cdot r_{\widehat{e}_h}([v_h])\ \mathrm{dA_{hk}}.
\end{aligned}
$$

Then

$$
\begin{aligned}
\mathcal{A}_h^k(u_h,v_h)=&\sum_{\widehat{K}_h\in\widehat{\mathcal{T}}_h}\int_{\widehat{K}_h}\nabla_{\Gamma_h^k}u_h\cdot\nabla_{\Gamma_h^k}v_h+u_hv_h\ \mathrm{dA_{hk}}\\
&-\sum_{\widehat{e}_h\in\widehat{\mathcal{E}}_h}\int_{\widehat{e}_h}\{\nabla_{\Gamma_h^k}u_h;n_h\}[v_h]+\{\nabla_{\Gamma_h^k}v_h;n_h\}[u_h]\ \mathrm{ds_{hk}}\\
&+\sum_{\widehat{K}_h\in\widehat{\mathcal{T}}_h}\int_{\widehat{K}_h}r_h([u_h])\cdot r_h([v_h])+\eta_{\widehat{e}_h}r_{\widehat{e}_h}([u_h])\cdot r_{\widehat{e}_h}([v_h])\ \mathrm{dA_{hk}}. \qquad (2.13)
\end{aligned}
$$

2.2.2.3 Surface IP method

To derive the surface IP method, based on [30, 9, 6], we choose the numerical fluxes $\widehat{u}$ and $\widehat{\sigma}$ as follows:

$$
\begin{aligned}
&\widehat{u}^+=\{u_h\}, && \widehat{u}^-=\{u_h\},\\
&\widehat{\sigma}^+=\Big(\{\nabla_{\Gamma_h^k}u_h;n_h\}-\beta_{\widehat{e}_h}[u_h]\Big)n_h^+, && \widehat{\sigma}^-=-\Big(\{\nabla_{\Gamma_h^k}u_h;n_h\}-\beta_{\widehat{e}_h}[u_h]\Big)n_h^-.
\end{aligned}
$$

Substituting them into (2.10), we obtain

$$
\begin{aligned}
\mathcal{A}_h^k(u_h,v_h)=&\sum_{\widehat{K}_h\in\widehat{\mathcal{T}}_h}\int_{\widehat{K}_h}\nabla_{\Gamma_h^k}u_h\cdot\nabla_{\Gamma_h^k}v_h+u_hv_h\ \ \mathrm{dA_{hk}}+\sum_{\widehat{e}_h\in\widehat{\mathcal{E}}_h}\int_{\widehat{e}_h}\beta_{\widehat{e}_h}[u_h][v_h]\ \ \mathrm{ds_{hk}}\\
&-\sum_{\widehat{e}_h\in\widehat{\mathcal{E}}_h}\int_{\widehat{e}_h}\big([u_h]\{\nabla_{\Gamma_h^k}v_h;n_h\}+[v_h]\{\nabla_{\Gamma_h^k}u_h;n_h\}\big)\ \mathrm{ds_{hk}} \qquad (2.14)
\end{aligned}
$$

which is exactly the surface IP method considered in [27].

2.2.2.4 Surface NIPG method

For the surface NIPG method, based on [63] (or equivalently the Baumann-Oden method in [13] with $\beta_{\widehat{e}_h} = 0$), we choose

$$\begin{aligned}
\widehat{u}^+ &= \{u_h\} + [u_h], & \widehat{u}^- &= \{u_h\} - [u_h],\\
\widehat{\sigma}^+ &= \Big(\{\nabla_{\Gamma_h^k} u_h; n_h\} - \beta_{\widehat{e}_h}[u_h]\Big) n_h^+, & \widehat{\sigma}^- &= -\Big(\{\nabla_{\Gamma_h^k} u_h; n_h\} - \beta_{\widehat{e}_h}[u_h]\Big) n_h^-.
\end{aligned}$$

We may derive the surface NIPG bilinear form in a similar way as for the surface IP method.

2.2.2.5 Surface IIPG method

For the surface IIPG method, based on [25], we choose the numerical fluxes $\widehat{u}$ and $\widehat{\sigma}$ as follows:

$$\begin{aligned}
\widehat{u}^+ &= u_h^+, & \widehat{u}^- &= u_h^-,\\
\widehat{\sigma}^+ &= \Big(\{\nabla_{\Gamma_h^k} u_h; n_h\} - \beta_{\widehat{e}_h}[u_h]\Big) n_h^+, & \widehat{\sigma}^- &= -\Big(\{\nabla_{\Gamma_h^k} u_h; n_h\} - \beta_{\widehat{e}_h}[u_h]\Big) n_h^-.
\end{aligned}$$

Here again, we may derive the surface IIPG bilinear form in a similar way as for the surface IP method.

2.2.2.6 Surface Bassi et al. method

For the surface Bassi et al. method, based on [11], we choose

$$\begin{aligned}
\widehat{u}^+ &= \{u_h\}, & \widehat{u}^- &= \{u_h\},\\
\widehat{\sigma}^+ &= \Big(\{\nabla_{\Gamma_h^k} u_h + \eta_{\widehat{e}_h} r_{\widehat{e}_h}([u_h]); n_h\}\Big) n_h^+, & \widehat{\sigma}^- &= -\Big(\{\nabla_{\Gamma_h^k} u_h + \eta_{\widehat{e}_h} r_{\widehat{e}_h}([u_h]); n_h\}\Big) n_h^-.
\end{aligned}$$

The resulting bilinear surface form can be easily obtained using the contributes of the surface IP and surface Brezzi et al. bilinear forms.

2.2.2.7 Surface LDG method

Finally for the surface LDG method, based on [23], the numerical fluxes are chosen as follows:

$$\begin{aligned}
\widehat{u}^+ &= \{u_h\} - \theta \cdot n_h^+ [u_h], \quad \widehat{u}^- = \{u_h\} - \theta \cdot n_h^+ [u_h],\\
\widehat{\sigma}^+ &= \Big(\{\sigma_h; n_h\} - \beta_{\widehat{e}_h}[u_h] + \theta \cdot n_h^+ [\sigma_h; n_h]\Big) n_h^+,\\
\widehat{\sigma}^- &= -\Big(\{\sigma_h; n_h\} - \beta_{\widehat{e}_h}[u_h] + \theta \cdot n_h^+ [\sigma_h; n_h]\Big) n_h^-,
\end{aligned}$$

where θ is a (possibly null) uniformly bounded vector of $\mathbb{R}^3$ that does not depend on the discretization parameters. We see that $\{\widehat{u}-u_h\} = -\theta\cdot n_h^+[u_h]$ and $[\widehat{u}-u_h] = -[u_h]$. So, from (2.8), we obtain:

$$\widehat{\sigma}^+ = \Big(\{\nabla_{\Gamma_h^k} u_h; n_h\} + \{r_h([u_h]); n_h\} + \{\theta\cdot n_h^+ l_h([u_h]); n_h\} - \beta_{\widehat{e}_h}[u_h] + \theta\cdot n_h^+ \Big([\nabla_{\Gamma_h^k} u_h; n_h] + [r_h([u_h]); n_h] + [\theta\cdot n_h^+ l_h([u_h]); n_h] \Big) \Big) n_h^+,$$

and in a similar way $\widehat{\sigma}^-$. Then

$$\begin{aligned}
&\sum_{\widehat{e}_h\in\widehat{\mathcal{E}}_h^k} \int_{\widehat{e}_h} \{\widehat{\sigma}; n_h\}[v_h] \, \mathrm{ds_{hk}} \\
&\quad = \sum_{\widehat{e}_h\in\widehat{\mathcal{E}}_h^k} \int_{\widehat{e}_h} \Big(\{\nabla_{\Gamma_h^k} u_h; n_h\}[v_h] + [\nabla_{\Gamma_h^k} u_h; n_h]\theta\cdot n_h^+[v_h] - \beta_{\widehat{e}_h}[u_h][v_h] \Big) \, \mathrm{ds_{hk}} \\
&\quad - \sum_{\widehat{K}_h\in\widehat{\mathcal{T}}_h} \int_{\widehat{K}_h} \Big(r_h([u_h]) + \theta\cdot n_h^+ l_h\big([u_h]\big) \Big) \cdot \Big(r_h([v_h]) + \theta\cdot n_h^+ l_h\big([v_h]\big) \Big) \, \mathrm{dA_{hk}},
\end{aligned}$$

and the surface LDG form can be written as

$$\begin{aligned}
&\mathcal{A}_h^k(u_h, v_h) \\
&\quad = \sum_{\widehat{K}_h\in\widehat{\mathcal{T}}_h} \int_{\widehat{K}_h} \nabla_{\Gamma_h^k} u_h \cdot \nabla_{\Gamma_h^k} v_h + u_h v_h \, \mathrm{dA_{hk}} \\
&\quad - \sum_{\widehat{e}_h\in\widehat{\mathcal{E}}_h} \int_{\widehat{e}_h} [u_h]\{\nabla_{\Gamma_h^k} v_h; n_h\} - \{\nabla_{\Gamma_h^k} u_h; n_h\}[v_h] \, \mathrm{ds_{hk}} \\
&\quad + \sum_{\widehat{e}_h\in\widehat{\mathcal{E}}_h} \int_{\widehat{e}_h} \Big(- [\nabla_{\Gamma_h^k} u_h; n_h]\theta\cdot n_h^+[v_h] - \theta\cdot n_h^+[u_h][\nabla_{\Gamma_h^k} v_h; n_h] + \beta_{\widehat{e}_h}[u_h][v_h] \Big) \, \mathrm{ds_{hk}} \\
&\quad + \sum_{\widehat{K}_h\in\widehat{\mathcal{T}}_h} \int_{\widehat{K}_h} \Big(r_h([u_h]) + \theta\cdot n_h^+ l_h\big([u_h]\big) \Big) \cdot \Big(r_h([v_h]) + \theta\cdot n_h^+ l_h\big([v_h]\big) \Big) \, \mathrm{dA_{hk}}.
\end{aligned} \tag{2.15}$$

Remark 2.2 *In the flat case, for which we have $n_h^+ = -n_h^-$, all of the surface DG methods yield the corresponding ones found in [7].*

Remark 2.3 *Notice that for all of our choices of the numerical fluxes $\widehat{u}$ and $\widehat{\sigma}$, we have that $[\widehat{u}] = 0$ and $[\widehat{\sigma}; n_h] = 0$. In addition, they are consistent with the corresponding fluxes in the flat case given in [7].*

2.3 Technical tools

In this section we introduce the necessary tools and geometric relations needed to work on discrete domains and prove boundedness and stability of the bilinear forms, following the framework introduced in [31].

2.3.1 Surface lifting

For any function w defined on Γ_h^k we define the surface *lift* onto Γ by

$$w^\ell(\xi) = w(x(\xi)),\ \xi \in \Gamma,$$

where, thanks to the invertibility of (2.1), $x(\xi)$ is defined as the unique solution of

$$x(\xi) = \pi(x) + d(x)\nu(\xi).$$

In particular, for every $\widehat{K}_h \in \widehat{\mathcal{T}}_h$, there is a unique curved triangle $\widehat{K}_h^\ell = \pi(\widehat{K}_h) \subset \Gamma$. We may then define the regular, conforming triangulation $\widehat{\mathcal{T}}_h^\ell$ of Γ given by

$$\Gamma = \bigcup_{\widehat{K}_h^\ell \in \widehat{\mathcal{T}}_h^\ell} \widehat{K}_h^\ell.$$

The triangulation $\widehat{\mathcal{T}}_h^\ell$ of Γ is thus induced by the triangulation $\widehat{\mathcal{T}}_h$ of Γ_h^k via the surface lift operator. Similarly, we denote by $\widehat{e}_h^\ell = \pi(\widehat{e}_h) \in \widehat{\mathcal{E}}_h^\ell$ the unique curved edge associated to $\widehat{e}_h$. The function space for surface lifted functions is chosen to be given by

$$\widehat{S}_{hk}^\ell = \{\chi \in L^2(\Gamma)\ :\ \chi = \widehat{\chi}^\ell \text{ for some } \widehat{\chi} \in \widehat{S}_{hk}\}.$$

We define the discrete right-hand side f_h such that $f_h^\ell = f$. We also denote by $w^{-\ell} \in \widehat{S}_{hk}$ the *inverse* surface lift of some function $w \in \widehat{S}_{hk}^\ell$ satisfying $(w^{-\ell})^\ell = w$.

As an extension of the results shown in [31, 29], for v_h defined on Γ_h^k, we have that

$$\nabla_{\Gamma_h^k} v_h = P_h(I - dH)P\nabla_\Gamma v_h^\ell. \tag{2.16}$$

Furthermore, let δ_h be the local area deformation when transforming $\widehat{K}_h$ to $\widehat{K}_h^\ell$, i.e.,

$$\delta_h \ \mathrm{dA_{hk}} = \ \mathrm{dA},$$

and let $\delta_{\widehat{e}_h}$ be the local edge deformation when transforming $\widehat{e}_h$ to $\widehat{e}_h^\ell$, i.e.,

$$\delta_{\widehat{e}_h} \ \mathrm{ds_{hk}} = \ \mathrm{ds}.$$

Finally, let

$$R_h = \frac{1}{\delta_h} P(I - dH)P_h(I - dH)P.$$

As a consequence of (2.16) we have that

$$\int_{\Gamma_h^k} \nabla_{\Gamma_h^k} u_h \cdot \nabla_{\Gamma_h^k} v_h + u_h v_h \, \mathrm{dA_{hk}} = \int_{\Gamma} R_h \nabla_\Gamma u_h^\ell \cdot \nabla_\Gamma v_h^\ell + \delta_h^{-1} u_h^\ell v_h^\ell \, \mathrm{dA}. \tag{2.17}$$

2.3.2 Geometric estimates

We next prove some geometric error estimates relating Γ to Γ_h^k.

Lemma 2.2 *Let Γ be a compact smooth connected and oriented surface in $\mathbb{R}^3$ and let Γ_h^k be its piecewise Lagrange interpolant of degree k. Furthermore, we denote by $n^\pm$ the unit (surface) conormals to respectively $\widehat{e}_h^{l+/-}$. Then, for sufficiently small h, we have that*

$$\|d\|_{L^\infty(\Gamma_h^k)} \lesssim h^{k+1}, \tag{2.18a}$$
$$\|1-\delta_h\|_{L^\infty(\Gamma_h^k)} \lesssim h^{k+1}, \tag{2.18b}$$
$$\|\nu-\nu_h\|_{L^\infty(\Gamma_h^k)} \lesssim h^{k}, \tag{2.18c}$$
$$\|P-R_h\|_{L^\infty(\Gamma_h^k)} \lesssim h^{k+1}, \tag{2.18d}$$
$$\|1-\delta_{\widehat{e}_h}\|_{L^\infty(\widehat{\mathcal{E}}_h)} \lesssim h^{k+1}, \tag{2.18e}$$
$$\sup_{\widehat{K}\in\widehat{\mathcal{T}}_h} \|P-R_{\widehat{e}_h}\|_{L^\infty(\partial\widehat{K}_h)} \lesssim h^{k+1}, \tag{2.18f}$$
$$\|n^\pm - P n_h^\pm\|_{L^\infty(\widehat{\mathcal{E}}_h)} \lesssim h^{k+1}, \tag{2.18g}$$

where $R_{\widehat{e}_h} = \frac{1}{\delta_{\widehat{e}_h}} P(I-dH)P_h(I-dH)$.

Proof. Proofs of (2.18a)-(2.18d) can be found in [28, Prop. 2.3 and Prop. 4.1]. The proof of (2.18f) will follow exactly the same lines as (2.18d) once we have proven (2.18e). Let e, K be the reference segment [0,1] and the (flat) reference element, respectively, and let $\widetilde{K}_h$, $\widehat{K}_h$ and $\widehat{K}_h^\ell$ be elements in Γ_h, Γ_h^k and Γ, respectively, such that $\pi_k(\widetilde{K}_h) = \widehat{K}_h$ and $\pi(\widehat{K}_h) = \widehat{K}_h^\ell$. Let also L_e be the inclusion operator that maps e into an edge of K and let $L_{\widetilde{K}_h}(K) = \widetilde{K}_h$.

A tangent on an edge $\widehat{e}_h \subset \widehat{K}_h$ in Γ_h^k is given by $\tau_h = \nabla(\pi_k \circ L_{\widetilde{K}_h} \circ L_e)$.

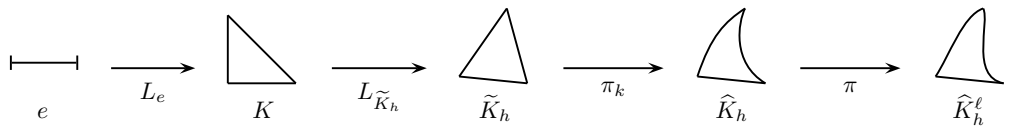

Figure 2.2: Mappings used in the proof of Lemma 2.2.

Analogously, a tangent on the surface lifted edge $\widehat{e}_h^\ell \subset \widehat{K}_h^\ell$ in Γ is given by $\tau = \nabla\pi\tau_h$. We denote by $\overline{\tau}_h$ and $\overline{\tau}$ respectively the unit tangents of $\widehat{e}_h$ and $\widehat{e}_h^\ell$,

and let $\lambda = \|\tau_h\|_{l^2}$. We will now prove estimate (2.18e). Let dx be the Lebesque measure on the reference interval e. We then have

$$\begin{aligned} \mathrm{ds_{hk}} &= \lambda \, \mathrm{dx}, \\ \mathrm{ds} &= \sqrt{\|(\nabla\pi\tau_h)^T \cdot \nabla\pi\tau_h\|_{l^2}} \, \mathrm{dx} = \lambda\sqrt{\|(\nabla\pi\overline{\tau}_h)^T \cdot \nabla\pi\overline{\tau}_h\|_{l^2}} \, \mathrm{dx} = \underbrace{\|\nabla\pi\overline{\tau}_h\|_{l^2}}_{\delta_{\widehat{e}_h}} \, \mathrm{ds_{hk}}. \end{aligned}$$

Having characterised $\delta_{\widehat{e}_h}$, we wish to show that

$$1 - Ch^{k+1} \leq \|\nabla\pi\overline{\tau}_h\|_{l^2} \leq 1 + Ch^{k+1}.$$

Making use of (2.2) and (2.18a), we have that

$$\|\nabla\pi\overline{\tau}_h\|_{l^2} \leq \|\nabla\pi\|_{l^2}\|\overline{\tau}_h\|_{l^2} \leq \|P - dH\|_{l^2} \leq 1 + Ch^{k+1}. \tag{2.19}$$

Next, to provide a lower bound for $\|\nabla\pi\overline{\tau}_h\|_{l^2}$, we consider

$$\tau - \tau_h = (\nabla\pi - P_h)\tau_h = \lambda(\nabla\pi - P_h)\overline{\tau}_h.$$

Recalling the definition of the projection matrices P and P_h, we have that

$$\|\tau - \tau_h\|_{l^2} \leq \lambda\|(P - P_h) - dH\|_{l^2}\|\overline{\tau}_h\|_{l^2} \leq \lambda Ch^k.$$

Using the reverse triangle inequality, we obtain

$$\lambda\|\nabla\pi\overline{\tau}_h\|_{l^2} = \|\tau\|_{l^2} \geq \|\tau_h\|_{l^2} - \|\tau - \tau_h\|_{l^2} \geq \lambda(1 - Ch^k) \tag{2.20}$$

and, dividing by λ and using (2.19), we obtain the sub-optimal estimate

$$1 - Ch^k \leq \|\nabla\pi\overline{\tau}_h\|_{l^2} \leq 1 + Ch^{k+1}. \tag{2.21}$$

The lower bound 2.21 can be improved in an iterative way as follows. We consider

$$\lambda\|\nabla\pi\overline{\tau}_h\|_{l^2} = \|\tau\|_{l^2} \geq \|P\tau_h\|_{l^2} - \|P\tau_h - \tau\|_{l^2}. \tag{2.22}$$

Then, using again the reverse triangular inequality, we have that

$$\|P\tau_h\|_{l^2} = \lambda\|P\overline{\tau}_h\|_{l^2} \geq \lambda(\|\overline{\tau}\|_{l^2} - \|\overline{\tau} - P\overline{\tau}_h\|_{l^2}) = \lambda(1 - \|\overline{\tau} - P\overline{\tau}_h\|_{l^2}). \tag{2.23}$$

Since $\overline{\tau}, n, \nu$ form an orthonormal basis of $\mathbb{R}^3$ and recalling that P maps vectors into the tangential space of Γ (hence have null normal component), we get

$$\begin{aligned} \lambda(1 - \|\overline{\tau} - P\overline{\tau}_h\|_{l^2}) &= \lambda(1 - \|1 - (\overline{\tau}, P\overline{\tau}_h)\overline{\tau} - (n, P\overline{\tau}_h)n\|_{l^2}) \\ &\geq \lambda(1 - \|(1 - (\overline{\tau}, \overline{\tau}_h))\|_{l^2} - \|(n, \overline{\tau}_h)\|_{l^2}) \\ &\geq \lambda(1 - \|\overline{\tau} - \overline{\tau}_h\|_{l^2}^2 - \|(n, \overline{\tau}_h)\|_{l^2}). \end{aligned} \tag{2.24}$$

Now

$$\overline{\tau}_h - \overline{\tau} = (P_h - \frac{\nabla\pi}{\|\nabla\pi\overline{\tau}_h\|_{l^2}})\overline{\tau}_h,$$

so using (2.21) and a Taylor expansion argument, it is easy to see that

$$\|\overline{\tau}_{\widehat{e}_h} - \overline{\tau}_{\widehat{e}_h^\ell}\|_{l^2} \lesssim h^k. \tag{2.25}$$

To deal with the last term of (2.24) we note that

$$(n, \overline{\tau}_h) = (\overline{\tau} \times \nu, \overline{\tau}_h) = (\nu, \overline{\tau}_h \times \overline{\tau}) = (\nu, \overline{\tau}_h \times \frac{\nabla\pi\overline{\tau}_h}{\|\nabla\pi\overline{\tau}_h\|_{l^2}}).$$

Then, using the sub-optimal lower bound (2.21) and a Taylor expansion argument, we get

$$(\nu, \overline{\tau}_h \times \frac{\nabla\pi\overline{\tau}_h}{\|\nabla\pi\overline{\tau}_h\|_{l^2}}) = \frac{1}{\|\nabla\pi\overline{\tau}_h\|_{l^2}}(\nu, \overline{\tau}_h \times \nabla\pi\overline{\tau}_h) \lesssim |(\nu, \overline{\tau}_h \times \nabla\pi\overline{\tau}_h)|\,.$$

Using the definition of P and (2.2), we have that

$$\nabla\pi\overline{\tau}_h = (P - dH)\overline{\tau}_h = \overline{\tau}_h - (\nu \cdot \overline{\tau}_h)\nu - dH\overline{\tau}_h. \tag{2.26}$$

Now, using (2.26), we can write

$$(\nu, \overline{\tau}_h \times \nabla\pi\overline{\tau}_h) = \Big(\nu, \overline{\tau}_h \times (\overline{\tau}_h - (\overline{\tau}_h \cdot \nu)\nu - dH\overline{\tau}_h)\Big) = -(\nu, \overline{\tau}_h \times dH\overline{\tau}_h).$$

Hence,

$$\|(n, \overline{\tau}_h)\|_{l^2} \lesssim \|d\|_{L^\infty}\|(\nu, \overline{\tau}_h \times H\overline{\tau}_h)\|_{l^2} \lesssim h^{k+1}. \tag{2.27}$$

Combining (2.27) and (2.25) with (2.24) we obtain that

$$\|P\tau_h\|_{l^2} \geq \lambda(1 - \|(1 - (\overline{\tau}, P\overline{\tau}_h))\overline{\tau} - (n, P\overline{\tau}_h)n\|_{l^2}) \geq \lambda(1 - Ch^{k+1}). \tag{2.28}$$

For the second term in the right-hand side of (2.22), notice that

$$\|\tau - P\tau_h\|_{l^2} = \|\nabla\pi\tau_h - P\tau_h\|_{l^2} = \|dH\tau_h\|_{l^2} \leq \lambda C h^{k+1}. \tag{2.29}$$

We are now ready to improve the lower bound in (2.21). By making use of (2.29) and (2.28) in (2.22), we get

$$\|\nabla\pi\overline{\tau}_h\|_{l^2} \geq 1 - Ch^{k+1} \tag{2.30}$$

which proves (2.18e).

To prove (2.18g), we need to first prove the following auxiliary estimates:

$$|(\overline{\tau}, n_h)| \lesssim h^{k+1}, \tag{2.31}$$

$$|1-(n,n_h)| \lesssim h^{2k}. \tag{2.32}$$

We start showing (2.31). Using the property of the cross product, we get

$$(\overline{\tau},n_h) = (\overline{\tau},\nu_h\times\overline{\tau}_h) = (\nu_h,\overline{\tau}_h\times\overline{\tau}) = (\nu_h,\overline{\tau}_h\times\nabla\pi\overline{\tau}_h). \tag{2.33}$$

Replacing (2.26) in (2.33), we obtain

$$(\overline{\tau},n_h) = [\nu\cdot(\overline{\tau}_h-\overline{\tau})](\overline{\tau}_h,\nu\times\nu_h) - (\nu_h,\overline{\tau}_h\times dH\overline{\tau}_h).$$

Taking the absolute value and using (2.18a), (2.18c) and (2.25), we find

$$|(\overline{\tau},n_h)| \lesssim h^{2k+1} + Ch^{k+1} \lesssim h^{k+1}.$$

In order to prove (2.32), we start showing that the following holds

$$|(\nu,n_h)| \lesssim h^k. \tag{2.34}$$

Indeed, using again the properties of the cross and scalar products, we obtain:

$$|(\nu,n_h)| = |(\nu,\nu_h\times\overline{\tau}_h)| = |(\nu_h,\overline{\tau}_h\times\nu)| = |(\nu_h,\overline{\tau}_h\times(\nu-\nu_h))| \lesssim h^k.$$

Since the vector n_h is of unit length, there exist $a(x),b(x),c(x)\in\mathbb{R}$ satisfying $a^2+b^2+c^2=1$ such that

$$n_h = a\overline{\tau}+bn+c\nu,$$

where $a=(\overline{\tau},n_h)$, $b=(n,n_h)$ and $c=(\nu,n_h)$. Hence, using (2.31), (2.34) and a Taylor expansion argument, we get

$$b = \pm\sqrt{1-a^2-c^2} = \pm\sqrt{1+O(h^{2k})} = \pm 1+O(h^{2k}).$$

The inequality (2.32) follows by assuming that the mesh size h of $\widehat{\mathcal{T}}_h$ is chosen small enough so that $b=1+O(h^{2k})$. Finally, writing $Pn_h = (\overline{\tau},Pn_h)\overline{\tau} + (n,Pn_h)n$, we obtain (2.18g), i.e.,

$$\begin{aligned}\|n-Pn_h\|_{L^\infty(\widehat{e}_h)} &= \|n-(\overline{\tau},Pn_h)\overline{\tau}+(n,Pn_h)n\|_{L^\infty(\widehat{e}_h)}\\ &\le |1-(n,Pn_h)| + |(\overline{\tau},Pn_h)|\\ &= |1-(n,n_h)| + |(\overline{\tau},n_h)| = O(h^{k+1}).\end{aligned}$$ ∎

2.3.3 Boundedness and stability

We define the space of piecewise polynomial functions on Γ_h as

$$\widetilde{S}_{hk} = \{\widetilde{\chi}\in L^2(\Gamma_h)\ :\ \widetilde{\chi}|_{\widetilde{K}_h}\in\mathbb{P}^k(\widetilde{K}_h)\quad \forall\widetilde{K}_h\in\widetilde{\mathcal{T}}_h\}.$$

We recall the following useful result from [28]:

Lemma 2.3 *Let $v \in H^j(\widehat{K}_h)$, $j \geq 2$, and let $\widetilde{v} = v \circ \pi_k$. Then, for h small enough, we have that*

$$\|v^\ell\|_{L^2(\widehat{K}_h^\ell)} \sim \|v\|_{L^2(\widehat{K}_h)} \sim \|\widetilde{v}\|_{L^2(\widetilde{K}_h)}, \tag{2.35a}$$

$$\|\nabla_\Gamma v^\ell\|_{L^2(\widehat{K}_h^\ell)} \sim \|\nabla_{\Gamma_h^k} v\|_{L^2(\widehat{K}_h)} \sim \|\nabla_{\Gamma_h} \widetilde{v}\|_{L^2(\widetilde{K}_h)}, \tag{2.35b}$$

$$\|D^j_{\Gamma_h^k} v\|_{L^2(\widehat{K}_h)} \lesssim \sum_{1\leq m\leq j} \|D^m_\Gamma v^\ell\|_{L^2(\widehat{K}_h^\ell)}, \tag{2.35c}$$

$$\|D^j_{\Gamma_h} \widetilde{v}\|_{L^2(\widetilde{K}_h)} \lesssim \sum_{1\leq m\leq j} \|D^m_{\Gamma_h^k} v\|_{L^2(\widehat{K}_h)}. \tag{2.35d}$$

We will also need the following inverse and trace inequalities. The following result is adapted from [22, Thm 3.2.6].

Lemma 2.4 *Let l, m be two integers such that $0 \leq l \leq m$. Then,*

$$|v_h|_{H^m(\widetilde{K}_h)} \lesssim h_{\widetilde{K}_h}^{l-m} |v_h|_{H^l(\widetilde{K}_h)} \qquad \forall v_h \in \widetilde{S}_{hk}.$$

Lemma 2.5 *Let $\widetilde{w} \in H^2(\widetilde{K}_h)$, $\widetilde{K}_h \in \widetilde{\mathcal{T}}_h$. Then, for each $\widetilde{e}_h \in \partial \widetilde{K}_h$, it holds that*

$$\|\widetilde{w}\|^2_{L^2(\widetilde{e}_h)} \lesssim h^{-1} \|\widetilde{w}\|^2_{L^2(\widetilde{K}_h)} + h \|\nabla_{\Gamma_h} \widetilde{w}\|^2_{H^2(\widetilde{K}_h)}.$$

Moreover, combining Lemma 2.5 and Lemma 2.4 we get the following result for polynomial functions:

Lemma 2.6 *For each $\widetilde{K}_h \in \widetilde{\mathcal{T}}_h$, it holds that*

$$\|\widetilde{w}\|^2_{L^2(\widetilde{e}_h)} \lesssim h^{-1} \|\widetilde{w}\|^2_{L^2(\widehat{K}_h)} \qquad \forall v_h \in \widetilde{S}_{hk},$$

with $\widetilde{e}_h \subseteq \partial \widetilde{K}_h$.

Finally, we prove the following trace inequality:

Lemma 2.7 *For sufficiently small h, we have that*

$$\|\nabla_{\Gamma_h^k} \widehat{w}_h\|^2_{L^2(\partial \widehat{K}_h)} \lesssim h^{-1} \|\nabla_{\Gamma_h^k} \widehat{w}_h\|^2_{L^2(\widehat{K}_h)} \qquad \forall \widehat{w}_h \in \widehat{S}_{hk}.$$

Proof. Defining $\delta_{\widetilde{e}_h} = \mathrm{ds}/\,\mathrm{ds_{h1}}$ and $\delta_{\widetilde{e}_h \to \widehat{e}_h} = \mathrm{ds_{hk}}/\,\mathrm{ds_{h1}}$, using (2.18e) and a Taylor expansion argument, we obtain

$$|1 - \delta_{\widetilde{e}_h \to \widehat{e}_h}| = \left| 1 - \frac{\delta_{\widetilde{e}_h}}{\delta_{\widehat{e}_h}} \right| = \left| 1 - \frac{1 + O(h^2)}{1 + O(h^{k+1})} \right| \lesssim h^2.$$

Now let $\widetilde{w}_h \in \widetilde{S}_{hk}$ be such that $\widetilde{w}_h = \widehat{w}_h \circ \pi_k$. From (2.21) and (2.22) in [28] we have that

$$\left|\nabla_{\Gamma_h^k} \widehat{w}_h(\pi_k(\tilde{x}))\right| \lesssim |\nabla_{\Gamma_h} \widetilde{w}_h(\tilde{x})| \tag{2.36}$$

for each $\tilde{x} \in \Gamma_h$, provided h is sufficiently small. Applying Lemma 2.6 we get

$$\int_{\partial \widetilde{K}_h} |\nabla_{\Gamma_h} \widetilde{w}_h|^2 \, \mathrm{ds_{h1}} \lesssim \frac{1}{h} \|\nabla_{\Gamma_h} \widetilde{w}_h\|^2_{L^2(\widetilde{K}_h)}.$$

Surface lifting the left-hand side to Γ_h^k, making use of (2.36) and using (2.35b) for the right-hand side we have that

$$\int_{\partial \widehat{K}_h} |\nabla_{\Gamma_h^k} \widehat{w}_h|^2 \delta^{-1}_{\widetilde{e}_h \to \widehat{e}_h} \, \mathrm{ds_{hk}} \lesssim \frac{1}{h} \|\nabla_{\Gamma_h^k} \widehat{w}_h\|^2_{L^2(\widehat{K}_h)}.$$

We thus obtain, using (2.18e),

$$(1 - Ch^2) \|\nabla_{\Gamma_h^k} \widehat{w}_h\|^2_{L^2(\partial \widehat{K}_h)} \lesssim \frac{1}{h} \|\nabla_{\Gamma_h^k} \widehat{w}_h\|^2_{L^2(\widehat{K}_h)},$$

which yields the desired result for h small enough. ∎

In order to perform a unified analysis of the surface DG methods presented in Section 2.2.2, we introduce the stabilisation function

$$S_h(u_h, v_h) = \begin{cases} \displaystyle\sum_{\widehat{e}_h \in \widehat{\mathcal{E}}_h} \beta_{\widehat{e}_h} \int_{\widehat{e}_h} [u_h][v_h] \, \mathrm{ds_{hk}}, & \text{(2.37a)} \\ \displaystyle\sum_{\widehat{e}_h \in \widehat{\mathcal{E}}_h} \eta_{\widehat{e}_h} \int_{\Gamma_h^k} r_{\widehat{e}_h}([u_h]) \cdot r_{\widehat{e}_h}([v_h]) \, \mathrm{dA_{hk}}, & \text{(2.37b)} \end{cases}$$

for $u_h,\ v_h \in \widehat{S}_{hk}$, cf. also Table 2.1.

Method	Stabilisation function $S_h(\cdot,\cdot)$
IP [30] NIPG [63] IIPG [25] LDG [23]	(2.37a)
Brezzi et al. [18] Bassi et al. [11]	(2.37b)

Table 2.1: Stabilisation function of the DG methods considered in our unified analysis.

The next result, together with Lax-Milgram, guarantees that there exists a unique solution $u_h \in \widehat{S}_{hk}$ of (2.10) that satisfies the stability estimate

$$\|u_h\|_{\mathrm{DG}} \lesssim \|f_h\|_{L^2(\Gamma_h^k)}, \tag{2.38}$$

where the DG norm $\|\cdot\|_{\mathrm{DG}}$ is given by

$$\|u_h\|_{\mathrm{DG}}^2 = \|u_h\|_{1,h}^2 + |u_h|_{*,h}^2 \quad \forall u_h \in \widehat{S}_{hk}, \tag{2.39}$$

with

$$\|u_h\|_{1,h}^2 = \sum_{\widehat{K}_h \in \widehat{\mathcal{T}}_h} \|u_h\|_{H^1(\widehat{K}_h)}^2,$$

and

$$|u_h|_{*,h}^2 = S_h(u_h, u_h),$$

where $S_h(\cdot,\cdot)$ depends on the method under investigation and is defined as in (2.37a)-(2.37b).

We will now consider boundedness and stability of the bilinear forms $\mathcal{A}_h^k(\cdot,\cdot)$ corresponding to the surface DG methods given in Table 2.1. We first state some estimates required for the analysis of the surface LDG method.

Lemma 2.8 *For any $v_h \in \widehat{S}_{hk}$,*

$$\alpha \|r_{\widehat{e}_h}([v_h])\|_{L^2(\Gamma_h^k)}^2 \lesssim \beta_{\widehat{e}_h} \|[v_h]\|_{L^2(\widehat{e}_h)}^2,$$
$$\alpha \|l_{\widehat{e}_h}([v_h])\|_{L^2(\Gamma_h^k)}^2 \lesssim \beta_{\widehat{e}_h} \|[v_h]\|_{L^2(\widehat{e}_h)}^2,$$

on each $\widehat{e}_h \in \widehat{\mathcal{E}}_h$.

Proof. The thesis straighforwally follows using the same arguements as in [4, Lemma 2.3] and recalling that here the average and jumps operators appearing in the definition of the local lifting operators are defined in a slightly different way than [4, Lemma 2.3]. ∎

Lemma 2.9 *The bilinear forms $\mathcal{A}_h^k(\cdot,\cdot)$ corresponding to the surface DG methods given in Table 2.1 are continuous and coercive in the DG norm* (2.39)*, i.e.,*

$$\mathcal{A}_h^k(u_h, v_h) \lesssim \|u_h\|_{DG} \|v_h\|_{DG}, \quad \mathcal{A}_h^k(u_h, u_h) \gtrsim \|u_h\|_{DG}^2,$$

for every $u_h, v_h \in \widehat{S}_{hk}$. For the surface IP, Bassi et al. and IIPG methods, coercivity holds provided the penalty parameter α appearing in the definition of $\beta_{\widehat{e}_h}$ or $\eta_{\widehat{e}_h}$ in (2.11) is chosen sufficiently large.

Proof. For all the methods stabilized with $S_h(\cdot,\cdot)$ defined as in (2.37a), Lemma 2.7 implies that

$$\begin{aligned}\sum_{\widehat{e}_h\in\widehat{\mathcal{E}}_h}\int_{\widehat{e}_h}[u_h]\{\nabla_{\Gamma_h^k}v_h;n_h\}\,\mathrm{ds_{hk}} &\leq \sum_{\widehat{e}_h\in\widehat{\mathcal{E}}_h}\left\|\beta_{\widehat{e}_h}^{1/2}[u_h]\right\|_{L^2(\widehat{e}_h)}\left\|\beta_{\widehat{e}_h}^{-1/2}\{\nabla_{\Gamma_h^k}v_h;n_h\}\right\|_{L^2(\widehat{e}_h)}\\ &\lesssim \sum_{\widehat{K}_h\in\widehat{\mathcal{T}}_h}\alpha^{-\frac{1}{2}}|u_h|_{*,h}\|\nabla_{\Gamma_h^k}v_h\|_{L^2(\widehat{K}_h)}\\ &\lesssim \alpha^{-\frac{1}{2}}|u_h|_{*,h}\|v_h\|_{1,h},\end{aligned}\tag{2.40}$$

where the hidden constant depends on the degree of the polynomial approximation but not on the penalty parameters $\beta_{\widehat{e}_h}$. Otherwise, if $S_h(\cdot,\cdot)$ is given as in (2.37b), we observe that for $u_h, v_h \in \widehat{S}_{hk}$ we have that

$$\sum_{\widehat{e}_h\in\widehat{\mathcal{E}}_h}\int_{\widehat{e}_h}[u_h]\{\nabla_{\Gamma_h^k}v_h;n_h\}\,\mathrm{ds_{hk}} = \sum_{\widehat{K}_h\in\widehat{\mathcal{T}}_h}\int_{\widehat{K}_h} r_h([u_h])\cdot\nabla_{\Gamma_h^k}v_h\,\mathrm{dA_{hk}}$$

and, making use of the fact that $r_{\widehat{e}_h}$ only has support on $\widehat{K}_h^+\bigcup\widehat{K}_h^-$ where $\partial\widehat{K}_h^+\bigcap\partial\widehat{K}_h^- = \widehat{e}_h$,

$$\|r_h(\phi)\|^2_{L^2(\widehat{K}_h)} = \|\sum_{\widehat{e}_h\subset\partial\widehat{K}_h} r_{\widehat{e}_h}(\phi)\|^2_{L^2(\widehat{K}_h)} \lesssim \sum_{\widehat{e}_h\subset\partial\widehat{K}_h}\|r_{\widehat{e}_h}(\phi)\|^2_{L^2(\widehat{K}_h)},\tag{2.41}$$

where the last step follows recalling that the support of $r_{\widehat{e}_h}(\cdot)$ is limited to the two neighboring elements sharing the edge $\widehat{e}_h$. Hence, applying Cauchy-Schwarz, we obtain

$$\sum_{\widehat{K}_h\in\widehat{\mathcal{T}}_h}\|\eta_{\widehat{e}_h}^{1/2}r_h([u_h])\|_{L^2(\widehat{K}_h)}\|\eta_{\widehat{e}_h}^{-1/2}\nabla_{\Gamma_h^k}v_h\|_{L^2(\widehat{K}_h)} \lesssim \alpha^{-\frac{1}{2}}|u_h|_{*,h}\|v_h\|_{1,h},\tag{2.42}$$

where the hidden constant depends on the degree of the polynomial approximation but not on the penalty parameters $\eta_{\widehat{e}_h}$. For the surface LDG method, using Lemma 2.8, Lemma 2.7 and the $L^\infty(\Gamma_h^k)$ bound on θ, we obtain

$$\left|\int_{\widehat{e}_h}[\nabla_{\Gamma_h^k}u_h;n_h]\theta\cdot n_h^+[v_h]\,\mathrm{ds_{hk}}\right| \lesssim \alpha^{-\frac{1}{2}}\|\beta\|_{L^\infty(\Gamma_h^k)}\|\nabla_{\Gamma_h^k}u_h\|_{L^2(\widehat{K}_h)}|v_h|_{*,h},$$

$$\left|\int_{\widehat{K}_h} r_h([u_h])\cdot l_h(\theta\cdot n_h^+[u_h])\,\mathrm{ds_{hk}}\right| \lesssim \alpha^{-1}\|\beta\|_{L^\infty(\Gamma_h^k)}|u_h|_{*,h}|v_h|_{*,h},$$

and, in a similar way, the remaining quantities. Continuity then follows from Cauchy-Schwarz and the above estimates. We next show coercivity of the DG bilinear forms. For the surface NIPG method, stability follows straightforwardly

from the Cauchy-Schwarz inequality. For the surface LDG method, we have that

$$\begin{aligned}\mathcal{A}_h^k(u_h,u_h) \geq &\|u_h\|_{1,h}^2 - 2\sum_{\widehat{e}_h\in\widehat{\mathcal{E}}_h^k}\int_{\widehat{e}_h}\left|[u_h]\{\nabla_{\Gamma_h^k}u_h;n_h\}\right|\ \mathrm{ds_{hk}}\\ &- 2\|\beta\|_{L^\infty(\Gamma_h^k)}\sum_{\widehat{e}_h\in\widehat{\mathcal{E}}_h^k}\int_{\widehat{e}_h}\left|[u_h][\nabla_{\Gamma_h^k}u_h;n_h]\right|\ \mathrm{ds_{hk}} + |u_h|_{*,h}^2.\end{aligned}$$

For the other methods involving $S_h(\cdot,\cdot)$ defined as in (2.37a) we obtain

$$\mathcal{A}_h^k(u_h,u_h) \geq \|u_h\|_{1,h}^2 - 2\sum_{\widehat{e}_h\in\widehat{\mathcal{E}}_h^k}\int_{\widehat{e}_h}\left|[u_h]\{\nabla_{\Gamma_h^k}u_h;n_h\}\right|\ \mathrm{ds_{hk}} + |u_h|_{*,h}^2,$$

otherwise, if $S_h(\cdot,\cdot)$ is given as in (2.37b), we have that

$$\mathcal{A}_h^k(u_h,u_h) \geq \|u_h\|_{1,h}^2 - 2\sum_{\widehat{K}_h\in\widehat{\mathcal{T}}_h^k}\int_{\widehat{K}_h}\left|r_h([u_h])\cdot\nabla_{\Gamma_h^k}u_h\right|\ \mathrm{dA_{hk}} + |u_h|_{*,h}^2.$$

The result follows by making use of the corresponding boundedness estimates, using using Cauchy-Schwarz inequality and Young's inequalities and choosing the penalty parameter α sufficiently large. ■

We now define the DG norm for functions in $\widehat{S}_{hk}^\ell$ as follows:

$$\|u_h^\ell\|_{\mathrm{DG},\ell}^2 = \|u_h^\ell\|_{1,h}^2 + |u_h^\ell|_{*,h}^2 \quad \forall u_h^\ell \in \widehat{S}_{hk}^\ell, \tag{2.43}$$

with

$$\|u_h^\ell\|_{1,h}^2 = \sum_{\widehat{K}_h^\ell\in\widehat{\mathcal{T}}_h^\ell}\|u_h^\ell\|_{H^1(\widehat{K}_h^\ell)}^2,$$

and

$$|u_h^\ell|_{*,h}^2 = S_h^\ell(u_h^\ell,u_h^\ell),$$

where $S_h^\ell(\cdot,\cdot)$ is given by

$$S_h^\ell(u_h^\ell,v_h^\ell) = \begin{cases}\displaystyle\sum_{\widehat{e}_h^\ell\in\widehat{\mathcal{E}}_h^\ell}\beta_{\widehat{e}_h}\int_{\widehat{e}_h^\ell}\delta_{\widehat{e}_h}^{-1}[u_h^\ell][v_h^\ell]\ \mathrm{ds}, & \text{(2.44a)}\\ \displaystyle\sum_{\widehat{e}_h^\ell\in\widehat{\mathcal{E}}_h^\ell}\eta_{\widehat{e}_h}\int_\Gamma\delta_h^{-1}\big(r_{\widehat{e}_h}([u_h])\big)^\ell\cdot\big(r_{\widehat{e}_h}([v_h])\big)^\ell\ \mathrm{dA}, & \text{(2.44b)}\end{cases}$$

for $u_h^\ell,\ v_h^\ell \in \widehat{S}_{hk}^\ell$.

Lemma 2.10 *Let $u_h \in \widehat{S}_{hk}$ satisfy (2.38). Then $u_h^\ell \in \widehat{S}_{hk}^\ell$ satisfies*

$$\|u_h^\ell\|_{DG,\ell} \lesssim \|f\|_{L^2(\Gamma)}, \tag{2.45}$$

for h small enough.

Proof. We first show that for any function $v_h \in \widehat{S}_{hk}$, for sufficiently small h,

$$\|v_h^\ell\|_{\mathrm{DG},\ell} \lesssim \|v_h\|_{\mathrm{DG}}. \tag{2.46}$$

The $\|\cdot\|_{1,h}^2$ component of the DG norm is dealt with in exactly the same way as in [28]. For the $|\cdot|_{*,h}^2$ component of the DG norm we have that

$$\int_{\widehat{e}_h} [v_h]^2 \,\mathrm{ds_{hk}} = \int_{\widehat{e}_h^\ell} \delta_{\widehat{e}_h}^{-1} [v_h^\ell]^2 \,\mathrm{ds} \quad \text{and} \quad \int_{\Gamma_h^k} |r_h([v_h])|^2 \,\mathrm{dA_{hk}} = \int_\Gamma \delta_h^{-1} |r_h([v_h])^\ell|^2 \,\mathrm{dA},$$

which straightforwardly yields (2.46). Making use of the discrete stability estimate (2.38) and noting that, by Lemma 2.8, $\|f_h\|_{L^2(\Gamma_h^k)} \lesssim \|f_h^\ell\|_{L^2(\Gamma)} = \|f\|_{L^2(\Gamma)}$, we get the desired result. ∎

For each of the surface DG bilinear forms given in Table 2.1, we define a corresponding bilinear form on Γ induced by the surface lifted triangulation $\widehat{\mathcal{T}}_h^\ell$ which is well defined for functions $w, v \in H^2(\Gamma) + \widehat{S}_{hk}^\ell$. For the surface IP bilinear form (2.14), we define

$$\begin{aligned}\mathcal{A}(w,v) = &\sum_{\widehat{K}_h^\ell \in \widehat{\mathcal{T}}_h^\ell} \int_{\widehat{K}_h^\ell} \nabla_\Gamma w \cdot \nabla_\Gamma v + wv \,\mathrm{dA} - \sum_{\widehat{e}_h^\ell \in \widehat{\mathcal{E}}_h^\ell} \int_{\widehat{e}_h^\ell} [w]\{\nabla_\Gamma v; n\} + [v]\{\nabla_\Gamma w; n\} \,\mathrm{ds} \\ &+ \sum_{\widehat{e}_h^\ell \in \widehat{\mathcal{E}}_h^\ell} \int_{\widehat{e}_h^\ell} \delta_{\widehat{e}_h}^{-1} \beta_{\widehat{e}_h} [w][v] \,\mathrm{ds}, \end{aligned} \tag{2.47}$$

where n^+ and n^- are respectively the unit surface conormals to $\widehat{K}_h^{\ell+}$ and $\widehat{K}_h^{\ell-}$ on $\widehat{e}_h^\ell \in \widehat{\mathcal{E}}_h^\ell$. For the Brezzi et al. bilinear form (2.13), we define

$$\begin{aligned}\mathcal{A}(w,v) = &\sum_{\widehat{K}_h^\ell \in \widehat{\mathcal{T}}_h^\ell} \int_{\widehat{K}_h^\ell} \nabla_\Gamma w \cdot \nabla_\Gamma v + wv \,\mathrm{dA} \\ &+ \sum_{\widehat{K}_h^\ell \in \widehat{\mathcal{T}}_h^\ell} \int_{\widehat{K}_h^\ell} \delta_h^{-1} \eta_{\widehat{e}_h} r_{\widehat{e}_h}([w^{-\ell}])^\ell \cdot r_{\widehat{e}_h}([v^{-\ell}])^\ell + \delta_h^{-1} \big(r_h([w^{-\ell}])\big)^\ell \cdot \big(r_h([v^{-\ell}])\big)^\ell \,\mathrm{dA} \\ &- \sum_{\widehat{e}_h^\ell \in \widehat{\mathcal{E}}_h^\ell} \int_{\widehat{e}_h^\ell} [w]\{\nabla_\Gamma v; n\} + [v]\{\nabla_\Gamma w; n\} \; - \delta_{\widehat{e}_h}^{-1} \beta_{\widehat{e}_h} [w][v] \,\mathrm{ds}. \end{aligned} \tag{2.48}$$

For the surface LDG bilinear form (2.15), we define

$$\begin{aligned}\mathcal{A}(w,v) = &\sum_{\widehat{K}_h^\ell \in \widehat{\mathcal{T}}_h^\ell} \int_{\widehat{K}_h^\ell} \nabla_\Gamma w \cdot \nabla_\Gamma v + wv \ \mathrm{dA} - \sum_{\widehat{e}_h^\ell \in \widehat{\mathcal{E}}_h^\ell} \int_{\widehat{e}_h^\ell} [w]\{\nabla_\Gamma v; n\} - \{\nabla_\Gamma w; n\}[v] \ \mathrm{ds} \\ &+ \sum_{\widehat{e}_h^\ell \in \widehat{\mathcal{E}}_h^\ell} \int_{\widehat{e}_h^\ell} \Big(- \delta_{\widehat{e}_h}^{-1} [\nabla_\Gamma w; n] \theta \cdot n_h^{\ell+}[v] - \delta_{\widehat{e}_h}^{-1} \theta \cdot n_h^{\ell+}[w][\nabla_\Gamma v; n] + \delta_{\widehat{e}_h}^{-1} \beta_{\widehat{e}_h}[w][v] \Big) \ \mathrm{ds} \\ &+ \sum_{\widehat{K}_h^\ell \in \widehat{\mathcal{T}}_h^\ell} \int_{\widehat{K}_h^\ell} \delta_h^{-1} \Big(r_h([w^{-\ell}]) + \theta \cdot n_h^{\ell+} l_h\big([w^{-\ell}]\big) \Big)^\ell \cdot \Big(r_h([v^{-\ell}]) + \theta \cdot n_h^{\ell+} l_h\big([v^{-\ell}]\big) \Big)^\ell \ \mathrm{dA}.\end{aligned} \tag{2.49}$$

The corresponding bilinear forms for the other surface DG methods can be derived in a similar manner. Since we assume that the weak solution u of (2.3) belongs to $H^2(\Gamma)$ they all satisfy

$$\mathcal{A}(u,v) = \sum_{\widehat{K}_h^\ell \in \widehat{\mathcal{T}_h}^\ell} \int_{\widehat{K}_h^\ell} fv \ \mathrm{dA}, \qquad \forall v \in H^2(\Gamma) + \widehat{S}_{hk}^\ell. \tag{2.50}$$

Finally, we require the following stability estimate for $\mathcal{A}(\cdot,\cdot)$, which follows by applying similar arguments as those found in the proof of Lemma 2.9.

Lemma 2.11 *The bilinear forms $\mathcal{A}(\cdot,\cdot)$ induced by the surface DG methods given in Table 2.1 are coercive in the DG norm* (2.43)*, i.e.,*

$$\|w_h^\ell\|_{DG,\ell}^2 \lesssim \mathcal{A}(w_h^\ell, w_h^\ell) \tag{2.51}$$

for all $w_h^\ell \in \widehat{S}_{hk}^\ell$ if, for the surface IP, Bassi et al. and IIPG methods, the penalty parameter α appearing in the definition of $\beta_{\widehat{e}_h}$ or $\eta_{\widehat{e}_h}$ in (2.11) is chosen sufficiently large.

2.4 Convergence

We now state the main result of this chapter.

Theorem 2.1 *Let $u \in H^{k+1}(\Gamma)$ and $u_h \in \widehat{S}_{hk}$ denote the solutions to (2.3) and (2.9), respectively. Let $\eta = 0$ for IIPG, NIPG formulations and let $\eta = 1$ otherwise. Then,*

$$\|u - u_h^\ell\|_{L^2(\Gamma)} + h^\eta \|u - u_h^\ell\|_{DG,\ell} \lesssim h^{k+\eta} (\|f\|_{L^2(\Gamma)} + \|u\|_{H^{k+1}(\Gamma)}),$$

provided the mesh size h is small enough and the penalty parameter α is large enough for the surface IP, Bassi et al. and IIPG methods. Here the hidden constant depends, in particular, on the signed-distance function d and its first/second derivatives.

In order to prove Theorem 2.1 we collect some useful technical results. For $\widehat{w} \in H^2(\Gamma_h^k)$, we define the interpolant $\widehat{I}_h^k : C^0(\Gamma_h^k) \to \widehat{S}_{hk}$ by

$$\widehat{I}_h^k \widehat{w} = \widetilde{I}_h^k(\widehat{w} \circ \pi_k),$$

where $\widetilde{I}_h^k : C^0(\Gamma_h) \to \widetilde{S}_{hk}$ is the standard Lagrange interpolant of degree k. We also define the interpolant $I_h^k : C^0(\Gamma) \to \widehat{S}_{hk}^\ell$ by

$$I_h^k w = \widehat{I}_h^k(w \circ \pi).$$

Lemma 2.12 *Let $w \in H^m(\Gamma)$ with $2 \le m \le k+1$. Then for $i = 0, 1$,*

$$|w - I_h^k w|_{H^i(\widehat{K}_h^\ell)} \lesssim h^{m-i} \|w\|_{H^m(\widehat{K}_h^\ell)}.$$

Proof. The proof follows easily by combining standard estimates for the Lagrange interpolant on Γ_h with Lemma 2.3. See [28] for further details. ∎

Lemma 2.13 *Let $w \in H^m(\Gamma)$ with $2 \le m \le k+1$. Then, for sufficiently small h, we have that*

$$\|w - I_h^k w\|^2_{L^2(\partial \widehat{K}_h^\ell)} + h^2 \|\nabla_\Gamma (w - I_h^k w)\|^2_{L^2(\partial \widehat{K}_h^\ell)} \lesssim h^{2m-1} \|w\|^2_{H^m(\widehat{K}_h^\ell)}.$$

Proof. Fix an arbitrary element $\widehat{K}_h^\ell \in \widehat{\mathcal{T}}_h^\ell$. We then define $\widehat{w} \in H^m(\widehat{K}_h)$ and $\widetilde{w} \in H^m(\widetilde{K}_h)$ such that $w = \widehat{w} \circ \pi$ and $\widetilde{w} = \widehat{w} \circ \pi_k$.

Using Lemma 2.5 on $\widetilde{K}_h \in \widetilde{\mathcal{T}}_h$ we get

$$\int_{\partial \widetilde{K}_h} |\nabla_{\Gamma_h}(\widetilde{w} - \widetilde{I}_h^k \widetilde{w})|^2 \, \mathrm{ds_{h1}} \lesssim \left(\frac{1}{h} \int_{\widetilde{K}_h} |\nabla_{\Gamma_h}(\widetilde{w} - \widetilde{I}_h^k \widetilde{w})|^2 \, \mathrm{dA_{h1}} + h \int_{\widetilde{K}_h} |\nabla^2_{\Gamma_h}(\widetilde{w} - \widetilde{I}_h^k \widetilde{w})|^2 \, \mathrm{dA_{h1}} \right).$$

Applying a classical interpolation result for the right-hand side (see, for example, Theorem 6.4 in [16]), we obtain

$$\int_{\partial \widetilde{K}_h} |\nabla_{\Gamma_h}(\widetilde{w} - \widetilde{I}_h^k \widetilde{w})|^2 \, \mathrm{ds_{h1}} \lesssim h^{2m-3} |\widetilde{w}|^2_{H^m(\widetilde{K}_h)}.$$

Then, lifting the left-hand side on Γ_h^k as in Lemma 2.7 and using (2.35b) with (2.35d) we have

$$(1 - Ch^2) \int_{\partial \widehat{K}_h} |\nabla_{\Gamma_h^k}(\widehat{w} - \widehat{I}_h^k \widehat{w})|^2 \, \mathrm{ds_{hk}} \lesssim h^{2m-3} \|\widehat{w}\|^2_{H^m(\widehat{K}_h)}.$$

In the same way, we lift the left-hand side onto Γ and use (2.35b) with (2.35d):

$$(1 - Ch^{k+1})(1 - Ch^2) \|\nabla_\Gamma (w - I_h^k w)\|^2_{L^2(\partial \widehat{K}_h^\ell)} \lesssim h^{2m-3} \|w\|^2_{H^m(\widehat{K}_h^\ell)}.$$

Similarly, using again Lemma 2.5 for $\widetilde{w} - \widetilde{I}_h^k \widetilde{w}$, we obtain

$$\int_{\partial \widetilde{K}_h} |\widetilde{w} - \widetilde{I}_h^k \widetilde{w}|^2 \, \mathrm{ds_{h1}} \lesssim \left(\frac{1}{h} \int_{\widetilde{K}_h} |\widetilde{w} - \widetilde{I}_h^k \widetilde{w}|^2 \, \mathrm{dA_{h1}} + h \int_{\widetilde{K}_h} |\nabla_{\Gamma_h} (\widetilde{w} - \widetilde{I}_h^k \widetilde{w})|^2 \, \mathrm{dA_{h1}} \right).$$

Then, using interpolation estimates on $\widetilde{K}_h$ we get

$$\int_{\partial \widetilde{K}_h} |\widetilde{w} - \widetilde{I}_h^k \widetilde{w}|^2 \, \mathrm{ds_{h1}} \lesssim h^{2m-1} |\widetilde{w}|^2_{H^m(\widetilde{K}_h)}.$$

Finally, doing as before the lifting of the left-hand side on Γ_h^k and then on Γ and using (2.35a) with (2.35b), we get the claim for h small enough. ∎

These interpolation estimates allow us to derive the following boundedness estimates for $\mathcal{A}(\cdot, \cdot)$:

Lemma 2.14 *Let $u \in H^m(\Gamma)$ and $w \in H^n(\Gamma)$ with $2 \leq m, n \leq k+1$. Then, for all $v_h^\ell \in \widehat{S}_{hk}^\ell$, we have that*

$$\mathcal{A}(u - I_h^k u, v_h^\ell) \lesssim h^{m-1} \|u\|_{H^m(\Gamma)} \|v_h^\ell\|_{DG,\ell}, \tag{2.52}$$

$$\mathcal{A}(u - I_h^k u, w - I_h^k w) \lesssim h^{m+n-2} \|u\|_{H^m(\Gamma)} \|w\|_{H^n(\Gamma)}. \tag{2.53}$$

Proof. Since $u \in H^m(\Gamma) \subset C^0(\Gamma)$ for $m \geq 2$ and $I_h^k u \in C^0(\Gamma)$, by the continuity of the *inverse* surface lift operator, we have $[(u - I_h^k u)^{-\ell}] = 0$ on each $\widehat{e}_h \in \widehat{\mathcal{E}}_h$. Then, by definition of $r_{\widehat{e}_h}$ and $l_{\widehat{e}_h}$, we obtain

$$\|r_{\widehat{e}_h}([(u - I_h^k u)^{-\ell}])\|^2_{L^2(\Gamma_h^k)} = \|l_{\widehat{e}_h}([(u - I_h^k u)^{-\ell}])\|^2_{L^2(\Gamma_h^k)} = 0.$$

Following the proof of Lemma 2.9, it is easy to obtain (2.52) and (2.53) from Lemma 2.12 and Lemma 2.13. ∎

For the first term on the right-hand side of (2.57), we require the following *perturbed* Galerkin orthogonality result:

Lemma 2.15 *Let $u \in H^s(\Gamma)$, $s \geq 2$, and $u_h \in \widehat{S}_{hk}$ denote the solutions to (2.3) and (2.9), respectively. We define the functional E_h on $\widehat{S}_{hk}^\ell$ by*

$$E_h(v_h^\ell) = \mathcal{A}(u - u_h^\ell, v_h^\ell).$$

Then, for all considered surface DG methods apart from LDG, E_h can be written as

$$\begin{aligned} E_h(v_h^\ell) = & \sum_{\widehat{K}_h^\ell \in \widehat{\mathcal{T}}_h^\ell} \int_{\widehat{K}_h^\ell} (R_h - P) \nabla_\Gamma u_h^\ell \cdot \nabla_\Gamma v_h^\ell + \left(\delta_h^{-1} - 1\right) u_h^\ell v_h^\ell + \left(1 - \delta_h^{-1}\right) f v_h^\ell \, dA \\ & + \sum_{\widehat{e}_h^\ell \in \widehat{\mathcal{E}}_h^\ell} \int_{\widehat{e}_h^\ell} [u_h^\ell] \left(\{\nabla_\Gamma v_h^\ell; n\} - \{\delta_{\widehat{e}_h}^{-1} P_h (I - dH) P \nabla_\Gamma v_h^\ell; n_h^\ell\} \right) \, ds \\ & + \zeta \sum_{\widehat{e}_h^\ell \in \widehat{\mathcal{E}}_h^\ell} \int_{\widehat{e}_h^\ell} [v_h^\ell] \left(\{\nabla_\Gamma u_h^\ell; n\} - \{\delta_{\widehat{e}_h}^{-1} P_h (I - dH) P \nabla_\Gamma u_h^\ell; n_h^\ell\} \right) \, ds \end{aligned} \tag{2.54}$$

where R_h is given as in Lemma 2.2 and

$$\zeta = \begin{cases} -1 & \textit{in NIPG and Baumann-Oden cases,} \\ 0 & \textit{in IIPG case,} \\ 1 & \textit{otherwise.} \end{cases}$$

The functional corresponding to the surface LDG method can be written as

$$\begin{aligned} E_h(v_h^\ell) =& (2.54) + \sum_{\widehat{e}_h^\ell \in \widehat{\mathcal{E}}_h^\ell} \int_{\widehat{e}_h^\ell} \delta_{\widehat{e}_h}^{-1} \theta \cdot n_h^{\ell+} [v_h^\ell] \left([\nabla_\Gamma u_h^\ell; n] - [P_h(I - dH) P \nabla_\Gamma u_h^\ell; n_h^\ell] \right) \, ds \\ &+ \sum_{\widehat{e}_h^\ell \in \widehat{\mathcal{E}}_h^\ell} \int_{\widehat{e}_h^\ell} \delta_{\widehat{e}_h}^{-1} \theta \cdot n_h^{\ell+} [u_h^\ell] \left([\nabla_\Gamma v_h^\ell; n] - [P_h(I - dH) P \nabla_\Gamma v_h^\ell; n_h^\ell] \right) \, ds. \end{aligned} \tag{2.55}$$

Furthermore, for all surface DG methods it holds

$$|E_h(v_h^\ell)| \lesssim h^{k+1} \|f\|_{L^2(\Gamma)} \|v_h^\ell\|_{DG,\ell}. \tag{2.56}$$

Proof. The proof is similar to that of Lemma 4.2 in [27] which considered a piecewise linear approximation of the surface. The expression for the error functional E_h is obtained by first noting that the solution u of (2.3) satisfies (2.50) and then considering the difference between (2.50) and (2.9):

$$\begin{aligned} \mathcal{A}(u, v_h^\ell) - \mathcal{A}_h^k(u_h, v_h) &= \sum_{\widehat{K}_h^\ell \in \widehat{\mathcal{T}_h}^\ell} \int_{\widehat{K}_h^\ell} f v_h^\ell \, \mathrm{dA} - \sum_{\widehat{K}_h \in \widehat{\mathcal{T}}_h} \int_{\widehat{K}_h} f_h v_h \, \mathrm{dA_{hk}} \\ &= \sum_{\widehat{K}_h^\ell \in \widehat{\mathcal{T}_h}^\ell} \int_{\widehat{K}_h^\ell} (1 - \delta_h^{-1}) f v_h^\ell \, \mathrm{dA}. \end{aligned}$$

By lifting $\mathcal{A}_h^k(u_h, v_h)$ onto Γ in a similar fashion to what has been done in (2.17) and using the definition of $\mathcal{A}(\cdot, \cdot)$ we get, after algebraic manipulations, relation (2.54). The estimate (2.56) is then obtained by making use of the geometric estimates in Lemma 2.2. In particular, following the proof of Lemma 4.2 in [27], we preliminary get

$$\begin{aligned} |E_h(v_h^\ell)| \lesssim & \|R_h - P\|_{L^\infty(\Gamma)} \|u_h^\ell\|_{\mathrm{DG},\ell} \|v_h^\ell\|_{\mathrm{DG},\ell} + \|\frac{1}{\delta_h} - 1\|_{L^\infty(\Gamma)} \|u_h^\ell\|_{\mathrm{DG},\ell} \|v_h^\ell\|_{\mathrm{DG},\ell} \\ &+ \|1 - \frac{1}{\delta_h}\|_{L^\infty(\Gamma)} \|f\|_{L^2(\Gamma)} \|v_h^\ell\|_{\mathrm{DG},\ell} + \max_{\widehat{e}_h^\ell \in \widehat{\mathcal{E}}_h^\ell} \|n - P n_h^\ell\|_{L^\infty(\widehat{e}_h^\ell)} \|u_h^\ell\|_{\mathrm{DG},\ell} \|v_h^\ell\|_{\mathrm{DG},\ell} \\ &+ \|d\|_{L^\infty(\Gamma)} \|u_h^\ell\|_{\mathrm{DG},\ell} \|v_h^\ell\|_{\mathrm{DG},\ell}. \end{aligned}$$

Then Lemma 2.2 and the stability estimate (2.45) yields the claimed bound. ∎

Remark 2.4 *Note that the error functional E_h in Lemma 2.15 includes all of the terms present in the high order surface FEM setting (see [28]) as well as additional terms arising from the surface DG methods.*

Proof of Theorem 2.1. The proof will follow an argument similar to the one outlined in [7]. Using the stability result (2.51), we have that

$$\|\phi_h^\ell - u_h^\ell\|_{\mathrm{DG},\ell}^2 \lesssim \mathcal{A}(\phi_h^\ell - u_h^\ell, \phi_h^\ell - u_h^\ell) = \mathcal{A}(u - u_h^\ell, \phi_h^\ell - u_h^\ell) + \mathcal{A}(\phi_h^\ell - u, \phi_h^\ell - u_h^\ell), \tag{2.57}$$

where $\phi_h^\ell \in \widehat{S}_{hk}^\ell$. Choosing the continuous interpolant $\phi_h^\ell = I_h^k u$, using the error functional estimate (2.56) and the boundedness estimate (2.52), the right-hand side of (2.57) can be bounded by

$$\begin{aligned}\|I_h^k u - u_h^\ell\|_{\mathrm{DG},\ell}^2 &\lesssim E_h(I_h^k u - u_h^\ell) + \mathcal{A}(I_h^k u - u, I_h^k u - u_h^\ell)\\ &\lesssim h^{k+1}\|f\|_{L^2(\Gamma)}\|I_h^k u - u_h^\ell\|_{\mathrm{DG},\ell} + h^k\|u\|_{H^{k+1}(\Gamma)}\|I_h^k u - u_h^\ell\|_{\mathrm{DG},\ell},\end{aligned}$$

which implies

$$\|I_h^k u - u_h^\ell\|_{\mathrm{DG},\ell} \lesssim h^k(\|f\|_{L^2(\Gamma)} + \|u\|_{H^{k+1}(\Gamma)}).$$

Recalling that $u - I_h^k u \in C^0(\Gamma)$, using Lemma 2.12 we obtain

$$\|u - u_h^\ell\|_{\mathrm{DG},\ell} \le \|u - I_h^k u\|_{\mathrm{DG},\ell} + \|I_h^k u - u_h^\ell\|_{\mathrm{DG},\ell} \lesssim h^k(\|f\|_{L^2(\Gamma)} + \|u\|_{H^{k+1}(\Gamma)}).$$

This concludes the first part of the proof. In the case of $\eta = 1$, to derive the L^2 estimate, we first observe that the solution $z \in H^2(\Gamma)$ to the dual problem

$$-\Delta_\Gamma z + z = u - u_h^\ell \tag{2.58}$$

satisfies

$$\|z\|_{H^2(\Gamma)} \lesssim \|u - u_h^\ell\|_{L^2(\Gamma)}. \tag{2.59}$$

Then, using the symmetry of the bilinear form $\mathcal{A}(\cdot,\cdot)$, we have that

$$\begin{aligned}\|u - u_h^\ell\|_{L^2(\Gamma)}^2 &= (u - u_h^\ell, u - u_h^\ell)_\Gamma = \mathcal{A}(z, u - u_h^\ell)\\ &= \mathcal{A}(u - u_h^\ell, z) = \mathcal{A}(u - u_h^\ell, z - I_h^k z) + E_h(I_h^k z).\end{aligned} \tag{2.60}$$

Using (2.56), a triangle inequality and the interpolation estimate in Lemma 2.12, we obtain

$$|E_h(I_h^k z)| \lesssim h^{k+1}\|f\|_{L^2(\Gamma)}\|I_h^k z\|_{H^1(\Gamma)} \lesssim h^{k+1}\|f\|_{L^2(\Gamma)}\|z\|_{H^2(\Gamma)}.$$

Hence, using (2.59),

$$|E_h(I_h^k z)| \lesssim h^{k+1}\|f\|_{L^2(\Gamma)}\|u - u_h^\ell\|_{L^2(\Gamma)}$$

Making use of the continuity of $I_h^k z - z$ and $I_h^k u - u$, the symmetry of the bilinear form $\mathcal{A}(\cdot,\cdot)$, Lemma 2.14 and the stability estimate (2.59) we get

$$\begin{aligned}
\mathcal{A}(u-u_h^\ell, z-I_h^k z) &= \mathcal{A}(z-I_h^k z, u-u_h^\ell) \\
&\lesssim \mathcal{A}(z-I_h^k z, I_h^k u-u_h^\ell) + \mathcal{A}(z-I_h^k z, u-I_h^k u) \\
&\lesssim h\|z\|_{H^2(\Gamma)}\|I_h^k u-u_h^\ell\|_{\mathrm{DG},\ell} + h^{k+1}\|z\|_{H^2(\Gamma)}\|u\|_{H^{k+1}(\Gamma)} \\
&\lesssim h\|z\|_{H^2(\Gamma)}(\|I_h^k u-u\|_{\mathrm{DG},\ell} + \|u-u_h^\ell\|_{\mathrm{DG},\ell} + h^{k+1}\|z\|_{H^2(\Gamma)}\|u\|_{H^{k+1}(\Gamma)} \\
&\lesssim (h^{k+1}\|u\|_{H^{k+1}(\Gamma)} + h\|u-u_h^\ell\|_{\mathrm{DG},\ell})\|u-u_h^\ell\|_{L^2(\Gamma)}.
\end{aligned}$$

Combining these estimates with (2.60) yields

$$\|u-u_h^\ell\|_{L^2(\Gamma)}^2 \lesssim \left(h\|u-u_h^\ell\|_{\mathrm{DG},\ell} + h^{k+1}(\|f\|_{L^2(\Gamma)} + \|u\|_{H^{k+1}(\Gamma)})\right)\|u-u_h^\ell\|_{L^2(\Gamma)},$$

which gives us the desired L^2 estimate and concludes the proof. In the case of $\eta = 0$, we can trivially obtain the (sub-optimal) bound for the error in the L^2 norm from bounding it by the error in the DG norm. ■

2.5 Numerical experiments

We show results for the IP method, cf. Section 2.2.2.3, implemented using DUNE-FEM, a discretization module based on the Distributed and Unified Numerics Environment (DUNE), [12, 26]. For the initial mesh generation we use the Computational Geometry Algorithms Library (CGAL) (see [61]). We consider the following test problem

$$-\Delta_\Gamma u + u = f, \tag{2.61}$$

on the unit sphere $\Gamma = \{x \in \mathbb{R}^3 \ : \ \|x\|_{l^2} = 1\}$, choosing f so that the exact solution is $u(x_1,x_2,x_3) = \cos(2\pi x_1)\cos(2\pi x_2)\cos(2\pi x_3)$. Figure 2.3 shows the DG approximate solutions obtained with $k = 1$ and $k = 4$ DG approximation orders. In Table 2.2 we report the computed errors measured in the DG norm (2.43) as well as the computed converge factors for *linear* ($k = 1$), *quadratic* ($k = 2$), and *quartic* ($k = 4$) DG/surface approximation orders. The same results obtained measuring the error in the L^2 norm are shown in Table 2.3. The numerical results validate the theoretical estimates of Theorem 2.1.

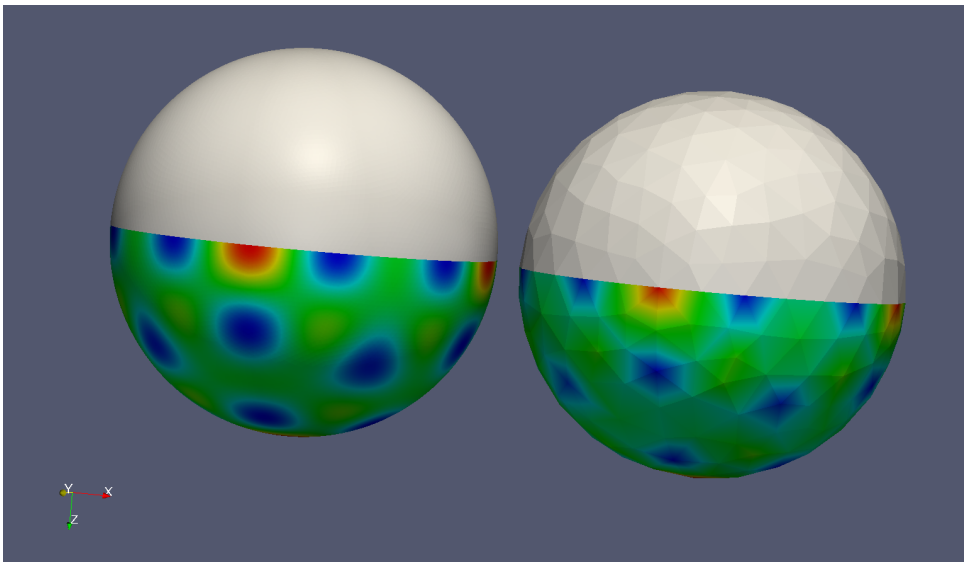

Figure 2.3: Paraview plots of the linear (right) and quartic (left) DG approximations of (2.61) on a mesh consisting of 623 elements.

N. elements	h	$k=1$		$k=2$		$k=4$	
632	0.220	5.0766		1.4205		4.7121e-2	
2528	0.110	2.6427	0.94	3.8696e-1	1.88	3.2585e-3	3.85
10112	0.056	1.3151	1.01	9.8648e-2	1.97	2.0765e-4	3.97
40448	0.028	6.5361e-1	1.01	2.4795e-2	1.99	1.3051e-5	4.00
161792	0.014	3.2596e-1	1.00	6.2087e-3	2.00	-	-
647168	0.007	1.6282e-1	1.00	-	-	-	-

Table 2.2: Computed errors measured in the DG norm (2.43) and computed convergence factors for the DG approximation of (2.61) with *linear* ($k=1$), quadratic ($k=2$), and *quartic* ($k=4$) approximation orders.

N. elements	h	$k=1$		$k=2$		$k=4$	
632	0.220	1.7146e-1		3.6978e-2		7.7900e-4	
2528	0.110	5.2882e-2	1.70	4.9040e-3	2.91	2.6808e-5	4.86
10112	0.056	1.4605e-2	1.86	6.1000e-4	3.00	8.4834e-7	4.98
40448	0.028	3.7830e-3	1.95	7.5856e-5	3.01	2.6582e-8	5.00
161792	0.014	9.5800e-4	1.98	9.4598e-6	3.00	-	-
647168	0.007	2.4100e-4	1.99	-	-	-	-

Table 2.3: Computed errors measured in the L^2 norm and computed convergence factors for the DG approximation of (2.61) with *linear* ($k=1$), quadratic ($k=2$), and *quartic* ($k=4$) approximation orders.

3

Discontinuous Galerkin approximation of parabolic problems with dynamic boundary conditions

In this chapter we present and analyze a DG approximation in SIPG framework of a parabolic problem with dynamic boundary conditions. To carry out the analysis we preliminary consider a suitable stationary problem with generalized Robin boundary conditions (see [48]). Several numerical experiments assess the validity of the theoretical analysis. The results presented in this chapter are contained in [3].

3.1 Basic notation

In this section we introduce some notation and the functional setting. Let $D \subset \mathbb{R}^2$ be an open, bounded, polygonal domain with boundary $\Gamma = \partial D$. On D we define the standard Sobolev space $H^s(D)$, $s \geq 0$, equipped with the usual inner scalar product $(\cdot,\cdot)_{H^s(D)}$, the usual seminorm $|\cdot|_{H^s(D)}$ and the norm $\|\cdot\|_{H^s(D)}$, cf. [1]. For $s = 0$ we will write $L^2(D)$ in lieu of $H^0(D)$. We next introduce on Γ the Laplace-Beltrami operator and the Sobolev surface spaces. We introduce the projection matrix $\mathbf{P} = \mathbf{I} - \mathbf{n} \otimes \mathbf{n} = (\delta_{ij} - n_i n_j)_{i,j=1}^2$, where $\mathbf{n}$ is the outward unit normal to D, and $\mathbf{a} \otimes \mathbf{b} = (a_i b_j)_{ij}$ is the dyadic product, and δ_{ij} is the Kroneker delta. We define the tangential gradient of a (regular enough) scalar function $u : \Gamma \to \mathbb{R}$ as $\nabla_\Gamma u = \mathbf{P}\nabla u$. The tangential divergence of a vector-valued function $\mathbf{A} : \Gamma \to \mathbb{R}^2$ is defined as $\mathrm{div}_\Gamma(\mathbf{A}) = \mathrm{Tr}\big((\nabla \mathbf{A})\mathbf{P}\big)$, where $\mathrm{Tr}(\cdot)$ is the trace operator. With the above notation, we define the Laplace-Beltrami operator as $\Delta_\Gamma u = \mathrm{div}_\Gamma(\nabla_\Gamma u)$. We next introduce the following Sobolev surface space, cf. [31]:

$$H^s(\Gamma) = \{v \in H^{s-1}(\Gamma) \ : \ \nabla_\Gamma v \in [H^{s-1}(\Gamma)]^2\}, \qquad s \geq 1,$$

with the convention that $H^0(\Gamma) \equiv L^2(\Gamma)$, $L^2(\Gamma)$ being the standard Sobolev space of square integrable functions (equipped with the usual inner scalar product $(\cdot,\cdot)_\Gamma$ and the usual induced norm $\|\cdot\|_{L^2(\Gamma)}$). We endow the space $H^s(\Gamma)$ with the following surface seminorm

$$|v|^2_{H^s(\Gamma)} = \|\nabla_\Gamma v\|^2_{H^{s-1}(\Gamma)} \qquad \forall v \in H^s(\Gamma),\ s \geq 1,$$

and the following norm

$$\|v\|_{H^s(\Gamma)} = \sqrt{\|v\|^2_{H^{s-1}(\Gamma)} + |v|^2_{H^s(\Gamma)}} \qquad \forall v \in H^s(\Gamma),\ s \geq 1.$$

In [48, Lemma 2.4] is proved that the above norm is equivalent to the usual surface norm present in literature [53], which is defined in local coordinates after a truncation by a partition of unity.

For a positive constant λ, we next introduce the space

$$H^s_\lambda(\Omega,\Gamma) = \{v \in H^s(D) : \lambda v_{|\Gamma} \in H^s(D)\}, \qquad s \geq 1,$$

and endow it with the norm

$$\|u\|_{H^s_\lambda(\Omega,D)} = \left(\|u\|^2_{H^s(D)} + \lambda\|u_{|\Gamma}\|^2_{H^s(D)}\right)^{1/2}.$$

We also set

$$L^2_\lambda(D,\Gamma) = \{v \in L^2(D) : \lambda v_{|\Gamma} \in L^2(\Gamma)\},$$

equipped with the norm

$$\|u\|_{L^2_\lambda(D,\Gamma)} = \sqrt{\|u\|^2_{L^2(D)} + \lambda\|u_{|\Gamma}\|^2_{L^2(\Gamma)}}.$$

To ease the notation, when $\lambda = 1$, we will omit the subscript.

3.2 The stationary problem

Let $\Omega = (a,b)\times(c,d) \subset \mathbb{R}^2$ be a rectangular domain and let Γ_1, Γ_2 be the union of the top and bottom/left and right edges, respectively. We consider the following Laplace problem with generalized Robin boundary conditions:

$$\begin{cases} -\Delta u &= f, & \text{in } \Omega, \\ \partial_n u &= -\alpha u + \beta\Delta_\Gamma u + g, & \text{on } \Gamma_1, \\ \text{periodic boundary conditions}, & & \text{on } \Gamma_2, \end{cases} \tag{3.1}$$

where α, β are positive constants, and $f \in L^2(\Omega)$, $g \in L^2(\Gamma_1)$ are given functions.

Defining the bilinear form $a(u,v) : H^1(\Omega,\Gamma_1)\times H^1(\Omega,\Gamma_1) \to \mathbb{R}$ as

$$a(u,v) = (\nabla u, \nabla v)_{L^2(\Omega)} + \beta(\nabla_\Gamma u, \nabla_\Gamma v)_{L^2(\Gamma_1)} + \alpha(u,v)_{L^2(\Gamma_1)},$$

the weak formulation of (3.1) reads: find $u \in H^1(\Omega, \Gamma_1)$ such that

$$a(u, v) = (f, v)_{L^2(\Omega)} + (g, v)_{L^2(\Gamma_1)} \qquad \forall v \in H^1(\Omega, \Gamma_1). \tag{3.2}$$

The following result shows that formulation (3.2) is well posed.

Theorem 3.1 *Problem (3.2) admits a unique solution $u \in H^2(\Omega, \Gamma_1)$ satisfying the following stability bound:*

$$\|u\|_{H^2(\Omega,\Gamma_1)} \lesssim \|f\|_{L^2(\Omega)} + \|g\|_{L^2(\Gamma_1)}. \tag{3.3}$$

Moreover, if $f \in H^{s-2}(\Omega)$ and $g \in H^{s-2}(\Gamma_1)$, $s \geq 2$, then $u \in H^s(\Omega, \Gamma_1)$ and

$$\|u\|_{H^s(\Omega,\Gamma_1)} \lesssim \|f\|_{H^{s-2}(\Omega)} + \|g\|_{H^{s-2}(\Gamma_1)}. \tag{3.4}$$

Proof. The existence and uniqueness of the solution are proved in [48, Theorem 3.2]. The proof of the regularity results is shown in [48, Theorem 3.3-3.4]. The same arguments used in [48, Theorem 3.3-3.4] apply also in our case thanks to periodic conditions. ■

Remark 3.1 *We observe that the forthcoming analysis holds in more general-shaped domains and/or more general type of boundary conditions provided that the exact solution of the differential problem analogous to (3.2) satisfies a stability bound of the form of (3.3).*

3.2.1 Discontinuous Galerkin space discretization

In this Section we present a discontinuous Galerkin (DG) approximation of problem (3.2).
Let $\mathcal{T}_h$ be a quasi-uniform partition of Ω into disjoint open triangles K such that $\overline{\Omega} = \cup_{K \in \mathcal{T}_h} \overline{T}$. We set $h = \max\{\text{diam}(K),\ K \in \mathcal{T}_h\}$. For $s \geq 0$, we define the following broken space

$$H^s(\mathcal{T}_h) = \{v \in L^2(\Omega) : v_{|K} \in H^s(K, \partial K),\ K \in \mathcal{T}_h\},$$

where, as before, $H^0(\mathcal{T}_h) = L^2(\mathcal{T}_h)$. For an integer $p \geq 1$, we also define the finite dimensional space

$$V_h^p = \{v \in L^2(\Omega) : v_{|K} \in \mathbb{P}^p(K),\ K \in \mathcal{T}_h\} \subset H^s(\mathcal{T}_h),$$

for any $s \geq 0$. An interior edge e is defined as the non-empty intersection of the closure of two neighboring elements, i.e., $\overline{e} = \overline{K_1} \cap \overline{K_2}$, for $K_1, K_2 \in \mathcal{T}_h$. We collect all the interior edges in the set $\mathcal{E}_h^0$. Recalling that on $\Gamma_2 \subset \partial\Omega$ we impose periodic boundary conditions, we decompose Γ_2 as $\Gamma_2 = \Gamma_2^+ \cup \Gamma_2^-$, cf. Figure 3.1 (left), and identify Γ_2^+ with Γ_2^-, cf. Figure 3.1 (right). Then we define the set $\mathcal{E}_h^{\Gamma_2}$ of the

periodic boundary edges as follows. An edge $e \in \mathcal{E}_h^{\Gamma_2}$ if $\overline{e} = \partial\overline{K}^- \cap \partial\overline{K}^+$, where $K^\pm \in \mathcal{T}_h$ such that $\partial K^\pm \subseteq \Gamma_2^\pm$, cf. Figure 3.1 (right). We also define a boundary edge e_{Γ_1} as the non-empty intersection between the closure of an element in $\mathcal{T}_h$ and Γ_1 and the set of those edges by $\mathcal{E}_h^{\Gamma_1}$. Finally, we define a boundary ridge r as the subset of the mesh vertexes that lie on Γ_1, and collect all the ridges r in the set $\mathcal{R}_h^{\Gamma_1}$. Clearly, the corner ridges have to be identified according to the periodic boundary conditions (cf. Figure 3.1, right). The set of all edge will be denoted by $\mathcal{E}_h$, i.e., $\mathcal{E}_h = \mathcal{E}_h^0 \cup \mathcal{E}_h^{\Gamma_1} \cup \mathcal{E}_h^{\Gamma_2}$.

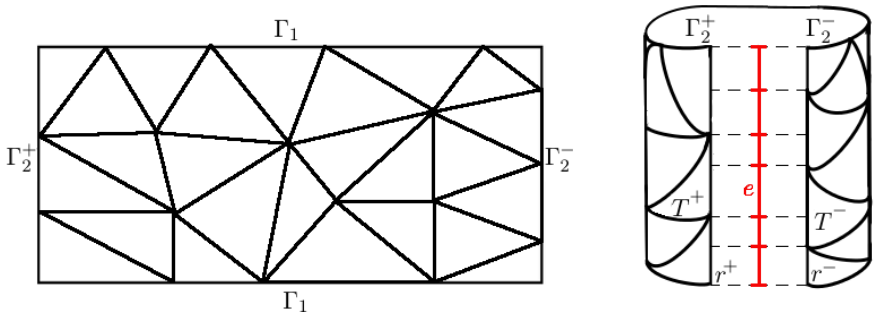

Figure 3.1: Example of a domain Ω and an admissible triangulation $\mathcal{T}_h$ (left). On the right, we highlight the edges $e \in \mathcal{E}_h^{\Gamma_2}$ with red lines.

For $v \in H^s(\mathcal{T}_h)$, $s \geq 1$, we define

$$|v|^2_{H^s(\mathcal{T}_h)} = \sum_{K\in\mathcal{T}_h} |v|^2_{H^s(K)}\,, \qquad |v|^2_{H^s(\mathcal{E}_h^{\Gamma_1})} = \sum_{e_{\Gamma_1}\in\mathcal{E}_h^{\Gamma_1}} |v|^2_{H^s(e_{\Gamma_1})}\,.$$

Next, for each $e \in \mathcal{E}_h^0 \cup \mathcal{E}_h^{\Gamma_2}$ we define the jumps and the averages of $v \in H^1(\mathcal{T}_h)$ as

$$[v]_e = (v^+)\mathbf{n}_e^+ + (v^-)\mathbf{n}_e^- \qquad \text{and} \qquad \{v\}_e = \frac{1}{2}(v^+ + v^-),$$

where $v^\pm = v_{|K^\pm}$ and $\mathbf{n}_e^\pm$ is the unit normal vector to e pointing outward of $K^\pm$. For each $e \in \mathcal{E}_h^{\Gamma_1}$ we define

$$[v]_e = v_{|e}\ \mathbf{n}_e, \qquad \{v\}_e = v_{|e}, \qquad v \in H^1(\mathcal{T}_h).$$

Analogously, for each $r \in \mathcal{R}_h^{\Gamma_1}$ and $v \in H^1(\mathcal{T}_h)$, we set

$$[v]_r = (v^+(r))\mathbf{n}_r^+ + (v^-(r))\mathbf{n}_r^- \qquad \text{and} \qquad \{v\}_r = \frac{1}{2}(v^+(r) + v^-(r)),$$

where, denoting by $e^\pm$ the two edges sharing the ridge r, $v^\pm(r) = v_{|e^\pm}(r)$ and $\mathbf{n}_r^\pm$ is the unit tangent vector to Γ_1 on r pointing outward of $e^\pm$. The above definitions can be immediately extended to a (regular enough) vector-valued function, cf. [7]. To simplify the notation, when the meaning will be clear from the context,

we remove the subscripts from the jump and average operators. Adopting the convention that

$$(v,w)_{\mathcal{E}_h} = \sum_{e\in\mathcal{E}_h}(v,w)_{L^2(e)}, \qquad (\xi,\eta)_{\mathcal{R}_h^{\Gamma_1}} = \sum_{r\in\mathcal{R}_h^{\Gamma_1}} \xi(r)\eta(r)$$

for regular enough functions v, w, ξ, η, we introduce the following bilinear forms

$$\begin{aligned}\mathcal{B}_h(v,w) = \sum_{K\in\mathcal{T}_h}(\nabla v,\nabla w)_K - ([v],\{\nabla w\})_{\mathcal{E}_h^0} - ([w],\{\nabla v\})_{\mathcal{E}_h^0} + \sigma([v],[w])_{\mathcal{E}_h^0} \\ - ([v],\{\nabla w\})_{\mathcal{E}_h^{\Gamma_2}} - ([w],\{\nabla v\})_{\mathcal{E}_h^{\Gamma_2}} + \sigma([v],[w])_{\mathcal{E}_h^{\Gamma_2}}\end{aligned}$$

and

$$b_h(v,w) = (\nabla_\Gamma v,\nabla_\Gamma w)_{\mathcal{E}_h^{\Gamma_1}} - ([v],\{\nabla_\Gamma w\})_{\mathcal{R}_h^{\Gamma_1}} - ([w],\{\nabla_\Gamma v\})_{\mathcal{R}_h^{\Gamma_1}} + \sigma([v],[w])_{\mathcal{R}_h^{\Gamma_1}},$$

for all $v, w \in H^2(\mathcal{T}_h)$. Here $\sigma = \frac{\mu}{h}$, μ being a positive constant at our disposal. We then set

$$\mathcal{A}_h(u,v) = \mathcal{B}_h(u,v) + \alpha\ (u,v)_{L^2(\Gamma_1)} + \beta\ b_h(u,v). \tag{3.5}$$

The discontinuous Galerkin approximation of problem (3.1) reads: find $u_h \in V_h^p$ such that

$$\mathcal{A}_h(u_h,v_h) = (f,v_h)_{L^2(\Omega)} + (g,v_h)_{L^2(\Gamma_1)} \qquad \forall v_h \in V_h^p. \tag{3.6}$$

In the following we show that the bilinear form $\mathcal{A}_h(\cdot,\cdot)$ is continuous and coercive in a suitable (mesh-dependent) energy norm. To this aim, for $w \in H^s(\mathcal{T}_h)$, we define the seminorm

$$|||w|||_{\mathcal{B}_h}^2 = |w|_{H^1(\mathcal{T}_h)}^2 + \sigma\|[w]\|_{L^2(\mathcal{E}_h^0\cup\mathcal{E}_h^{\Gamma_2})}^2 + \frac{1}{\sigma}\|\{\nabla w\}\|_{L^2(\mathcal{E}_h^0\cup\mathcal{E}_h^{\Gamma_2})}^2$$

and the norm

$$\begin{aligned}|||w|||_*^2 = |||w|||_{\mathcal{B}_h}^2 + \alpha\|w\|_{L^2(\Gamma_1)}^2 \\ + \beta\,|w|_{H^1(\mathcal{E}_h^{\Gamma_1})}^2 + \beta\sigma\|[w]\|_{L^2(\mathcal{R}_h^{\Gamma_1})}^2 + \frac{\beta}{\sigma}\|\{\nabla_\Gamma w\}\|_{L^2(\mathcal{R}_h^{\Gamma_1})}^2,\end{aligned} \tag{3.7}$$

where we adopted the notation

$$\|w\|_{L^2(\mathcal{E}_h)}^2 = \sum_{e\in\mathcal{E}_h}\|w\|_{L^2(e)}^2, \qquad \|w\|_{L^2(\mathcal{R}_h^{\Gamma_1})}^2 = \sum_{e\in\mathcal{R}_h^{\Gamma_1}}\|w\|_{L^2(r)}^2.$$

Reasoning as in [6], it is easy to prove the following result.

Lemma 3.1 *It holds*

$$\mathcal{A}_h(v,w) \lesssim |||v|||_* |||w|||_* \qquad \forall v,w \in H^2(\mathcal{T}_h). \tag{3.8}$$

Moreover, for μ large enough, it holds

$$|||v|||_*^2 \lesssim \mathcal{A}_h(v,v) \qquad \forall v \in V_h^p. \tag{3.9}$$

Proof. Let us first prove (3.8). The term $\mathcal{B}_h(\cdot,\cdot)$ can be bounded by Cauchy-Schwarz inequality as in [6]. Also the term $b_h(\cdot,\cdot)$ can be handled using the Cauchy-Schwarz inequality:

$$\begin{aligned}
|b_h(v,w)| = \Big| &(\nabla_\Gamma v, \nabla_\Gamma w)_{\mathcal{E}_h^{\Gamma_1}} - ([v], \{\nabla_\Gamma w\})_{\mathcal{R}_h^{\Gamma_1}} \\
&\qquad -([w], \{\nabla_\Gamma v\})_{\mathcal{R}_h^{\Gamma_1}} + \sigma([v],[w])_{\mathcal{R}_h^{\Gamma_1}} \Big| \\
\lesssim \Big(&|v|^2_{H^1(\mathcal{E}_h^{\Gamma_1})} + \sigma \|[v]\|^2_{L^2(\mathcal{R}_h^{\Gamma_1})} + \frac{1}{\sigma}\|\{\nabla_\Gamma v\}\|^2_{L^2(\mathcal{R}_h^{\Gamma_1})} \Big)^{1/2} \times \\
&\Big(|w|^2_{H^1(\mathcal{E}_h^{\Gamma_1})} + \sigma \|[w]\|^2_{L^2(\mathcal{R}_h^{\Gamma_1})} + \frac{1}{\sigma}\|\{\nabla_\Gamma w\}\|^2_{L^2(\mathcal{R}_h^{\Gamma_1})} \Big)^{1/2},
\end{aligned}$$

and (3.8) follows employing the definition (3.7) of the norm $|||\cdot|||_*$.
We now prove (3.9). As before the term $\mathcal{B}_h(\cdot,\cdot)$ can be bounded as in [6]: using the classical polynomial inverse inequality [22] we obtain

$$|||v|||^2_{\mathcal{B}_h} \lesssim |v|^2_{H^1(\mathcal{T}_h)} + \sigma\|[v]\|^2_{L^2(\mathcal{E}_h^0 \cup \mathcal{E}_h^{\Gamma_2})} \lesssim \mathcal{B}_h(v,v)$$

for all $v \in V_h^p$. The term $b_h(\cdot,\cdot)$ can be estimated as follows:

$$b_h(v,v) \geq |v|^2_{H^1(\mathcal{E}_h^{\Gamma_1})} - 2\Big|([v], \{\nabla_\Gamma v\})_{\mathcal{R}_h^{\Gamma_1}}\Big| + \sigma\|[v]\|^2_{L^2(\mathcal{R}_h^{\Gamma_1})}.$$

Employing the arithmetic-geometric inequality we get:

$$\begin{aligned}
\Big|([v], \{\nabla_\Gamma v\})_{\mathcal{R}_h^{\Gamma_1}}\Big| &\leq \|\sigma^{1/2}[v]\|_{L^2(\mathcal{R}_h^{\Gamma_1})} \|\{\sigma^{-1/2}\nabla_\Gamma v\}\|_{L^2(\mathcal{R}_h^{\Gamma_1})} \\
&\leq \frac{1}{\epsilon}\sigma\|[v]\|^2_{L^2(\mathcal{R}_h^{\Gamma_1})} + 4\epsilon\sigma^{-1}\|\{\nabla_\Gamma v\}\|^2_{L^2(\mathcal{R}_h^{\Gamma_1})},
\end{aligned}$$

for a positive $\epsilon > 0$. Finally, estimate (3.9) follows using the polynomial inverse inequality

$$h\|\{\nabla_\Gamma v\}\|^2_{L^2(\mathcal{R}_h^{\Gamma_1})} \lesssim |v|^2_{H^1(\mathcal{E}_h^{\Gamma_1})} \qquad \forall v \in V_h^p$$

and choosing μ sufficiently large. ■

The following result shows that problem (3.6) admits a unique solution and that the Galerkin orthogonality property is satisfied. The proof is straightforward and we omit it for sake of brevity.

Lemma 3.2 *Assume that μ is sufficiently large. Then, the discrete solution u_h of problem (3.6) exists and is unique. Moreover, formulation (3.6) is strongly consistent, i.e.,*

$$\mathcal{A}_h(u - u_h, v) = 0 \qquad \forall v \in V_h^p. \tag{3.10}$$

For $v \in H^s(\Omega, \Gamma_1)$, $s \geq 2$, let $I_p^h v$ be the piecewise Lagrangian interpolant of order p of u on $\mathcal{T}_h$. Note that $(I_p^h u)_{|\Gamma_1}$ interpolates u on the set of degrees of freedom that lie on $\mathcal{E}_h^{\Gamma_1}$. By standard approximation results we get the following interpolation estimate.

Lemma 3.3 *For all $v \in H^s(\Omega, \Gamma_1)$, $s \geq 2$, it holds*

$$|||v - I_p^h v|||_* \lesssim h^{\min(s-1,p)} \|v\|_{H^s(\Omega,\Gamma_1)}.$$

Proof. Using the definition (3.7) of $|||\cdot|||_*$ norm and that $I_p^h v(r) = v(r)$ for all $r \in \mathcal{R}_h^{\Gamma_1}$, we get

$$|||v - I_p^h v|||_*^2 = |||v - I_p^h v|||_{\mathcal{B}_h}^2 + \alpha \|v - I_p^h v\|_{L^2(\Gamma_1)}^2 + \beta \left|v - I_p^h v\right|_{H^1(\mathcal{E}_h^{\Gamma_1})}^2. \tag{3.11}$$

Expanding the first term at right-hand side and using the multiplicative trace inequalities

$$\begin{aligned} \|v\|_{L^2(\mathcal{E}_h)}^2 &\lesssim h^{-1} \|v\|_{L^2(\Omega)}^2 + h \, |v|_{H^1(\Omega)}^2, \\ \|\nabla v\|_{L^2(\mathcal{E}_h)}^2 &\lesssim h^{-1} \, |v|_{H^1(\Omega)}^2 + h \, |v|_{H^2(\Omega)}^2, \end{aligned}$$

cf. [62], we get

$$\begin{aligned} |||v - I_p^h v|||_{\mathcal{B}_h}^2 &= \left|v - I_p^h v\right|_{H^1(\Omega)}^2 + \sigma \|[v - I_p^h v]\|_{L^2(\mathcal{E}_h^0 \cup \mathcal{E}_h^{\Gamma_2})}^2 \\ &\qquad + \frac{1}{\sigma} \|\{\nabla(v - I_p^h v)\}\|_{L^2(\mathcal{E}_h^0 \cup \mathcal{E}_h^{\Gamma_2})}^2 \\ &\lesssim h^{-2} \|v - I_p^h v\|_{L^2(\Omega)}^2 + \left|v - I_p^h v\right|_{H^1(\Omega)}^2 + h^2 \left|v - I_p^h v\right|_{H^2(\Omega)}^2. \end{aligned}$$

Using standard interpolation estimates [59] we get the thesis. ■

Now we show that the discrete solution u_h of (3.6) converges to the weak solution of (3.2).

Theorem 3.2 *Let $u \in H^s(\Omega, \Gamma_1)$, $s \geq 2$, be the solution of the problem (3.2) and let u_h be the solution of the problem (3.6). Then,*

$$\|u - u_h\|_{L^2(\Omega,\Gamma_1)} + h|||u - u_h|||_* \lesssim h^{\min(s,p+1)} \|u\|_{H^s(\Omega,\Gamma_1)},$$

provided μ is chosen sufficiently large.

Proof. By the triangular inequality we have

$$|||u-u_h|||_* \leq |||u-I_p^h u|||_* + |||I_p^h u - u_h|||_*.$$

We first bound the second term on the right-hand side. Combining the Galerkin orthogonality (3.10) with the continuity and the coercivity estimates (3.8)-(3.9), we obtain:

$$\begin{aligned} |||I_p^h u - u_h|||_*^2 &\lesssim \mathcal{A}_h(I_p^h u - u_h, I_p^h u - u_h) \\ &= \mathcal{A}_h(I_p^h u - u, I_p^h u - u_h) + \mathcal{A}_h(u - u_h, I_p^h u - u_h) \\ &\lesssim |||I_p^h u - u_h|||_* |||I_p^h u - u|||_*. \end{aligned}$$

Therefore,

$$|||I_p^h u - u_h|||_* \lesssim |||I_p^h u - u|||_*,$$

and

$$|||u - u_h|||_* \lesssim |||u - I_p^h u|||_*.$$

Then, using Lemma 3.3, we get

$$|||u-u_h|||_* \lesssim h^{\min(s-1,p)} \|u\|_{H^s(\Omega,\Gamma_1)}. \tag{3.12}$$

For the L^2 error estimate, we consider the following adjoint problem: find ζ such that

$$\begin{cases} -\Delta\zeta &= u - u_h, & \text{in } \Omega, \\ \partial_n \zeta &= -\alpha\zeta + \beta\Delta_\Gamma\zeta + (u-u_h), & \text{on } \Gamma_1, \end{cases}$$

As $u - u_h \in L^2(\Omega,\Gamma_1)$, using Theorem 3.1 yields an unique $\zeta \in H^2(\Omega,\Gamma_1)$ satisfiying the following stability estimate

$$\|\zeta\|_{H^2(\Omega,\Gamma_1)} \lesssim \|u-u_h\|_{L^2(\Omega,\Gamma_1)}.$$

Using Lemma 3.3 with $p=1$, we get

$$|||\zeta - I_1^h\zeta|||_* \lesssim h\|\zeta\|_{H^2(\Omega,\Gamma_1)} \lesssim h\|u-u_h\|_{L^2(\Omega,\Gamma_1)}. \tag{3.13}$$

Since $\mathcal{A}_h(\cdot,\cdot)$ defined in (3.5) is symmetric, it is easy to see that it holds

$$\mathcal{A}_h(\chi,\zeta) = (u-u_h,\chi)_{L^2(\Omega)} + (u-u_h,\chi)_{L^2(\Gamma_1)} \qquad \forall \chi \in H^2(\mathcal{T}_h). \tag{3.14}$$

Next, choosing $\chi = u - u_h$ in (3.14) and employing (3.10) together with (3.8), we find

$$\begin{aligned} \|u-u_h\|_{L^2(\Omega,\Gamma_1)}^2 &= \mathcal{A}_h(u-u_h,\zeta) \\ &= \mathcal{A}_h(u-u_h,\zeta - I_1^h\zeta) \\ &\lesssim |||u-u_h|||_* |||\zeta - I_1^h\zeta|||_*. \end{aligned}$$

The thesis follows using (3.12) and (3.13). ∎

3.3 The parabolic problem and its fully-discretization

In this section we employ the result obtained in the previous sections to present and analyze a a DG space semi-discretization combined with an backward Euler time advancing scheme for solving the following parabolic problem:

$$\begin{cases} \partial_t u & = \Delta u + f, & \text{in } \Omega,\ 0 < t \le T, \\ \partial_n u & = -\alpha u + \beta \Delta_\Gamma u - \lambda \partial_t u + g, & \text{on } \Gamma_1,\ 0 < t \le T, \\ \text{periodic boundary conditions}, & & \text{on } \Gamma_2,\ 0 < t \le T, \\ u_{|t=0} & = u_0, & \text{in } \overline{\Omega}, \end{cases} \tag{3.15}$$

where $T > 0$, α, β, λ are positive constants and f, g, u_0 are (regular enough) given data. The weak formulation of (3.15) reads: *For any $t \in (0, T]$, find u such that:*

$$\begin{cases} (\partial_t u, v)_{L^2(\Omega)} + \lambda (\partial_t u, v)_{L^2(\Gamma_1)} + a(u, v) = (f, v)_{L^2(\Omega)} + (g, v)_{L^2(\Gamma_1)}, \\ u_{|t=0} = u_0, \end{cases} \tag{3.16}$$

for any $v \in H^1(\Omega, \Gamma_1)$.

It is possible to prove the following result dealing with the existence and (higher) regularity of the weak solution of (3.15).

Theorem 3.3 *If $u_0 \in H^2(\Omega, \Gamma_1)$, $f \in H^1(0, T; L^2(\Omega))$ and $g \in H^1(0, T; L^2(\Gamma_1))$ and the following compatibility conditions holds*

1. $u_1 = \Delta u_0 + f(0, \cdot) \in L^2(\Omega)$,
2. $u_{1|\Gamma_1} = \beta \Delta_\Gamma u_0 - \partial_n u_0 - \alpha u_0 + g(0, \cdot) \in L^2(\Gamma_1)$,

then problem (3.15) admits a unique solution u with

$$u \in C([0, T]; H^2(\Omega, \Gamma_1)) \cap C^1([0, T]; L^2_\lambda(\Omega, \Gamma_1)) \cap H^1(0, T; H^1_\lambda(\Omega, \Gamma_1)).$$

Moreover, if $u_0 \in H^{2m}_\lambda(\Omega; \Gamma_1)$, $\frac{d^k f}{dt^k} \in H^1(0, T; H^{2m-2k-2}(\Omega))$ and $\frac{d^k g}{dt^k} \in H^1(0, T; H^{2m-2k-2}(\Gamma_1))$, for $k = 0, \dots, m-1$, and the following higher order compatibility conditions hold for $k = 1, \dots, m$

3. $u_1^{(k)} = \Delta u_1^{(k-1)} + \frac{d^{k-1}}{dt^{k-1}} f(0, \cdot) \in L^2(\Omega)$
4. $u_{1|\Gamma_1}^{(k)} = \beta \Delta_\Gamma u_{1|\Gamma_1}^{(k-1)} - \partial_n u_1^{(k-1)} - \alpha u_{1|\Gamma_1}^{(k-1)} + \frac{d^{k-1}}{dt^{k-1}} g(0, \cdot) \in L^2(\Gamma_1)$,

where we set $u_1^{(0)} = u_1$ and $u_{1|\Gamma_1}^{(0)} = u_{1|\Gamma_1}$, it holds for $k = 0, \dots, m-1$

$$\begin{aligned} \frac{d^k u}{dt^k} \ \in \ & C([0, T]; H^{2m-2k}(\Omega, \Gamma_1)) \cap C^1(0, T; H^{2m-2k-2}_\lambda(\Omega, \Gamma_1)) \\ & \cap H^1(0, T; H^{2m-2k-1}_\lambda(\Omega, \Gamma_1)). \end{aligned} \tag{3.17}$$

Proof. As the proof follows standard steps (see, e.g., [36, Chapter 7.1]), we only sketch the main steps of the argument.

1. *Construction of the discrete space.* Let $\{e_i\}_{i\geq 1}$ be an orthonormal basis of $L^2(\Omega)$ such that

$$\int_\Omega \nabla e_i \cdot \nabla z = \lambda_i \int_\Omega e_i z \qquad \forall z \in H^1(\Omega),\ i \geq 1,$$

i.e., λ_i and e_i are respectively the eigenvalues and eigenfunctions of the weak form of eigenvalue problem $-\Delta e = \lambda e$ with homogeneous Neumann and periodic boundary conditions on Γ_1 and Γ_2, respectively. Reordering $\{e_i\}_{i\geq 1}$ such that $\lambda_1 = 0$, it is easy to see that there holds

$$\int_\Omega \nabla e_i \cdot \nabla e_j = 0, \quad \text{for } i \neq j \qquad \text{and} \qquad \int_\Omega |\nabla e_i|^2 = \lambda_i > 0, \quad \text{for } i > 1.$$

Let $V^n = \text{span}\{e_i : i = 1, ..., n\}$, $n \geq 1$, and let u_0^n be the $L^2(\Omega)$- projection of u_0 on V^n. Since the domain is regular, the eigenfunctions e_i belong to $H^2(\Omega)$.

2. *Finite-dimensional approximation of (3.16).* We introduce the following finite dimensional problem: find $u^n \in H^1(0,T;V^n)$ such that, for $t \in (0,T)$,

$$\begin{cases} (\partial_t u^n, z)_{L^2(\Omega)} + \lambda(\partial_t u^n, z)_{L^2(\Gamma_1)} + a(u^n, z) = (f, z)_{L^2(\Omega)} + (g, z)_{L^2(\Gamma_1)}, \\ u^n{}_{|t=0} = u_0^n, \end{cases} \tag{3.18}$$

for all $z \in V^n$, In the sequel we prove that problem (3.18) admits a unique solution in $H^1(0,T;V^n)$. We write

$$u^n(t) = \sum_{j=1}^n u_j(t) e_j.$$

The problem (3.18) is equivalent to find $\mathbf{u}(t) = (u_1(t), ..., u_n(t))^T \in H^1(0,T;\mathbb{R}^n)$ such that, for each $t \in (0,T)$,

$$\begin{cases} M\dot{\mathbf{u}}(t) + A\mathbf{u}(t) = \mathbf{F}(t), \\ \mathbf{u}(0) = (u_{0,1}, ..., u_{0,n})^T, \end{cases}$$

where, for $i, j = 1, .., n$,

$$M_{ij} = M^\Omega + \lambda M^{\Gamma_1} = \delta_{ij} + \lambda(e_i, e_j)_{L^2(\Gamma_1)},$$

$$A_{ij} = a(e_i, e_j), \qquad F_i = (f, e_i)_{L^2(\Omega)} + (g, e_i)_{L^2(\Gamma_1)}, \qquad u_{0,i} = (u_0, e_i)_{L^2(\Omega)}.$$

Since the matrix M^{Γ_1} is semi-positive definite, we see that M is positive definite. In addition, $\mathbf{F}(t) \in L^2(0,T;\mathbb{R}^n)$ and $A : \mathbb{R}^n \to \mathbb{R}^n$ is Lipschitz continuous.

Therefore, by standard existence theory of ordinary differential equations, there exists a unique solution $\mathbf{u}(t)$ for a.e. $0 \leq t \leq T$.

3. *Energy estimates.* Taking $z = u^n$ in (3.18) and using Cauchy-Schwarz inequality, we obtain

$$\frac{d}{dt}\left(\|u^n\|^2_{L^2_\lambda(\Omega,\Gamma_1)}\right) + \|\nabla u^n\|^2_{L^2(\Omega)} + \alpha\|u^n\|^2_{L^2(\Gamma_1)} + \beta\|\nabla_\Gamma u^n\|^2_{L^2(\Gamma_1)} \lesssim \|u^n\|^2_{L^2_\lambda(\Omega,\Gamma_1)} + \|f\|^2_{L^2(\Omega)} + \|g\|^2_{L^2(\Gamma_1)} \quad (3.19)$$

for a.e. $t \in [0,T]$. Using the differential form of Gronwall's inequality, data regularity and Lemma 3.4 we obtain

$$\max_{0\leq t\leq T}\|u^n(t)\|_{L^2_\lambda(\Omega,\Gamma_1)} \lesssim \|u_0\|^2_{L^2_\lambda(\Omega,\Gamma_1)} + \|f\|^2_{L^2(0,T;L^2(\Omega))} + \|g\|^2_{L^2(0,T;L^2(\Gamma_1))} \leq C.$$

Integrating (3.19) in $[0,T]$ and employing the above inequality together with data regularity and Lemma 3.4 we get

$$\|u^n\|_{L^2(0,T;H^1_\lambda(\Omega,\Gamma_1))} \lesssim \|u_0\|^2_{L^2_\lambda(\Omega,\Gamma_1)} + \|f\|^2_{L^2(0,T;L^2(\Omega))} + \|g\|^2_{L^2(0,T;L^2(\Gamma_1))} \leq C.$$

On the other hand, taking $z = \partial_t u^n$ in (3.18), integrating in t and using Cauchy-Schwarz inequality, we obtain, for every $\tau \in (0,T]$,

$$\begin{aligned}\frac{1}{2}\int_0^\tau \|\partial_t u^n\|^2_{L^2_\lambda(\Omega,\Gamma_1)} + \frac{1}{2}\|\nabla u^n(\tau)\|^2_{L^2(\Omega)} + \frac{\alpha}{2}\|u^n(\tau)\|^2_{L^2(\Gamma_1)} + \frac{\beta}{2}\|\nabla_\Gamma u^n(\tau)\|^2_{L^2(\Gamma_1)} \\ \leq \frac{1}{2}\|\nabla u_0^n\|^2_{L^2(\Omega)} + \frac{\alpha}{2}\|u_0^n\|^2_{L^2(\Gamma_1)} + \frac{\beta}{2}\|\nabla_\Gamma u_0^n\|^2_{L^2(\Omega)} \\ + \frac{1}{2}\int_0^\tau \|f\|^2_{L^2(\Omega)} + \frac{1}{2\lambda}\int_0^\tau \|g\|^2_{L^2(\Gamma_1)},\end{aligned}$$

where the right-hand side of the above inequality can be bounded using Lemma 3.4 and data regularity.

Moreover, differentiating (3.18) with respect to t and setting $\tilde{u}^n = \partial_t u^n$ we get for any $t \in [0,T]$

$$(\partial_t \tilde{u}^n, z)_{L^2(\Omega)} + \lambda(\partial_t \tilde{u}^n, z)_{L^2(\Gamma_1)} + a(\tilde{u}^n, z) = (\partial_t f, z)_{L^2(\Omega)} + (\partial_t g, z)_{L^2(\Gamma_1)}, \quad (3.20)$$

for all $z \in V^n$. Testing (3.20) with $z = \tilde{u}^n$, it is easy to show that it holds

$$\begin{aligned}\|\partial_t u^n\|^2_{L^2_\lambda(\Omega,\Gamma_1)} + \int_0^t \|\partial_t u^n(s)\|^2_{H^1_\lambda(\Omega,\Gamma_1)}\,ds \lesssim \int_0^t \|\partial_t f(s)\|^2_{L^2(\Omega)}\,ds \\ + \int_0^t \|\partial_t g(s)\|^2_{L^2(\Gamma_1)}\,ds + \|\partial_t u^n(0)\|^2_{L^2_\lambda(\Omega,\Gamma_1)}. \quad (3.21)\end{aligned}$$

Taking $t = 0$ in (3.18), testing with $z = \partial_t u^n(0)$, integrating by parts and employing Cauchy-Schwarz inequality we obtain

$$\|\partial_t u^n(0)\|^2_{L^2_\lambda(\Omega,\Gamma_1)} \lesssim \|u^n(0)\|^2_{H^2_\lambda(\Omega,\Gamma_1)} + \|f(0,\cdot)\|^2_{L^2(\Omega)} + \|g(0,\cdot)\|^2_{L^2(\Gamma_1)},$$

whose right-hand side can be bounded by resorting to compatibility conditions, Lemma 3.4 and data regularity.

Hence, collecting all the above results, we get

$$u^n \in C([0,T]; H^1_\lambda(\Omega,\Gamma_1)) \cap C^1(0,T; L^2_\lambda(\Omega,\Gamma_1)) \cap H^1(0,T; H^1_\lambda(\Omega,\Gamma_1)).$$

4. *Existence of the solution u.* Resorting to subsequences $\{u_{m_l}\}_{l=1}^\infty$ of $\{u_m\}_{m=1}^\infty$, passing to the limit for $m \to \infty$ and using standard arguments it is possible to prove that there exists a solution u to problem (3.16) with

$$u \in C([0,T]; H^1_\lambda(\Omega,\Gamma_1)) \cap C^1(0,T; L^2_\lambda(\Omega,\Gamma_1)) \cap H^1(0,T; H^1_\lambda(\Omega,\Gamma_1)).$$

5. *Uniqueness of the weak solution.* Let u_1 and u_2 be two solutions of weak problem (3.16) and set $w = u_1 - u_2$. By definition, taking $z = w$, we get from (3.16)

$$\frac{d}{dt}\left(\|w\|^2_{L^2_\lambda(\Omega,\Gamma_1)}\right) + \|\nabla w\|^2_{L^2(\Omega)} + \alpha\|w\|^2_{L^2(\Gamma_1)} + \beta\|\nabla_\Gamma w\|^2_{L^2(\Gamma_1)} = 0,$$

that implies $w = 0$, or $u_1 = u_2$ for a.e. $0 \le t \le T$.

6. *Improved regularity.* Rewriting (3.16) as

$$a(u,v) = (\tilde f, v)_{L^2(\Omega)} + (\tilde g, v)_{L^2(\Gamma_1)},$$

where $\tilde f = f - \partial_t u \in L^2(0,T,L^2(\Omega))$ and $\tilde g = g - \partial_t u \in L^2(0,T,L^2(\Gamma_1))$. Employing Theorem 3.1 we get $u(t) \in H^2_\lambda(\Omega,\Gamma_1)$ for a.e. $0 \le t \le T$.

7. *Higher regularity.* We prove (3.17) by induction. From the above discussion the result holds true for $m = 1$. Assume now the validity of (3.17) for some $m > 1$, together with the associated higher order compatibility and regularity conditions. Differentiating (3.15) with respect to t, it is immediate to verify that $\tilde u = \partial_t u$ verifies

$$\begin{cases} \partial_t \tilde u &= \Delta \tilde u + \tilde f, & \text{in } \Omega,\ 0 < t \le T,\\ \partial_n \tilde u &= -\alpha \tilde u + \beta \Delta_\Gamma \tilde u - \lambda \partial_t \tilde u + \tilde g, & \text{on } \Gamma_1,\ 0 < t \le T,\\ \text{periodic boundary conditions}, & & \text{on } \Gamma_2,\ 0 < t \le T,\\ \tilde u_{|t=0} &= \tilde u_0, & \text{in } \overline{\Omega}, \end{cases} \tag{3.22}$$

where $\tilde f = \partial_t f$, $\tilde g = \partial_t g$, $\tilde u_0 = f(0,\cdot) + \Delta u_0$ in Ω and $\tilde u_0|_\Gamma = \beta\Delta_\Gamma u_0 - \partial_n u_0 - \alpha u_0 + g(0,\cdot)$ on Γ. Since the pair (f,g) satisfies the higher order compatibility conditions

for $k = 1, \ldots, m$ then the pair $(\tilde{f}, \tilde{g})$ satisfies the same type of compatibility conditions for $k = 1, \ldots, m-1$. Hence, it follows for $k = 0, \ldots, m-1$

$$\begin{aligned} \frac{d^k \tilde{u}}{dt^k} \;\in\; & C([0,T]; H^{2m-2k}(\Omega, \Gamma_1)) \cap C^1(0,T; H^{2m-2k-2}_{\lambda}(\Omega, \Gamma_1)) \\ & \cap\, H^1(0,T; H^{2m-2k-1}_{\lambda}(\Omega, \Gamma_1)) \end{aligned} \tag{3.23}$$

which immediately implies the validity of (3.17) for $k = 0, \ldots, m$. ■

The following result has been proof in [41, Lemmas 4.4 and 4.5].

Lemma 3.4 *Let $z \in Z = \{z \in H^2(\Omega) \mid \partial_n z = 0 \text{ on } \Gamma_1\}$. If z_n is the $L^2(\Omega)$-projection of z on V^n, then*

$$\|z_n - z\|_{H^1_{\lambda}(\Omega;\Gamma_1)} \to 0 \text{ when } n \to \infty. \tag{3.24}$$

Let $V_\infty = \cup_{n=1}^{\infty} V_n$. Moreover, Z and V_∞ are dense in $H^1_{\lambda}(\Omega; \Gamma_1)$.

Employing the DG notation introduced in Section 3.2.1, the space semi-discretization of problem (3.15) becomes: *Find $u_h \in C^0([0,T]; V_h^p)$ such that, for any $t \in (0,T]$,*

$$\begin{cases} (\partial_t u_h, v_h)_{L^2(\Omega)} + \lambda(\partial_t u_h, v_h)_{L^2(\Gamma_1)} + \mathcal{A}_h(u_h, v_h) = (f, v_h)_{L^2(\Omega)} + (g, v_h)_{L^2(\Gamma_1)}, \\ u_{h|t=0} = u_{h0}, \end{cases} \tag{3.25}$$

for any $v_h \in V_h^p$, where $u_{h0} \in V_h^p$ is the L^2-projection of u_0 into V_h^p. The following result shows the existence of a unique solution u_h of problem (3.25).

Theorem 3.4 *The semi-discrete problem (3.25) admits a unique local solution.*

Proof. As the proof is standard, we only sketch it. Let $\{\phi_j\}_{j=1}^N$ be an orthogonal basis of V_h^p. The semi-discrete problem (3.25) is equivalent to solve, for any $t \in (0,T]$, the following system of ordinary differential equations

$$\begin{cases} (\partial_t u_h, \phi_j)_{L^2(\Omega)} + \lambda(\partial_t u_h, \phi_j)_{L^2(\Gamma_1)} + \mathcal{A}_h(u_h, \phi_j) = (f, \phi_j)_{L^2(\Omega)} + (g, \phi_j)_{L^2(\Gamma_1)}, \\ u_{h|t=0} = u_{h0}, \end{cases} \tag{3.26}$$

for $j = 1, ..., N$. Setting $u_h = \sum_{i=1}^N c_i(t)\phi_i$, (3.26) can be equivalently written as

$$\begin{cases} M\dot{\mathbf{c}}(t) + A\mathbf{c}(t) = \mathbf{F}(t), \\ \mathbf{c}(0) = \mathbf{c}^0, \end{cases} \tag{3.27}$$

where $\mathbf{c}(t) = (c_i(t))_{1 \le i \le N}$, $\mathbf{c}^0 = (c_i^0)_{1 \le i \le N}$ with $u_{h0} = \sum_{i=1}^N c_i^0 \phi_i$, and, for $i, j = 1, .., N$,

$$A_{ij} = \mathcal{A}(\phi_i, \phi_j), \qquad M_{ij} = (\phi_i, \phi_j)_{L^2(\Omega)} + \lambda(\phi_i, \phi_j)_{L^2(\Gamma_1)},$$

$$F_i = (f, \phi_i)_{L^2(\Omega)} + (g, \phi_i)_{L^2(\Gamma_1)}.$$

Since the matrix M is positive definite and $\mathbf{F}(t) \in L^2(0,T;\mathbb{R}^N)$ invoking the well-known Picard-Lindelöf theorem yields the existence and uniqueness of a local solution $\mathbf{c} \in H^1(0,T_N;\mathbb{R})$, i.e., $u_h \in H^1(0,T_N;V_h^p) \subset C^0(0,T_N;V_h^p)$ with $T_N \in (0,T]$. ■

The next result shows the stability of the semi-discrete solution of (3.25).

Lemma 3.5 *Let u_h be the solution of (3.25). Then it holds*

$$\|u_h(T)\|^2_{L^2_\lambda(\Omega,\Gamma_1)} + \int_0^T |||u_h|||^2_* dt \lesssim \|u_{h0}\|^2_{L^2_\lambda(\Omega,\Gamma_1)} + \int_0^T (\|f\|^2_{L^2(\Omega)} + \|g\|^2_{L^2(\Gamma_1)})dt. \quad (3.28)$$

Proof. Choosing $v_h = u_h$ in (3.25) and using (3.9) we get

$$\frac{1}{2}\frac{d}{dt}\|u_h\|^2_{L^2_\lambda(\Omega,\Gamma_1)} + |||u_h|||^2_* \lesssim \big(\|f\|_{L^2(\Omega)} + \|g\|_{L^2(\Gamma_1)}\big)\|u_h\|_{L^2_1(\Omega,\Gamma_1)}.$$

Using the arithmetic-geometric inequality and the Poincaré-Friedrich inequality for functions in the broken Sobolev space $H^1(\mathcal{T}_h)$, i.e.,

$$\begin{aligned} \|v_h\|_{L^2(\Omega)} &\lesssim \big(|v_h|^2_{H^1(\mathcal{T}_h)} + \|[v_h]\|^2_{L^2(\mathcal{E}_h \cup \mathcal{E}_h^{\Gamma_2})}\big)^{1/2}, \quad \forall v_h \in H^1(\mathcal{T}_h), \\ \|v_h\|_{L^2(\Gamma_1)} &\lesssim \big(|v_h|^2_{H^1(\mathcal{E}_h^{\Gamma_1})} + \|[v_h]\|^2_{\mathcal{R}_h^{\Gamma_1}}\big)^{1/2}, \quad \forall v_h \in H^1(\mathcal{T}_h), \end{aligned}$$

cf. [17], we obtain

$$\frac{d}{dt}\|u_h\|^2_{L^2_\lambda(\Omega,\Gamma_1)} + |||u_h|||^2_* \lesssim \|f\|^2_{L^2(\Omega)} + \|g\|^2_{L^2(\Gamma_1)}. \quad (3.29)$$

The thesis follows integrating between 0 and T and noting that

$$\|u_{h0}\|^2_{L^2_\lambda(\Omega,\Gamma_1)} \lesssim \|u_0\|^2_{L^2_\lambda(\Omega,\Gamma_1)}$$

because u_{h0} is the L^2-projection of u_0 into V_h^p. ■

Finally, we consider the fully discretization of problem (3.16) by resorting to the Implicit Euler method with time-step $\Delta t > 0$. Let $t_k = k\Delta t$, $0 \le k \le K$, with $K = T/\Delta t$, and denote by u_h^k, $k \ge 0$, the approximation of $u_h(t_k)$. The fully-discrete problem reads as follows: given $u_h^0 = u_{h0}$, find $u_h^{k+1} \in V_h^p$, $0 < k \le K-1$, such that

$$\left(\frac{u_h^{k+1} - u_h^k}{\Delta t}, v_h\right)_{L^2(\Omega)} + \lambda\left(\frac{u_h^{k+1} - u_h^k}{\Delta t}, v_h\right)_{L^2(\Gamma_1)} + \mathcal{A}_h(u_h^{k+1}, v_h) = (f(t_{k+1}), v_h)_{L^2(\Omega)} + (g(t_{k+1}), v_h)_{L^2(\Gamma_1)} \quad (3.30)$$

for all $v_h \in V_h^p$.

3.4 Stability and error estimates

This section is devoted to show that the solution of problem (3.30) converges with optimal rate to the continuous solution of (3.15). We first prove the following stability result.

Lemma 3.6 *Let $f^k = f(t_k)$ and $g^k = g(t_k)$, $k = 1, ..., K$. Then it holds*

$$\|u_h^K\|^2_{L^2_\lambda(\Omega,\Gamma_1)} + \Delta t \sum_{k=1}^{K} |||u_h^k|||^2_* \lesssim \|u_{h0}\|^2_{L^2_\lambda(\Omega,\Gamma_1)} + \Delta t \sum_{k=1}^{K} \left(\|f^k\|^2_{L^2(\Omega)} + \|g^k\|^2_{L^2(\Gamma_1)} \right). \quad (3.31)$$

Proof. We choose $v_h = u_h^{k+1}$ in (3.30). Using (3.9), the identity

$$(z - y, z) = \frac{1}{2}\|z\|^2 - \frac{1}{2}\|y\|^2 + \frac{1}{2}\|z - y\|^2,$$

and the Cauchy-Schwarz inequality, we obtain

$$\|u_h^{k+1}\|^2_{L^2_\lambda(\Omega,\Gamma_1)} - \|u_h^k\|^2_{L^2_\lambda(\Omega,\Gamma_1)} + \|u_h^{k+1} - u_h^k\|^2_{L^2_\lambda(\Omega,\Gamma_1)} + \Delta t |||u_h^{k+1}|||^2_* \lesssim \Delta t \left(\|f^{k+1}\|_{L^2(\Omega)} \|u_h^{k+1}\|_{L^2(\Omega)} + \|g^{k+1}\|_{L^2(\Gamma_1)} \|u_h^{k+1}\|_{L^2(\Gamma_1)} \right).$$

Employing Young's inequality, Poincaré-Friedrich inequality and summing over k we get the thesis. ∎

We next state the main result of this section.

Theorem 3.5 *Let $u \in C([0,T]; H^s(\Omega,\Gamma_1)) \cap H^1(0,T; L^2_\lambda(\Omega,\Gamma_1))$, $s \geq 2$, be the solution of (3.16) and let u_h be the solution of (3.30). If $\partial_t u \in L^2(0,T; H^s(\Omega,\Gamma_1))$, $\partial_t^2 u \in L^2(0,T; L^2(\Omega,\Gamma_1))$ and u_h^0 satisfies*

$$\|u_0 - u_h^0\|_{L^2_\lambda(\Omega,\Gamma_1)} \lesssim h^{\min(s,p+1)} \|u_0\|_{H^s(\mathcal{T}_h)}, \quad (3.32)$$

then

$$\|u^K - u_h^K\|^2_{L^2_\lambda(\Omega,\Gamma_1)} \lesssim h^{2\min(s,p+1)} \left(\|u^K\|^2_{H^s_\lambda(\Omega,\Gamma_1)} + \|u_0\|^2_{H^s_\lambda(\Omega,\Gamma_1)} + \int_0^T \|\partial_t u(t)\|^2_{H^s_\lambda(\Omega,\Gamma_1)}\, dt \right) + \Delta t^2 \int_0^T \|\partial_t^2 u(t)\|^2_{L^2_\lambda(\Omega,\Gamma_1)}\, dt,$$

and

$$\Delta t\sum_{k=1}^{K}|||u^k-u_h^k|||_*^2\lesssim h^{2\min(s-1,p)}\bigg(\Delta t\sum_{k=1}^{K}\|u^k\|_{H^s_\lambda(\Omega,\Gamma_1)}^2 + h^2\|u_0\|_{H^s_\lambda(\Omega,\Gamma_1)}^2+h^2\int_0^T\|\partial_t u(t)\|_{H^s_\lambda(\Omega,\Gamma_1)}^2\,dt\bigg) + \Delta t^2\int_0^T\|\partial_t^2 u(t)\|_{L^2_\lambda(\Omega,\Gamma_1)}^2\,dt,$$

where $u^k=u(t_k),\ k=1,...,K.$

Proof. We first define the elliptic projection $P:H^2(\Omega,\Gamma_1)\to V_h^p$ as

$$\mathcal{A}_h(Pw-w,v_h)=0\qquad\forall v_h\in V_h^p,\tag{3.33}$$

where $\mathcal{A}_h(\cdot,\cdot)$ is defined as in (3.5). We note (see Theorem 3.2) that P satisfies the bound

$$\|Pw-w\|_{L^2_\lambda(\Omega,\Gamma_1)}+h|||Pw-w|||_*\lesssim h^{\min(s,p+1)}\|w\|_{H^s_\lambda(\Omega,\Gamma_1)},\tag{3.34}$$

for all $w\in H^s(\Omega,\Gamma_1)$, $s\geq 2$. We next write $u^k-u_h^k=(u^k-Pu^k)+(Pu^k-u_h^k)$ and start to focus on the second term. Considering problem (3.25) at time t_{k+1}, we easily get

$$\begin{aligned}&\left(\frac{Pu^{k+1}-Pu^k}{\Delta t},v_h\right)_{L^2(\Omega)}+\lambda\left(\frac{Pu^{k+1}-Pu^k}{\Delta t},v_h\right)_{L^2(\Gamma_1)}+\mathcal{A}_h(Pu^{k+1},v_h)\\&\quad=(f(t_k),v_h)_{L^2(\Omega)}+(g(t_k),v_h)_{L^2(\Gamma_1)}-(E^{k+1},v_h)_{L^2(\Omega)}-\lambda(E^{k+1},v_h)_{L^2(\Gamma_1)},\end{aligned}\tag{3.35}$$

for all $v_h\in V_h^p$, where

$$E^{k+1}=\partial_t u(t_{k+1})-\frac{1}{\Delta t}(Pu^{k+1}-Pu^k).$$

Subtracting (3.30) from (3.35), we get that $e_h^k=Pu^k-u_h^k$ satisfies

$$\begin{aligned}&\left(\frac{e_h^{k+1}-e_h^k}{\Delta t},v_h\right)_{L^2(\Omega)}+\lambda\left(\frac{e_h^{k+1}-e_h^k}{\Delta t},v_h\right)_{L^2(\Gamma_1)}+\mathcal{A}_h(e_h^{k+1},v_h)\\&\qquad=-(E^{k+1},v_h)_{L^2(\Omega)}-\lambda(E^{k+1},v_h)_{L^2(\Gamma_1)},\end{aligned}$$

for all $v_h\in V_h^p$. Then, reasoning as in the proof of Lemma 3.6 , we obtain

$$\|e_h^K\|_{L^2_\lambda(\Omega,\Gamma_1)}^2+\Delta t\sum_{k=1}^{K}|||e_h^k|||_*^2\lesssim\|e_h^0\|_{L^2_\lambda(\Omega,\Gamma_1)}^2+\Delta t\sum_{k=1}^{K}\|E^k\|_{L^2_\lambda(\Omega,\Gamma_1)}^2.\tag{3.36}$$

We bound the first term on the right-hand side of (3.36) using (3.32) and (3.34):

$$\begin{aligned}\|e_h^0\|_{L^2_\lambda(\Omega,\Gamma_1)} &= \|Pu_0 - u_{h0}\|_{L^2_\lambda(\Omega,\Gamma_1)} \\ &\leq \|Pu_0 - u_0\|_{L^2_\lambda(\Omega,\Gamma_1)} + \|u_0 - u_{h0}\|_{L^2_\lambda(\Omega,\Gamma_1)} \\ &\lesssim h^{\min(s,p+1)}\|u_0\|_{H^s(\mathcal{T}_h)}. \end{aligned} \tag{3.37}$$

In order to bound the second term on the right-hand side of (3.36) we observe that it holds:

$$\begin{aligned} E^{k+1} &= \left(\partial_t u(t_{k+1}) - \frac{u^{k+1}-u^k}{\Delta t}\right) + \frac{(u^{k+1}-Pu^{k+1}) - (u^k - Pu^k)}{\Delta t} \\ &= -\frac{1}{\Delta t}\int_{t_k}^{t_{k+1}} \big(t-t_k\big)\ \partial_t^2 u(t)\ dt + \frac{1}{\Delta t}\int_{t_k}^{t_{k+1}} \partial_t\big(u(t)-Pu(t)\big)\ dt \end{aligned}$$

where we employed Taylor's formula. Therefore, employing the commutation of the operators P and ∂t, we have

$$\begin{aligned}\|E^{k+1}\|^2_{L^2_\lambda(\Omega,\Gamma_1)} \lesssim\ & \frac{1}{\Delta t}\left|\left|\int_{t_k}^{t_{k+1}} \big(t-t_k\big)\ \partial_t^2 u(t)\ dt\right|\right|^2_{L^2_\lambda(\Omega,\Gamma_1)} \\ &+ \frac{1}{\Delta t}\left|\left|\int_{t_k}^{t_{k+1}} \big(\partial_t u(t) - P\partial_t u(t)\big)dt\right|\right|^2_{L^2_\lambda(\Omega,\Gamma_1)}. \end{aligned}$$

Using the Cauchy-Schwarz inequality we get

$$\begin{aligned}&\left|\left|\int_{t_k}^{t_{k+1}} \big(t-t_k\big)\partial_t^2 u(t)\ dt\right|\right|_{L^2_\lambda(\Omega,\Gamma_1)} \\ &\quad\leq \left(\int_{t_k}^{t_{k+1}} (t-t_k)^2\ dt\right)^{1/2}\left(\int_{t_k}^{t_{k+1}} \|\partial_t^2 u(t)\|^2_{L^2_\lambda(\Omega,\Gamma_1)}\ dt\right)^{1/2} \\ &\quad\lesssim \Delta t^{3/2}\left(\int_{t_k}^{t_{k+1}} \|\partial_t^2 u(t)\|^2_{L^2_\lambda(\Omega,\Gamma_1)}\ dt\right)^{1/2}. \end{aligned}$$

Hence,

$$\frac{1}{\Delta t}\left|\left|\int_{t_k}^{t_{k+1}} \big(t-t_k\big)\partial_t^2 u(t)\ dt\right|\right|^2_{L^2_\lambda(\Omega,\Gamma_1)} \lesssim \Delta t^2 \int_{t_k}^{t_{k+1}} \|\partial_t^2 u(t)\|^2_{L^2_\lambda(\Omega,\Gamma_1)}\ dt.$$

Employing $\partial_t u \in L^2(0,T;H^s(\mathcal{T}_h))$, $s \geq 2$, and (3.34), we obtain

$$\begin{aligned}
&\left|\left|\int_{t_k}^{t_{k+1}} \big(\partial_t u(t) - P\partial_t u(t)\big)dt\right|\right|_{L^2_\lambda(\Omega,\Gamma_1)} \\
&\quad\leq \left(\int_{t_k}^{t_{k+1}} (1)^2 \, dt\right)^{1/2} \left(\int_{t_k}^{t_{k+1}} \|\partial_t u(t) - P\partial_t u(t)\|^2_{L^2_\lambda(\Omega,\Gamma_1)} \, dt\right)^{1/2} \\
&\quad\lesssim \Delta t^{1/2} \left(\int_{t_k}^{t_{k+1}} \|\partial_t u(t) - P\partial_t u(t)\|^2_{L^2_\lambda(\Omega,\Gamma_1)} \, dt\right)^{1/2} \\
&\quad\lesssim \Delta t^{1/2} h^{\min(s,p+1)} \left(\int_{t_k}^{t_{k+1}} \|\partial_t u(t)\|^2_{H^s_\lambda(\Omega,\Gamma_1)} \, dt\right)^{1/2}.
\end{aligned}$$

Hence,

$$\begin{aligned}
\frac{1}{\Delta t}\left|\left|\int_{t_k}^{t_{k+1}} \big(\partial_t u(t) - P\partial_t u(t)\big)dt\right|\right|^2_{L^2_\lambda(\Omega,\Gamma_1)} \\
\lesssim h^{2\min(s,p+1)} \int_{t_k}^{t_{k+1}} \|\partial_t u(t)\|^2_{H^s_\lambda(\Omega,\Gamma_1)} \, dt. \quad (3.38)
\end{aligned}$$

Finally, summing over k we get

$$\begin{aligned}
&\Delta t \sum_{k=1}^{K} \|E^k\|^2_{L^2_\lambda(\Omega,\Gamma_1)} \qquad (3.39)\\
&\quad\lesssim \Delta t^2 \int_0^T \|\partial_t^2 u(t)\|^2_{L^2_\lambda(\Omega,\Gamma_1)} \, dt + h^{2\min(s,p+1)} \int_0^T \|\partial_t u(t)\|^2_{H^s_\lambda(\Omega,\Gamma_1)} \, dt,
\end{aligned}$$

which concludes the bound for e_h^k. Finally, the thesis follows employing the triangle inequality and the bounds (3.36)-(3.37) together with (3.34)-(3.39). ■

3.5 Numerical experiments

In this section we present some numerical results to validate our theoretical estimates. In the first two examples (cf. Sections 3.5.1 and 3.5.2) we consider a test case with periodic boundary conditions and validate our theoretical error estimates. In the last example (cf. Section 3.5.3) we show that our theoretical results seem to hold in the case of more general boundary conditions, provided the exact solution of problem (3.15) is smooth enough.

3.5.1 Example 1

We consider problem (3.15) on $\Omega = (0,1)^2$ and choose f and g such that $u = e^{-10t}(1-\cos(2\pi x))\cos(4\pi y)$ is the exact solution.

We have tested our scheme on a sequence of uniformly refined structured triangular grids with meshsize $h = \sqrt{2}/2^{\ell}$, $\ell = 2, ..., 7$. In those sets of numerical experiments we have measured the error $e(T) = u(T) - u_h(T)$ at the final observation time $T = 0.001$ in the $\|\cdot\|_{L^2(\Omega)}$ and $\|\cdot\|_{L^2(\Gamma_1)}$ norms. We have also measured the quantity $(\Delta t \sum_{k=1}^{K} |||e^k|||_*^2)^{1/2}$, being $e^k = u^k - u_h^k$.
In the first set of experiments we used piecewise linear elements ($p = 1$) and the following parameters: $\sigma = 10$, $\Delta t = 10^{-5}$, $\lambda = 10$, $\beta = 5$ $\alpha = 2$. The computed errors and the corresponding computed convergence rates are reported in Table 3.1. We have repeated the same set of experiments employing piecewise quadratic elements ($p = 2$); the results are reported in Table 3.2. From the results shown in Table 3.1 and Table 3.2, it is clear that the expected convergence rates are obtained.

h	$\|e(T)\|_{L^2(\Omega)}$	rate	$\|e(T)\|_{L^2(\Gamma_1)}$	rate	$(\Delta t \sum_{k=1}^{K} \|\|\|e^k\|\|\|_*^2)^{1/2}$	rate
$\sqrt{2}/2^2$	1.836048e-01	-	1.908256e-01	-	2.281359e-01	
$\sqrt{2}/2^3$	5.455936e-02	1.75	5.035380e-02	1.92	1.186343e-01	0.94
$\sqrt{2}/2^4$	1.451833e-02	1.91	1.278655e-02	1.98	5.939199e-02	1.00
$\sqrt{2}/2^5$	3.688202e-03	1.98	3.208881e-03	1.99	2.962468e-02	1.00
$\sqrt{2}/2^6$	9.258142e-04	1.99	8.028862e-04	2.00	1.480150e-02	1.00
$\sqrt{2}/2^7$	2.316573e-04	2.00	2.006754e-04	2.00	7.399580e-03	1.00

Table 3.1: Example 1. Computed errors, $p = 1$, $\sigma = 10$, $\Delta t = 10^{-5}$, $T = 0.001$, $\lambda = 10$, $\beta = 5$ and $\alpha = 2$.

h	$\|e(T)\|_{L^2(\Omega)}$	rate	$\|e(T)\|_{L^2(\Gamma_1)}$	rate	$(\Delta t \sum_{k=1}^{K} \|\|\|e^k\|\|\|_*^2)^{1/2}$	rate
$\sqrt{2}/2^2$	2.470397e-02	-	1.751588e-02	-	5.281897e-02	-
$\sqrt{2}/2^3$	3.027272e-03	3.03	2.232268e-03	2.97	1.405198e-02	1.91
$\sqrt{2}/2^4$	3.827204e-04	2.98	2.822643e-04	2.98	3.602372e-03	1.96
$\sqrt{2}/2^5$	4.797615e-05	3.00	3.539247e-05	3.00	9.081101e-04	1.99
$\sqrt{2}/2^6$	5.992844e-06	3.00	4.421683e-06	3.00	2.276766e-04	2.00
$\sqrt{2}/2^7$	7.507474e-07	3.00	5.632338e-07	2.97	5.593742e-05	2.02

Table 3.2: Example 1. Computed errors, $p = 2$, $\sigma = 10$, $\Delta t = 10^{-5}$, $T = 0.001$, $\lambda = 10$, $\beta = 5$ and $\alpha = 2$.

3.5.2 Example 2

In the second example, we explore the dependencies of the error on the time-step Δt. To this aim, we set f and g as in Section 3.5.1. In Table 3.3 we report the

computed errors and convergence rates obtained with piecewise linear elements ($p = 1$) and the following parameters: $k = 7$, $\sigma = 10$, $T = 0.1$, $\lambda = 10$, $\beta = 5$, $\alpha = 2$, $h = \sqrt{2}/2^7$ and vary the time integration step Δt. The numerical results are in agreement with the theoretical estimate.

Δt	$\|e(T)\|_{L^2(\Omega)}$	rate	$\|e(T)\|_{L^2(\Gamma_1)}$	rate
0.1×2^0	2.682138e-02	-	8.678953e-02	-
0.1×2^{-1}	1.487984e-02	0.85	4.905898e-02	0.82
0.1×2^{-2}	7.889826e-03	0.92	2.630006e-02	0.90
0.1×2^{-3}	4.050365e-03	0.96	1.360794e-02	0.95
0.1×2^{-4}	2.028095e-03	1.00	6.881036e-03	0.98
0.1×2^{-5}	9.897726e-04	1.03	3.415646e-03	1.01
0.1×2^{-6}	4.664660e-04	1.08	1.656678e-03	1.04

Table 3.3: Example 2. Computed errors, $k = 7$, $p = 1$, $\sigma = 10$, $T = 0.1$, $\lambda = 10$, $\beta = 5$ and $\alpha = 2$.

3.5.3 Example 3

Finally, we consider problem (3.15) on $\Omega = (0, 1)^2$ with homogeneous Dirichlet boundary conditions applied on Γ_2 and dynamic boundary conditions on Γ_1. In this case we choose f and g such that $u = t(1 - \cos(2\pi x)) \cos(\pi y)$ is the exact solution. In Table 3.4 we report the computed errors and computed convergence rates at the final time $T = 0.1$. Those results have been obtained with piecewise linear elements ($p = 1$) and with the following choice of parameters: $\sigma = 10$, $\Delta t = 0.001$, $\lambda = 10$, $\beta = 5$ and $\alpha = 2$. We have ran the same set of experiments employing piecewise quadratic elements ($p = 2$); the computed results are shown in Table 3.5. The results reported in Table 3.4 and Table 3.5 clearly confirm the theoretical rates of convergence even in the cases of Dirichlet boundary conditions instead of periodic ones, at least whenever the exact solution is sufficiently smooth (see Remark 3.1).

h	$\|e(T)\|_{L^2(\Omega)}$	rate	$\|e(T)\|_{L^2(\Gamma_1)}$	rate	$(\Delta t \sum_{k=1}^{K} \|\|\|e^k\|\|\|_*^2)^{1/2}$	rate
$\sqrt{2}/2^2$	9.185918e-03	-	1.111234e-02	-	1.347859e-01	-
$\sqrt{2}/2^3$	2.704819e-03	1.76	2.849404e-03	1.96	6.413467e-02	1.07
$\sqrt{2}/2^4$	7.279868e-04	1.89	7.169369e-04	1.99	3.155837e-02	1.02
$\sqrt{2}/2^5$	1.875124e-04	1.96	1.797070e-04	2.00	1.571196e-02	1.01
$\sqrt{2}/2^6$	4.745622e-05	1.98	4.501545e-05	2.00	7.847606e-03	1.00
$\sqrt{2}/2^7$	1.192746e-05	1.99	1.127502e-05	2.00	3.922783e-03	1.00

Table 3.4: Example 3. Computed errors, $p = 1$, $\sigma = 10$, $\Delta t = 0.001$, $T = 0.1$, $\lambda = 10$, $\beta = 5$ and $\alpha = 2$.

h	$\|e(T)\|_{L^2(\Omega)}$	rate	$\|e(T)\|_{L^2(\Gamma_1)}$	rate	$(\Delta t \sum_{k=1}^{K} \|\|\|e^k\|\|\|_*^2)^{1/2}$	rate
$\sqrt{2}/2^2$	1.239177e-03	-	1.607590e-03	-	2.589798e-02	-
$\sqrt{2}/2^3$	1.543449e-04	3.01	2.189412e-04	2.88	6.771702e-03	1.93
$\sqrt{2}/2^4$	1.911957e-05	3.01	2.788057e-05	2.97	1.715537e-03	1.98
$\sqrt{2}/2^5$	2.386211e-06	3.00	3.496808e-06	3.00	4.307186e-04	1.99
$\sqrt{2}/2^6$	2.990873e-07	3.00	4.364171e-07	3.00	1.079691e-04	2.00
$\sqrt{2}/2^7$	3.777961e-08	2.98	5.420558e-08	3.01	2.621607e-05	2.04

Table 3.5: Example 3. Computed errors, $p = 2$, $\sigma = 10$, $\Delta t = 0.001$, $T = 0.1$, $\lambda = 10$, $\beta = 5$ and $\alpha = 2$.

4

Fast solution techniques for the Cahn-Hilliard problem

In this chapter we present a numerical comparison of several multigrid techniques for the efficient solution of the fully discretized Cahn-Hilliard equation.

4.1 Problem discretization

Let $\Omega \subset \mathbb{R}^d$, $d = 2, 3$, be an open bounded domain and define $\Gamma = \partial\Omega$. The Cahn-Hilliard equation reads as: *Find* $u : \Omega \times [0, T] \to \mathbb{R}$, $T > 0$, *such that*

$$\begin{cases} \partial_t u + \Delta(\gamma^2 \Delta u - \Phi'(u)) = 0 & \text{in } \Omega \times (0, T], \\ \partial_n u = \partial_n(\Delta u) = 0 & \text{on } \Gamma \times (0, T], \\ u(\cdot, 0) = u_0(\cdot) & \text{in } \Omega, \end{cases} \tag{4.1}$$

where $\partial_t \eta = \frac{\partial \eta}{\partial t}$, $\partial_n \eta = \frac{\partial \eta}{\partial n}$ and $\gamma > 0$ is a given constant called interface parameter. This parameter is usually assumed to be small, e.g. in the range $10^{-3} - 10^{-2}$.

We rewrite (4.1) in a mixed form, introducing the chemical potential $w = \Phi'(u) - \gamma^2 \Delta u$: *Find* $u, w : \Omega \times [0, T] \to \mathbb{R}$, $T > 0$, *such that*

$$\begin{cases} \partial_t u - \Delta w = 0 & \text{in } \Omega \times (0, T], \\ w = \Phi'(u) - \gamma^2 \Delta u & \text{in } \Omega \times (0, T], \\ \partial_n u = \partial_n w = 0 & \text{on } \Gamma \times (0, T], \\ u(\cdot, 0) = u_0(\cdot) & \text{in } \Omega. \end{cases} \tag{4.2}$$

In the following, the free energy $\phi(\cdot)$ is taken as the quartic polynomial

$$\Phi(s) = \frac{1}{4}(1 - s^2)^2. \tag{4.3}$$

As shown in [56], this is a good approximation of the (more general) logarithmic potential (1.3). We point out that (4.3) is easier to be treated than (1.3) from the numerical point of view since it does not have singularities in ± 1 that can be source of numerical instabilities when the modulus of the solution is near to 1.

4.1.1 Space-time discretization of the Cahn-Hilliard equation

We begin by stating the weak formulation of the Cahn-Hilliard problem (4.2): *For any* $t \in (0, T]$, *find* $\{u(\cdot, t), w(\cdot, t)\} \in H^1(\Omega) \times H^1(\Omega)$, *such that*

$$\begin{cases} (\partial_t u, \eta)_{L^2(\Omega)} - (\Delta w, \eta)_{L^2(\Omega)} = 0 & \forall \eta \in H^1(\Omega), \\ (w, \eta)_{L^2(\Omega)} = (\phi'(u), \eta)_{L^2(\Omega)} - \gamma^2 (\Delta u, \eta)_{L^2(\Omega)} & \forall \eta \in H^1(\Omega), \\ u(\cdot, 0) = u_0(\cdot) \in H^2_N(\Omega), \end{cases} \tag{4.4}$$

where

$$H^2_N(\Omega) = \{v \in H^2(\Omega) : \partial_n v = 0 \text{ on } \Gamma\}.$$

Let $\mathcal{T}_h$ be a shape-regular partition of the domain Ω and let V_h^p be the test and trial space of piecewise discontinuous polynomial functions of order $p \geq 1$, defined on $\mathcal{T}_h$, i.e.

$$V_h^p = \{v \in L^2(\Omega) : v_{|K} \in \mathbb{P}^p \quad \forall K \in \mathcal{T}_h\}.$$

We also define

$$H^m(\Omega, \mathcal{T}_h) = \{w \in L^2(\Omega) \ : \ w_{|K} \in H^m(K) \quad \forall K \in \mathcal{T}_h\}.$$

We denote by $\mathcal{E}_h^0$ the set of interior edges (or faces) of the triangulation $\mathcal{T}_h$ and by $\mathcal{E}_h^\Gamma$ the set of the edges (or faces) belongs to Γ. We also define $\mathcal{E}_h = \mathcal{E}_h^0 \cup \mathcal{E}_h^\Gamma$.

Let us to introduce some notation about jump and average operators. For each $e \in \mathcal{E}_h^0$ there exist K and $K^* \in \mathcal{T}_h$ such that $\overline{e} = \partial\overline{K} \cap \partial\overline{K^*}$, and, similarly, for each $e \in \mathcal{E}_h^\Gamma$ there exists a $K \in \mathcal{T}_h$ such that $\overline{e} = \partial\overline{K} \cap \partial\overline{\Omega}$. Then, for each $e \in \mathcal{E}_h^0$ we define

$$\{\boldsymbol{\tau}\}_{|e} = \frac{\boldsymbol{\tau}_{|K} \ + \ \boldsymbol{\tau}_{|K^*}}{2}, \qquad [\boldsymbol{\tau}]_{|e} = \boldsymbol{\tau}_{|K} \cdot \mathbf{n}_K \ - \ \boldsymbol{\tau}_{|K^*} \cdot \mathbf{n}_K,$$

$$\{v\}_{|e} = \frac{v_{|K} \ + \ v_{|K^*}}{2}, \qquad [v]_{|e} = v_{|K}\mathbf{n}_K \ + \ v_{|K^*}\mathbf{n}_K,$$

and for $e \in \mathcal{E}_h^\Gamma$

$$\{\boldsymbol{\tau}\}_{|e} = \boldsymbol{\tau}_{|K}, \qquad [v]_{|e} = v\mathbf{n}_{|K},$$

where v and $\boldsymbol{\tau}$ are a scalar and a vector-valued smooth enough functions, respectively. In the following, to improve the readability, we remove the subscript index.

We introduce the bilinear form $\mathcal{B}_h(\cdot,\cdot) : V_h^p \times V_h^p \to \mathbb{R}$ defined as

$$\mathcal{B}_h(v,w) = \sum_{K\in\mathcal{T}_h} (\nabla v, \nabla w)_{L^2(K)} - (\{\nabla v\},[w])_{L^2(\mathcal{E}_h^0)} - ([v],\{\nabla w\})_{L^2(\mathcal{E}_h^0)} + \sigma([v],[w])_{L^2(\mathcal{E}_h^0)}, \quad (4.5)$$

where $(\cdot,\cdot)_{L^2(\mathcal{E}_h^0)} = \sum_{e\in\mathcal{E}_h^0}(\cdot,\cdot)_{L^2(e)}$. We also define the DG norm $\|\cdot\|_{DG}$ on V_h^p as

$$\|w_h\|_{DG}^2 = \sum_{K\in\mathcal{T}_h} \|\nabla w_h\|_{L^2(K)}^2 + \frac{1}{\sigma}\|\{\nabla w_h\}\|_{L^2(\mathcal{E}_h^0)} + \sigma\|[w_h]\|_{L^2(\mathcal{E}_h^0)}^2.$$

The parameter σ is taken as

$$\begin{cases} \sigma_{|e} = \frac{\mu[\max(p_K,p_{K^*})]^2}{\min(h_K,h_{K^*})} & \text{if } e\in\mathcal{E}_h^0, \\ \sigma_{|e} = \frac{\mu p_K^2}{h_K} & \text{if } e\in\mathcal{E}_h^\Gamma, \end{cases}$$

where $\mu \in \mathbb{R}^+$ and p_K, h_K are the polynomial degree and the diameter of the element K, respectively.

The bilinear form $\mathcal{B}_h(\cdot,\cdot)$ satisfies the following properties [49]:

- Consistency: let $v \in H_N^2(\Omega)$ such that $(v,1)_{L^2(\Omega)} = 0$. Then we have
$$\mathcal{B}_h(v,w_h) = (-\Delta v, w_h)_{L^2(\Omega)} \qquad \forall w_h \in V_h^p;$$
- Continuity: For all $v, w \in H^2(\Omega,\mathcal{T}_h)$, it holds
$$|\mathcal{B}_h(v,w)| \lesssim \|v\|_{DG}\|w\|_{DG};$$
- Coercivity: If μ is large enough, there holds
$$\|v\|_{DG}^2 \lesssim \mathcal{B}_h(v,v) \qquad \forall v \in V_h^p.$$

We define the discontinuous Galerkin space semi-discretization of the Cahn-Hilliard problem (4.2) as: *For any* $t \in (0,T]$, *find* $\{u_h(\cdot,t), w_h(\cdot,t)\} \in V_h^p \times V_h^p$, $t \in (0,T]$, *such that*

$$\begin{cases} (\partial_t u_h, \eta_h)_{L^2(\Omega)} + \mathcal{B}_h(w_h,\eta_h)_{L^2(\Omega)} = 0 & \forall \eta_h \in V_h^p, \\ (w_h,\eta_h)_{L^2(\Omega)} = (\phi'(u_h),\eta_h)_{L^2(\Omega)} + \gamma^2\mathcal{B}_h(u_h,\eta_h)_{L^2(\Omega)} & \forall \eta_h \in V_h^p, \\ u_h(\cdot,0) = \Pi_h u_0(\cdot) \in V_h^p, \end{cases} \quad (4.6)$$

where the orthogonal projector $\Pi_h : L^2(\Omega) \to V_h^p$ is defined as

$$(v - \Pi_h v, \chi_h)_{L^2(\Omega)} = 0 \quad \forall \chi_h \in V_h^p. \tag{4.7}$$

We now introduce the fully discretization of problem (4.2). Let $0 = t_0 < t_1 < ... < t_N = T$ be a partition of $[0, T]$, with step size Δt, i.e., $t_n = t_0 + n\Delta t$, $n = 0, ..., N$.

There are several type of time-discretization method for (4.6). The first method that we present is the backward Euler method (cf. [49]). In this case the fully discrete problem reads as follows: *For* $1 \leq n \leq N$, *find* $\{u_h^n, w_h^n\} \in V_h^p \times V_h^p$ *such that*

$$\begin{cases} (\delta_t u_h^n, \chi_h)_{L^2(\Omega)} + \mathcal{B}_h(w_h^n, \chi_h) = 0 & \forall \chi_h \in V_h^p, \\ (w_h^n, \chi_h)_{L^2(\Omega)} = (\phi'(u_h^n), \chi_h)_{L^2(\Omega)} + \gamma^2 \mathcal{B}_h(u_h^n, \chi_h)_{L^2(\Omega)} & \forall \chi_h \in V_h^p, \\ u_h^0 = \Pi_h u_0 \in V_h^p, \end{cases} \tag{4.8}$$

where

$$\delta_t u_h^n = \frac{u_h^n - u_h^{n-1}}{\Delta t}, \qquad 1 \leq n \leq N.$$

To numerically solve (4.8), we linearize it using the Newton's method (cf. Appendix A.1).
Applying the Newton's method to the function

$$F(u) = \phi'(u) - \gamma^2 \Delta u - w,$$

we obtain

$$\lim_{\epsilon \to 0} \frac{-\gamma^2 \Delta(u^{(k)} + \epsilon \delta u) + \gamma^2 \Delta(u^{(k)}) + \phi'(u^{(k)} + \epsilon \delta u) - \phi'(u^{(k)})}{\epsilon} = \gamma^2 \Delta u^{(k)} - \phi'(u^{(k)}) + w,$$

hence,

$$-\gamma^2 \Delta u^{(k+1)} + u^{(k+1)} \phi''(u^{(k)}) = u^{(k)} \phi''(u^{(k)}) - \phi'(u^{(k)}) + w.$$

Using the definition of ϕ we get

$$-\gamma^2 \Delta u^{(k+1)} + u^{(k+1)}(3(u^{(k)})^2 - 1) = 2(u^{(k)})^3 + w.$$

Therefore, after the Newton linearization, the numerical solution of (4.8) becomes: *For* $k = 0, 1, ..K$, *given* $u_h^n = u_h^{n,K}$ *and* $u_h^{n+1,k}$, *find* $u_h^{n+1,k+1}, w_h^{n+1,k+1}$ *that satisfy*

$$\begin{cases} \left(u_h^{n+1,k+1} - u_h^n, \chi_h\right) + \Delta t \ \mathcal{B}_h(w_h^{n+1,k+1}, \chi_h) = 0 & \forall \chi_h \in V_h^p, \\ (w_h^{n+1,k+1}, \chi_h) = \gamma^2 \ \mathcal{B}_h(u_h^{n+1,k+1}, \chi_h) & \\ \qquad + \left(3u_h^{n+1,k+1}(u_h^{n+1,k})^2 - 2(u_h^{n+1,k})^3 - u_h^{n+1,k}, \chi_h\right) & \forall \chi_h \in V_h^p. \end{cases} \tag{4.9}$$

Another type of time-discretization for Cahn-Hilliard problem is the convex-splitting proposed in [5]. In this case, the fully discretization of problem (4.2) reads as: *For* $1 \leq n \leq N$, *find* $\{u_h^n, w_h^n\} \in V_h^p \times V_h^p$ *such that*

$$\begin{cases} (\delta_t u_h^n, \chi_h)_{L^2(\Omega)} + \mathcal{B}_h(w_h^n, \chi_h) = 0 & \forall \chi_h \in V_h^p, \\ (w_h^n, \chi)_{L^2(\Omega)} = ((u_h^n)^3 - u_h^{n-1}, \chi_h)_{L^2(\Omega)} + \gamma^2 \mathcal{B}_h(u_h^n, \chi_h)_{L^2(\Omega)} & \forall \chi_h \in V_h^p, \\ u_h^0 = \Pi_h u_0 \in V_h^p, \end{cases} \tag{4.10}$$

We can linearize the above formulation proceeding as before. Then we obtain: *For* $k = 0, 1, ..K$, *given* $u_h^n = u_h^{n,K}$ *and* $u_h^{n+1,k}$, *find* $u_h^{n,k+1}, w_h^{n,k+1}$ *such that*

$$\begin{cases} \left(u_h^{n+1,k+1} - u_h^n, \chi_h\right) + \Delta t \ \mathcal{B}_h(w_h^{n+1,k+1}, \chi_h) = 0 & \forall \chi_h \in V_h^p, \\ (w_h^{n+1,k+1}, \chi_h) = \gamma^2 \ \mathcal{B}_h(u_h^{n+1,k+1}, \chi_h) & \\ \qquad + \left(3u_h^{n+1,k+1}(u_h^{n+1,k})^2 - 2(u_h^{n+1,k})^3 - u_h^{n,k}, \chi_h\right) & \forall \chi_h \in V_h^p. \end{cases} \tag{4.11}$$

For both linearized formulations, we set $u_h^{n+1,0} = u_h^{n,K}$. The number K is commonly taken equal to 3 as suggested in [49].

4.1.2 Numerical examples

In this section we consider four test cases taken from [49] and we report the numerical results obtained by employing backward Euler (4.8).

4.1.2.1 Example 1

In the first example we choose $\Delta t = 0.01$, $\gamma = 0.01$, $\mu = 10$ and

$$u_0(x, y) = \begin{cases} 0.95 & \text{if } 9(x - 0.5)^2 + (y - 0.5)^2 < \frac{1}{9}, \\ \text{-0.95} & \text{otherwise.} \end{cases}$$

In Figure 4.1 we report the numerical solutions computed employing piecewise linear ($p = 1$) and quadratic ($p = 2$) elements on a mesh made of 8192 triangles on different time snapshots.

From the theoretical point of view, at each time steps the energy functional (1.4) decreases. This behaviour is represented in Figure 4.1 by the length reduction of the layer in which the two phases coexist.

4.1.2.2 Example 2

In the second example we set $\Delta t = 10^{-3}$, $\gamma = 0.01$, $\mu = 10$ and consider a cross-shaped initial datum. In Figure 4.2 we report the result performed on the same mesh employed in Example 1. As in Example 1, the pattern of the solution minimizes the energy functional (1.4) and, therefore, the length of the interface layer. Indeed, for $t \gg 0$, this layer becomes circular.

(a) $p = 1$

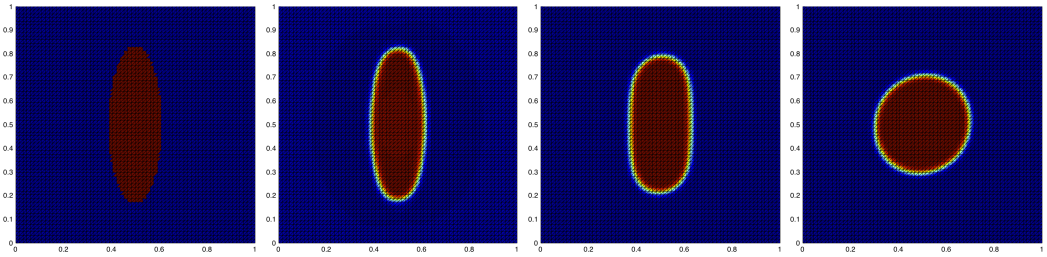

(b) $p = 2$

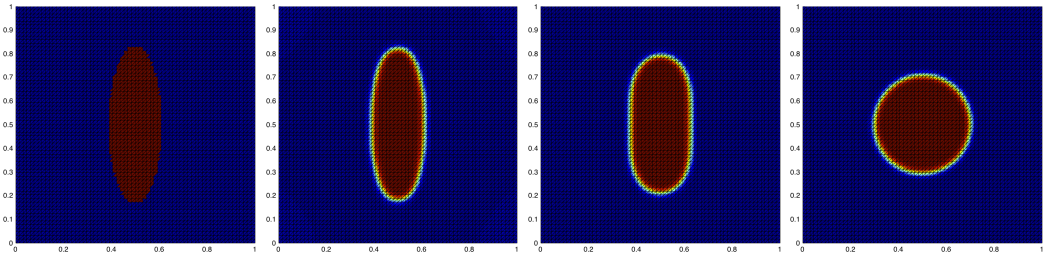

Figure 4.1: Example 1. Computed solutions with $p = 1$ (top) and $p = 2$ (bottom) polynomial approximation degrees. From left to right we report the solution at time $t = 0, 0.01, 0.1, 1.0$.

(a) $p = 1$

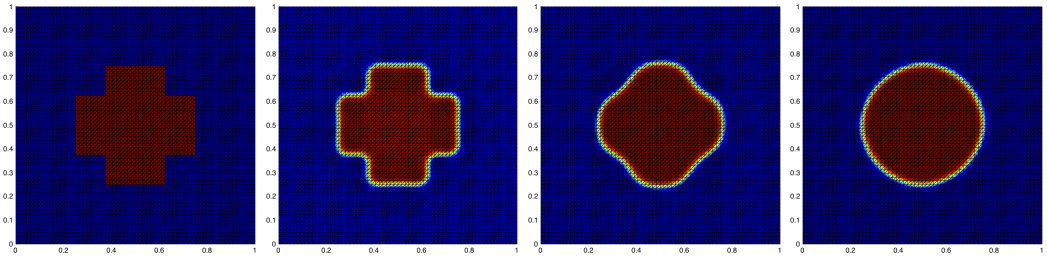

(b) $p = 2$

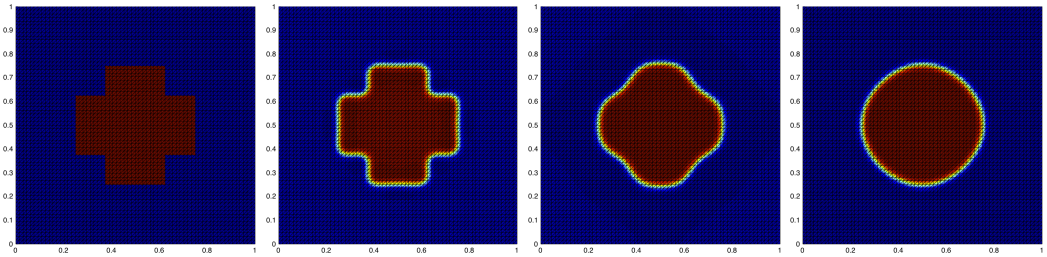

Figure 4.2: Example 2. Computed solutions with $p = 1$ (top) and $p = 2$ (bottom) polynomial approximation degrees. From left to right we report the solution at time $t = 0, 0.001, 0.01, 0.1$.

4.1.2.3 Example 3

The third example regards the spinodal decomposition: the separation of a mixture of two or more components to bulk regions, like the rapidly cooling down of an alloy at high-temperature. The initial piecewise constant datum is chosen uniform randomly with amplitude 0.9. In Figure 4.3 it can be seen the expected behaviour of a spinodal decomposition dynamic. Indeed, the two phases are rapidly unmixing into growing subregions.

(a) $p = 1$

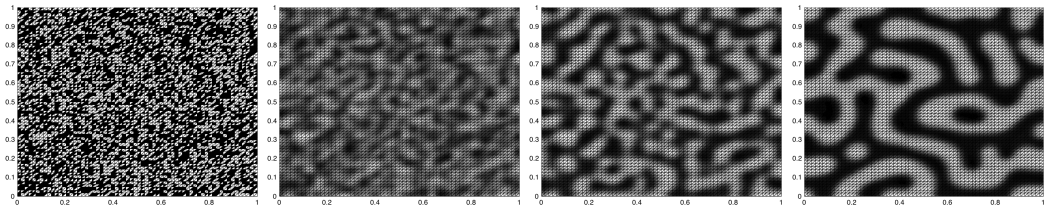

Figure 4.3: Example 3. Computed solutions with $p = 1$ polynomial approximation degree with random initial datum. From left to right we report the solution at time $t = 0, 0.0001, 0.001, 0.01$.

4.1.2.4 Example 4

In this test case we consider the Cahn-Hilliard equation (4.1) and choose the data such that the exact solution is given by

$$u(x, y, t) = \cos(t)\cos(\pi x)\cos(\pi y).$$

We choose $\Delta t = 0.001$, $\gamma = 0.1$ and $\mu = 10$. In Table 4.1 are shown the computed errors as a function of the mesh size h measured in the $L^\infty(0, T; H^1(\Omega))$ and $L^\infty(0, T; L^2(\Omega))$ norms employing $p = 1$ elements.

h	$L^\infty(0, T; H^1(\Omega))$	rate	$L^\infty(0, T; L^2(\Omega))$	rate
1/8	0.254617	-	0.026940	-
1/16	0.102218	1.31	0.008124	1.73
1/32	0.045502	1.16	0.002124	1.93
1/64	0.021994	1.05	0.000537	1.98

Table 4.1: Computed errors and corresponding convergence rates ($\gamma = 0.1$, $\mu = 10$, $\Delta t = 0.001$, $T = 0.1$, $p = 1$).

The computed results are in agreement with the theoretical estimates presented in [49]: linear and quadratic rates are observed in the $L^\infty(0, T; H^1(\Omega))$ and $L^\infty(0, T; L^2(\Omega))$ norms, respectively.

4.2 Multigrid-based solution algorithms

In the rest of this chapter we discuss several numerical startegies to solve the system of non-linear equations arising from the fully DG disctretization of the Cahn-Hilliard problem like the one reported in (4.8) and (4.10). To ease the presentation, we refer to these systems of non-linear equations as to the solution of the following problem: find u_h such that

$$A_h(u_h) = f_h, \tag{4.12}$$

where, for simplicity, we omit the temporal superscript. A general iterative algorithm for a problem of the form (4.12) reads as in Algorithm 1.

Algorithm 1 Solution of (4.12)

Set $k = 0$ and $\mathbf{u}_h^{(0)}$;
repeat
  $\mathbf{u}_h^{(k+1)} = \texttt{solver}(\mathbf{f}_h, \mathbf{u}_h^{(k)}, h)$;
  k=k+1;
until `stopping_criterion`
$\mathbf{u}_h = \mathbf{u}_h^{(k)}$.

The `stopping_criterion` can be taken as a test on the residual, i.e.,

$$\|r_h^{(k+1)}\| = \|A_h(u_h^{(k+1)}) - f_h\| < \epsilon_1$$

or as a criterion on the absolute value of the difference of successive iterations, i.e.,

$$\|u_h^{(k+1)} - u_h^{(k)}\| < \epsilon_1,$$

with $0 < \epsilon_1 \ll 1$.
The module `solver` will be the core of the algorithm and it is composed by an iterative scheme that improves the approximate solution. In the following numerical experiments we employ the latter criterion with $\epsilon_1 = 10^{-6}$. Since the Cahn-Hilliard equation is a non-linear problem we implement two different strategies in the routine `solver`: a classical multigrid procedure applied to the Newton linearization of the problem, namely Newton multigrid strategy (NMG), or a non-linear multigrid procedure, namely Fully Approximation Scheme (FAS). We refer to Appendix A for some useful result on Newton and linear multigrid method that will be used through the chapter.

4.3 FAS algorithm

The generic FAS iteration to solve problem (4.12) reads as described in Algorithm 2.

Algorithm 2 $\mathbf{u}_h^{\text{new}}$=FAS($\mathbf{f}_h$,$\mathbf{u}_h$,$h$)

Pre-smoothing: Apply ν_1 smoothing steps to obtain $\mathbf{u}_h^{pre}$ from $\mathbf{u}_h$;
Compute the defect: $\mathbf{r}_h = \mathbf{f}_h - A_h(\mathbf{u}_h^{pre})$;
Restrict the defect: $\mathbf{r}_{2h} = I_h^{2h}\mathbf{r}_h$;
Restrict the approximation: $\mathbf{u}_{2h} = \tilde{I}_h^{2h}\mathbf{u}_h^{pre}$;
Compute $\mathbf{f}_{2h} = \mathbf{r}_{2h} + A_{2h}(\mathbf{u}_{2h})$;
if $2h$ is the coarsest mesh size **then**
    Linearize and solve $A_{2h}(\mathbf{v}_{2h}) = \mathbf{f}_{2h}$;
else
    $\mathbf{v}_{2h}$=FAS($\mathbf{f}_{2h}$,$\mathbf{u}_{2h}$,$2h$);
end if
Compute the coarse grid correction: $\mathbf{e}_{2h} = \mathbf{v}_{2h} - \mathbf{u}_{2h}$;
Interpolate the correction: $\mathbf{e}_h = I_{2h}^h\mathbf{e}_{2h}$;
Correct the approximation: $\mathbf{u}_h^c = \mathbf{u}_h^{pre} + \mathbf{e}_h$;
Post-smoothing: Apply ν_2 smoothing steps to obtain $\mathbf{u}_h^{\text{new}}$ from $\mathbf{u}_h^c$.

If we have to solve a non-linear problem, as in the Cahn-Hilliard case, the smoothing steps consist in ν_1 or ν_2 applications of an iterative solver applied to the linearized problem. In Algorithm 2 I_h^{2h} and $\tilde{I}_h^{2h}$ are suitable prolongation operators whereas I_{2h}^h is a restriction operator. In particular, in our case, we define I_h^{2h} to be the full-weighted prolongation operator, I_{2h}^h as the transpose of I_h^{2h}, and $\tilde{I}_h^{2h}$ such that it enforces in a weak sense the state equality between the coarse and fine levels, i.e., $\tilde{I}_h^{2h} = (M^{2h})^{-1}N^{2h}$, where M^{2h} is the mass matrix on the coarse grid and $(N^{2h})_{kj} = \int_\Omega \phi_k^{2h}\phi_j^h dx$ (cf. [37]).
We test the FAS algorithm by solving (4.8) on $\Omega = (0,1)^2$ using a sequence of uniform structured triangular meshes with $h = \sqrt{2}/2^n$, $n = 1, ..., 6$. In all the simulation we used as the finest level the grid with $h = \sqrt{2}/2^6$ and we set $\nu_1 = \nu_2 = \nu$ and used piecewise linear element ($p = 1$). We use as a pre- and post-smoother the symmetric Gauss-Seidel algorithm. In the first example, we consider as initial datum the discontinuous cross-shaped function

$$u_h^0 = \begin{cases} 0.95 & \text{if } x \text{ belongs to the cross,} \\ \text{-}0.95 & \text{elsewhere,} \end{cases} \tag{4.13}$$

cf. Figure 4.4 (a).
Where not specified, we assume the time-step $\Delta t = 10^{-6}$, the residual stopping criterion (4.14) with $\epsilon_2 = 10^{-6}$ and $\nu = 6$.
First of all we test the dependency of the number of iterations needed to achieve convergence on the number of the pre- and post-smoothing iterations. In Table 4.2 we report the iteration counts for the first 10 discrete time steps. As expected, the faster scheme in terms of number of FAS iterations are the ones with the larger values of ν. However, large values of ν has a negative effect on the computational cost.

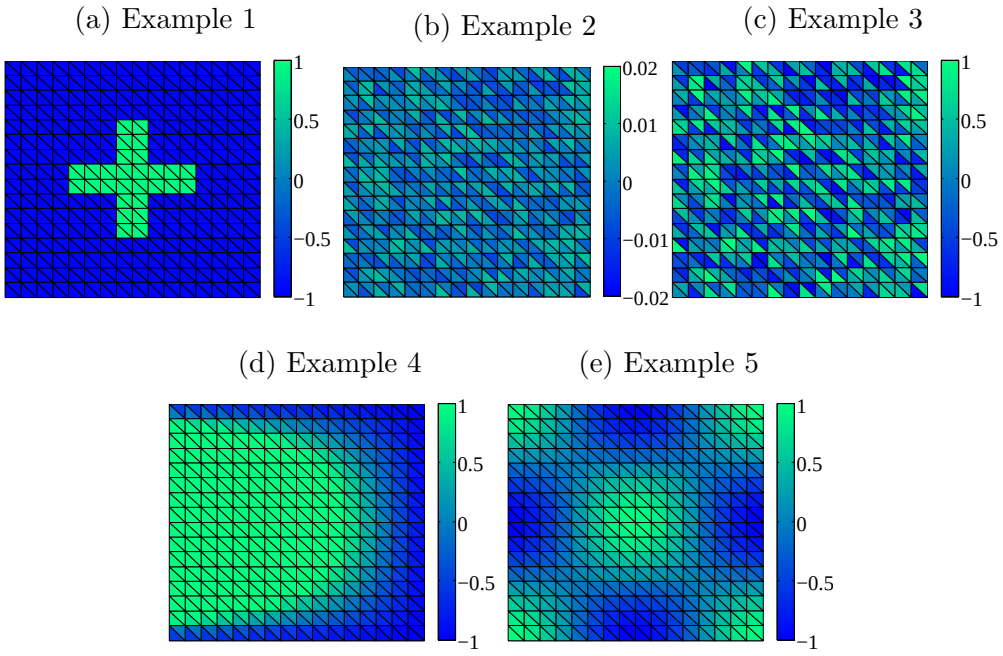

Figure 4.4: Initial data u_h^0 for the test case 1-5.

ν	Discrete time values $t_n = t_0 + n\Delta t,\ n = 1, 2, ..., 10.$									
	$n=1$	$n=2$	$n=3$	$n=4$	$n=5$	$n=6$	$n=7$	$n=8$	$n=9$	$n=10$
5	34	27	24	23	22	22	21	20	20	20
6	31	25	23	21	20	20	19	19	18	18
7	29	24	21	20	19	18	18	17	17	16
8	27	22	20	19	18	17	17	16	16	15
9	26	21	19	18	17	16	16	15	15	15
10	25	20	18	17	16	16	15	15	14	14
11	24	20	18	16	16	15	15	14	14	13

Table 4.2: Number of FAS iterations at different snapshots using different number ν of smoothing steps with initial datum u_h^0 defined in (4.13).

In Table 4.3 we explore the dependency of the FAS algorithm on the number of levels. More precisely, in Table 4.3 we report the FAS iteration counts at different time-step $t_n = t_0 + n\Delta t$ and employing a variable number of levels. We observe that, as expected, the best performance is the one achieved by the two-grid scheme. However, we recall that in this case solving the problem on the coarse level is more expensive than in the other cases.
Next, we investigate the performance of the FAS solver when varying the initial datum. To this aim, in Table 4.4 we report the number of FAS iterations needed to solve (at different time steps) problem (4.8) with the following initial data:

a) the cross-shape u_h^0 defined in (4.13), cf. Figure 4.4 (a);

Number of levels	Discrete time values $t_n = t_0 + n\Delta t,\ n = 1, 2, ..., 10.$									
	$n=1$	$n=2$	$n=3$	$n=4$	$n=5$	$n=6$	$n=7$	$n=8$	$n=9$	$n=10$
5	31	25	23	21	20	20	19	19	18	18
4	31	25	23	21	20	20	19	19	18	18
3	31	26	23	21	21	20	19	19	18	18
2	28	23	20	19	18	18	17	16	16	16

Table 4.3: Number of FAS iterations at different snapshots using $\nu = 6$ and different number of levels with initial datum u_h^0 defined in (4.13).

b) random initial datum u_h^0 with $\max|u_h| \leq 0.01$, cf. Figure 4.4 (b);

c) random initial datum u_h^0 with $\max|u_h| \leq 1$, , cf. Figure 4.4 (c);

d) $u_h^0 = 25((1-x)y(1-y)) - 1$, cf. Figure 4.4 (d);

e) $u_h^0 = \cos(2\pi x)\cos(2\pi y)$, cf. Figure 4.4 (e);

We observe that the number of FAS iterations decreases as n grows up, at least for the first phase of the Cahn-Hilliard problem. This is, for example, the case of the first three data: the discontinuous initial data becomes more regular for increasing values of t_n and the corresponding number of FAS iterations decreases. Afterwards the spinodal decomposition, where the solution changes faster its shape, the successive coarsening phase requires less FAS iterations because the solution changes very slowly due to the different time-length of the process.

Type	Discrete time values $t_n = t_0 + n\Delta t,\ n = 1, 2, ..., 10.$									
	$n=1$	$n=2$	$n=3$	$n=4$	$n=5$	$n=6$	$n=7$	$n=8$	$n=9$	$n=10$
case a	31	25	23	21	20	20	19	19	18	18
case b	23	12	9	8	7	6	6	5	5	4
case c	35	24	21	19	17	16	14	13	13	13
case d	24	21	22	21	21	21	21	20	20	20
case e	20	17	16	16	16	16	16	15	15	15

Table 4.4: Number of FAS iterations at different snapshots using $\nu = 6$, 5 levels and with initial data u_h^0 showed in Figure 4.4.

Finally, we perform some experiments to study the dependency of the FAS algorithm on the size of the time-step. We collect the results in Table 4.5. As expected, we observe that the number of iterations needed to perform a single time-step decreases when a smaller value of Δt is employed. In fact, smaller values of Δt imply that the searched solution is closer to the solution at the previous time-step.

Δt	Discrete time values $t_n = t_0 + n\Delta t,\ n = 1, 2, ..., 10.$									
	$n=1$	$n=2$	$n=3$	$n=4$	$n=5$	$n=6$	$n=7$	$n=8$	$n=9$	$n=10$
10^{-3}	37	31	27	24	22	21	20	19	19	19
10^{-4}	31	25	23	21	20	20	19	19	18	18
10^{-5}	25	23	20	18	17	16	15	15	14	14
10^{-6}	16	16	15	15	14	13	13	13	12	12
10^{-7}	8	7	7	7	7	7	7	7	7	6
10^{-8}	3	3	3	3	3	3	3	3	3	3

Table 4.5: Number of FAS iterations at different snapshots using $\nu = 6$ and different time-step Δt with initial datum u_h^0 defined in (4.13).

4.4 Newton-Multigrid solver

The Newton-Multigrid (NMG) algorithm, reported in Algorithm 3, solves the linearization of the problem with the MG method that is described in details in Appendix A.2.

Algorithm 3 $\mathbf{u}_h^{\text{new}}$=NMG($\mathbf{f}_h$,$\mathbf{u}_h$,$h$)

Linearize problem (4.12) to obtain the linear problem $A_h^{lin} v_h = \mathbf{f}_h^{lin}$;
Set $i = 0$ and $\mathbf{u}_h^{(0)} = \mathbf{u}_h$;
repeat
  $\mathbf{u}_h^{(i+1)} = \text{MG}(\mathbf{f}_h^{lin}, \mathbf{u}_h^{(i)}, h)$;
  $i = i + 1$;
until `stopping_criterion`
$\mathbf{u}_h^{\text{new}} = \mathbf{u}_h^{(i)}$.

For the `stopping_criterion` there will be several different choices. The classical one is test the normalized residual, i.e.,

$$\|r_h^{(i)}\| = \|f_h^{lin} - A_h^{lin} u_h^{(i)}\| < \epsilon_2 \|f_h^{lin}\|, \text{ with } 0 < \epsilon_2 \ll 1. \tag{4.14}$$

A possibility to recover the quadratic convergence of inexact-Newton strategy can be reached satisfying the following condition

$$\|J_F(u^{(i)})(u^{(i+1)} - u^{(i)}) + F(u^{(i)})\| \leq \eta_i \|F(u^{(i)})\|, \tag{4.15}$$

The behaviour of the inexact Newton method is well known in literature (see Appendix A.1). Setting η_i as

$$\eta_i = \begin{cases} \eta_{max} & i = 0, \\ \min(\eta_{max}, \tilde{\gamma}\|r_h^{(i)}\|^2/\|r_h^{(i-1)}\|^2) & i \geq 1 \text{ and } \tilde{\gamma}\eta_{i-1}^2 \leq 0.1, \\ \min(\eta_{max}, \max(\tilde{\gamma}(\|r_h^{(i)}\|^2/\|r_h^{(i-1)}\|^2, \tilde{\gamma}\eta_{i-1}^2)) & i \geq 1 \text{ and } \tilde{\gamma}\eta_{i-1}^2 > 0.1, \end{cases} \tag{4.16}$$

with $\tilde{\gamma} = 0.9$ and $\eta_{max} = 0.9999$, guarantees the second order of convergence for NMG, cf. [32].

We perform several numerical experiments to study the performance of NMG algorithm. In all the subsequent tables, we employ the notation x/y where x refers to the total number of MG cycles to perform a single time-step and y is the total number of Newton linearizations performed to satisfy the inner criterion within the Newton algorithm. In all the following experiments we set $\nu_1 = \nu_2 = 6$. We test the NMG algorithm by solving (4.8) on $\Omega = (0,1)^2$ using the same set of meshes defined for the FAS examples. In the first test case we consider (4.13) as initial datum, cf. also Figure 4.4 (a). We also set $\Delta t = 10^{-6}$ and $p = 1$. In Table 4.6 we report the computed results employing the adaptive criteria (4.15). As in the FAS case, it seems that using fewer levels requires less iterations to satisfy the stopping condition.
In Table 4.7 we study the relation between the number of multigrid iterations and Newton linearizations needed to satisfy the stopping criteria (4.14) on the normalized residual with different values of the tolerance and different number of levels. We point out that using smaller values of the tolerance requires more Newton linearization but smaller number of multigrid iterations.

Number of levels	Discrete time values $t_n = t_0 + n\Delta t,\ n = 1, 2, ..., 10.$									
	$n=1$	$n=2$	$n=3$	$n=4$	$n=5$	$n=6$	$n=7$	$n=8$	$n=9$	$n=10$
5	40/20	34/11	31/8	29/7	28/7	26/7	25/7	24/7	24/7	23/7
4	40/20	34/11	31/8	29/7	28/7	26/7	25/7	24/7	24/7	23/7
3	39/19	33/11	30/7	27/7	26/7	25/7	24/7	23/7	23/7	22/7
2	29/17	24/10	22/7	20/7	19/7	19/7	18/7	17/7	17/7	17/7

Table 4.6: Number of NMG iterations at different snapshots using different number of levels. We employ the adaptive stopping criterion (4.15) with η defined by (4.16) with initial datum u_h^0 defined in (4.13)

ϵ_2	Discrete time values $t_n = t_0 + n\Delta t,\ n = 1, 2, ..., 10.$									
	$n=1$	$n=2$	$n=3$	$n=4$	$n=5$	$n=6$	$n=7$	$n=8$	$n=9$	$n=10$
10^{-6}	105/4	87/4	76/4	65/3	61/3	59/3	56/3	55/3	53/3	51/3
10^{-5}	83/4	65/4	56/4	50/3	46/3	43/3	41/3	39/3	37/3	36/3
10^{-4}	67/10	51/8	44/9	39/8	37/9	34/8	32/9	30/9	29/8	27/8
10^{-3}	53/16	42/16	36/15	32/15	30/16	27/15	26/14	24/13	23/14	22/13
10^{-2}	44/23	36/22	31/22	28/21	26/20	25/20	24/19	23/19	23/19	22/19
10^{-1}	40/29	34/29	30/27	28/26	27/26	25/24	24/23	23/22	23/22	22/22

Table 4.7: Number of NMG iterations at different snapshots using 5 levels with initial datum u_h^0 defined in (4.13). We employ (4.14) as a stopping criterion using different values of ϵ_2.

We also test the performance of the NMG algorithm depending on the choice of

the initial datum. In Table 4.8 we report the results where we employed the same initial data employed in Table 4.4.

Type	Discrete time values $t_n = t_0 + n\Delta t,\ n = 1, 2, ..., 10.$									
	$n = 1$	$n = 2$	$n = 3$	$n = 4$	$n = 5$	$n = 6$	$n = 7$	$n = 8$	$n = 9$	$n = 10$
case a	40/20	34/11	31/8	29/7	28/7	26/7	25/7	24/7	24/7	23/7
case b	30/11	18/7	14/6	11/5	10/5	8/4	7/3	7/3	6/3	6/3
case c	47/24	35/13	30/7	27/7	24/7	22/7	21/7	20/7	19/7	18/7
case d	28/13	28/9	28/9	28/8	28/8	27/8	27/8	27/7	28/7	28/7
case e	25/13	23/7	23/7	22/7	21/7	21/7	20/7	20/7	20/7	20/7

Table 4.8: Number of NMG iterations at different snapshots using 5 levels and with initial data u_h^0 showed in Figure 4.4. We employ (4.14) as a stopping criterion using different values of $\epsilon_2 = 10^{-6}$.

We notice that, for each initial condition, the number of Newton linearizations and multigrid iterations needed to satisfy the stopping criterion decreases as t_n increases, at least for the time interval considered here. In Table 4.9 we collect the number of iterations needed to perform the first 10 time-steps with different values of Δt. By comparing those values with the ones reported in Table 4.5 we notice that, for smaller values of Δt, the number of FAS and NMG cycles are similar. On the other hand, for larger values of Δt, the NMG solver needs a larger number of linearizations and MG cycles.

Δt	Discrete time values $t_n = t_0 + n\Delta t,\ n = 1, 2, ..., 10.$									
	$n = 1$	$n = 2$	$n = 3$	$n = 4$	$n = 5$	$n = 6$	$n = 7$	$n = 8$	$n = 9$	$n = 10$
10^{-3}	58/23	52/7	45/7	40/7	36/7	32/7	30/7	29/7	27/6	27/6
10^{-4}	40/20	34/11	31/8	29/7	28/7	26/7	25/7	24/7	24/7	23/7
10^{-5}	28/17	26/14	23/11	22/10	20/9	19/8	18/8	18/8	18/8	17/8
10^{-6}	17/13	17/13	16/12	15/11	15/11	14/10	14/10	14/10	13/10	13/9
10^{-7}	8/8	7/7	7/7	7/7	7/7	7/7	7/7	7/7	7/7	6/6
10^{-8}	3/3	3/3	3/3	3/3	3/3	3/3	3/3	3/3	3/3	3/3

Table 4.9: Number of NMG iterations at different snapshots using 5 levels and different values of Δt with initial datum u_h^0 defined in (4.13). We employ (4.14) as a stopping criterion using different values of $\epsilon_2 = 10^{-6}$.

5

Collective block Gauss-Seidel smoothers

5.1 Motivation

This chapter is devoted to the introduction and testing of a new set of smoothers to accelerate the convergence of the FAS algorithm, cf. Algorithm 2. To validate the performance of the new class of smoothers we will employ the Local Fourier Analysis (LFA) approach, cf. [67].

From Algorithm 2, it is clear that at each FAS iteration we have to approximate the solution of a non-linear problem by an inexact Newton-like algorithm which requires $\nu_1 + \nu_2$ iterations of a classical linear smoother (e.g., Jacobi or Gauss-Seidel). This indeed represent the bottleneck of the whole algorithm. Therefore, to accelerate the convergence of the FAS algorithm in the following we incorporate and test different type of smoothers called collective block Gauss-Seidel smoothers.

The main difficulty in constructing effective smoothers is how to group together the degrees of freedom in such a way the resulting blocks guarantee that the convergence is as fast as possible. The local blocks that we consider in the following are composed by the (DG) degrees of freedom associated to one or more elements (element-wise blocks) or by the degrees of freedom across one or more interfaces (interface-wise blocks). Moreover, we recall that in discontinuous methods the boundary conditions are always imposed weakly. For this reason we will introduce suitable "ghost" points for any boundary degree of freedom such that the smoother can deal with the boundary unknowns as internal points.

Remark 5.1 *All the following results can be extended to higher-order odd polynomial as in [44].*

5.2 Definition of the smoother for linear problem

As a first step, we will introduce and test our smoothers on a one dimensional simplify (toy) model problem, namely the diffusion-reaction equation:

$$\begin{cases} -u'' + au &= f \quad \text{in } \Omega, \\ u &= 0 \quad \text{on } \Gamma_D, \\ \partial_n u &= 0 \quad \text{on } \Gamma_N, \end{cases} \tag{5.1}$$

where $a \geq 0$ and where $\Gamma_D \cap \Gamma_N = \emptyset$ and $\overline{\Gamma}_D \cup \overline{\Gamma}_N = \partial\Omega$. Moreover, in the case of $a = 0$, we set $\Gamma_D \neq \emptyset$ to guarantee the uniqueness of the solution.

Let $\mathcal{T}_h$ be a uniform partition of Ω into disjoint open intervals K such that $\overline{\Omega} = \cup_{i=1}^{n} \overline{K}_i$. Let h be the mesh-size of the partition $\mathcal{T}_h$ and $\mathcal{E}_h$ be the set of all points e of $\mathcal{T}_h$. Furthermore, we define by $\mathcal{E}_h^0$ the set of all internal points, i.e.,

$$\mathcal{E}_h^0 = \{e \in \mathcal{E}_h \ : \ e \cap \partial\Omega = \emptyset\},$$

and by $\mathcal{E}_h^{\Gamma_D}$ the set of Dirichlet points, i.e.,

$$\mathcal{E}_h^{\Gamma_D} = \{e \in \mathcal{E}_h \ : \ e \cap \Gamma_D \neq \emptyset\}.$$

We set V_h^1 as

$$V_h^1 = \{v_h \in L^2(\Omega) \ : \ (v_h)_{|K} \in \mathbb{P}^1(K) \ \ \forall K \in \mathcal{T}_h\}.$$

The DG approximation of problem (5.1) reads as: *Find* $u_h \in V_h^1$ *such that*

$$\mathcal{B}_h(u_h, v_h) + a\ (u_h, v_h)_{L^2(\Omega)} = (f, v_h)_{L^2(\Omega)} \qquad \forall v_h \in V_h^1,$$

where $\mathcal{B}_h(\cdot,\cdot)$ is defined as

$$\begin{aligned} \mathcal{B}_h(v_h, w_h) = &\sum_{K \in \mathcal{T}_h} \int_K v_h' w_h' dx \\ &- \sum_{e \in \mathcal{E}_h^0 \cup \mathcal{E}_h^{\Gamma_D}} \left(\{v_h'\}_{|e} [w_h]_{|e} + \{w_h'\}_{|e} [v_h]_{|e} - \sigma [v_h]_{|e} [w_h]_{|e} \right). \end{aligned} \tag{5.2}$$

Let $n = \dim(V_h^1)/2$ and let $\{\phi_i\}_{i=1,..,2n}$ be an admissible set of basis function for V_h^1. We define the stiffness and the mass matrices by

$$S_{ij} = \mathcal{B}_h(\phi_i, \phi_j) \qquad \text{and} \qquad M_{ij} = (\phi_i, \phi_j)_{L^2(\Omega)}, \qquad 0 \leq i, j \leq 2n. \tag{5.3}$$

Writing

$$u_h = \sum_{i=1}^{2n} u_i \phi_i,$$

problem (5.1) becomes: *Find* $\boldsymbol{u} \in \mathbb{R}^{2n}$ *such that*

$$A\mathbf{u} = \mathbf{f}, \tag{5.4}$$

with $\mathbf{u} = [u_1, ..., u_{2n}]^T$ *and* $A = (S + aM)$.

We now present some collective block Gauss-Seidel smoothers for the linear system (5.4). Let us suppose to number from left to the right the elements K and the interface points e of $\mathcal{T}_h$. We also define I as the set of all degrees of freedom of the space V_h^1.
The first collective smoother that we consider is based on element-wise blocks. Let $s \geq 1$ the number of elements involved in a single smoother block. For any $i = 1, ..., n - s + 1$ we define $I_s(K_i) \subset I$ as the set of degrees of freedom that belong to the elements K_i, $K_{i+1}, ...,$ K_{i+s-1}, cf. Figure 5.1 (left) for a sketch in the case $s = 1, 2, 3$.

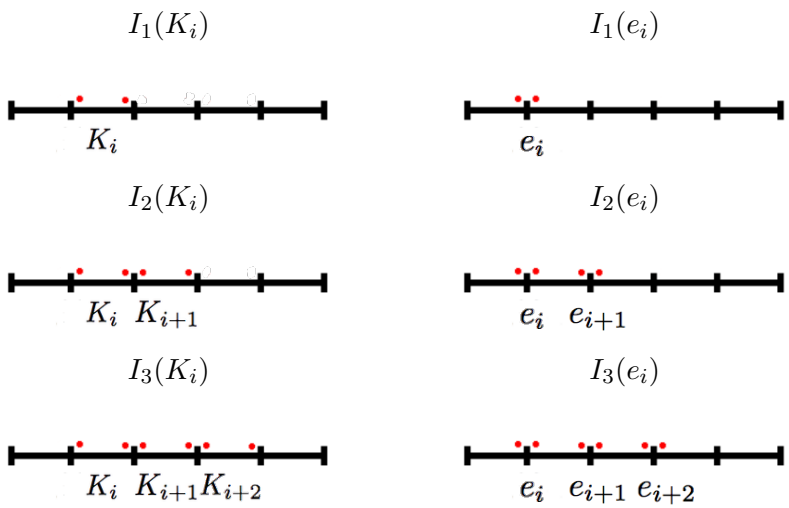

Figure 5.1: Examples of the sets $I_s(K_i)$ (left) and $I_s(e_i)$ (right) for $s = 1, 2, 3$.

Then, at each iteration for $i = 1, ...n-s+1$, we update (sequentially) only the unknowns $\mathbf{u}_{I_s(K_i)}$ associated to the degrees of freedom in $I_s(K_i)$. More precisely, for fixed values of i between 1 and $n - s + 1$, we subdivide the set I into three subsets $I_s^-(K_i)$, $I_s(K_i)$, $I_s^+(K_i)$, where $I_s^-(K_i)$ ($I_s^+(K_i)$) is the set of degrees of freedom that belong to the elements K_j with $j < i$ ($j \geq i + s$, respectively), cf. Figure 5.2 for $s = 2$.

With the above notation, system (5.4) can be rewritten as

$$\begin{bmatrix} A_{I_s^-(K_i),I_s^-(K_i)} & A_{I_s^-(K_i),I_s(K_i)} & A_{I_s^-(K_i),I_s^+(K_i)} \\ A_{I_s(K_i),I_s^-(K_i)} & A_{I_s(K_i),I_s(K_i)} & A_{I_s(K_i),I_s^+(K_i)} \\ A_{I_s^+(K_i),I_s^-(K_i)} & A_{I_s^+(K_i),I_s(K_i)} & A_{I_s^+(K_i),I_s^+(K_i)} \end{bmatrix} \begin{bmatrix} \mathbf{u}_{I_s^-(K_i)} \\ \mathbf{u}_{I_s(K_i)} \\ \mathbf{u}_{I_s^+(K_i)} \end{bmatrix} = \begin{bmatrix} f_{I_s^-(K_i)} \\ f_{I_s(K_i)} \\ f_{I_s^+(K_i)} \end{bmatrix}.$$

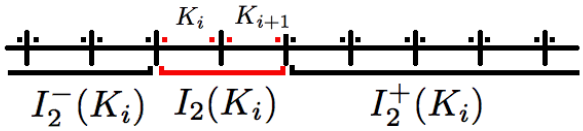

Figure 5.2: Example of the sets $I_2^-(K_i)$, $I_2(K_i)$, $I_2^+(K_i)$.

Then, for each $i = 1, \ldots, n - s + 1$, we update the unknowns $\mathbf{u}_{I_s(K_i)}$ as described in Algorithm 4, where the element-wise collective Gauss-Seidel ($ECGS$) algorithm is reported.

Algorithm 4 (One iteration of the $ECGS$ algorithm for Laplace problem)
$\mathbf{u}^{new} = ECGS(\mathbf{u}, s)$

for $i = 1, \ldots, n - s + 1$ **do**
  Solve $A_{I_s(K_i),I_s(K_i)}\ \tilde{\mathbf{u}}_{I_s(K_i)} = \mathbf{f}_{I_s(K_i)} - A_{I_s(K_i),I_s^-(K_i)}\ \mathbf{u}_{I_s^-(K_i)} - A_{I_s(K_i),I_s^+(K_i)}\ \mathbf{u}_{I_s^+(K_i)}$;
  Update $\mathbf{u} = [\mathbf{u}^T_{I_s^-(K_i)}, \tilde{\mathbf{u}}^T_{I_s(K_i)}, \mathbf{u}^T_{I_s^+(K_i)}]^T$.
end for
Set $\mathbf{u}^{new} = \mathbf{u}$;

We can proceed in an analogous manner and grouping the unknowns in an interface-wise manner, to obtain the interface-wise collective Gauss-Seidel ($ICGS$). More precisely, in this case we define $I_s(e_i)$ as the set of degrees of freedom that belong to the interface e_i, e_{i+1}, ..., e_{i+s-1} and, as before, we divide the remaining degrees of freedom into two sets called $I_s^{\pm}(e_i)$ as shown in Figure 5.3.

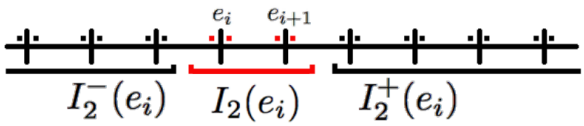

Figure 5.3: Example of the sets $I_2^-(e_i)$, $I_2(e_i)$, $I_2^+(e_i)$.

As before, for any $i = 1, \ldots, n-s+2$, we update only the unknowns associated to the degrees of freedom in $I_s(e_i)$ as described in Algorithm 5.

In the next section we generalize the $ECGS$ and $ICGS$ smoothers to the case where the system of equations result from a fully discretization of the CH equation.

Algorithm 5 (One iteration of the $ICGS$ algorithm for Laplace problem)
$\mathbf{u}^{new} = ICGS(\mathbf{u}, s)$

for $i = 1, \ldots, n - s + 2$ **do**
  Solve $A_{I_s(e_i),I_s(e_i)}\ \tilde{\mathbf{u}}_{I_s(e_i)} = \mathbf{f}_{I_s(e_i)} - A_{I_s(e_i),I_s^-(e_i)}\ \mathbf{u}_{I_s^-(e_i)} - A_{I_s(e_i),I_s^+(e_i)}\ \mathbf{u}_{I_s^+(e_i)}$;
  Update $\mathbf{u} = [\mathbf{u}^T_{I_s^-(K_i)}, \tilde{\mathbf{u}}^T_{I_s(K_i)}, \mathbf{u}^T_{I_s^+(K_i)}]^T$.
end for
Set $\mathbf{u}^{new} = \mathbf{u}$;

5.3 Definition of the smoothers for the CH problem

Let us consider the one dimensional Cahn-Hilliard problem. Let $\Omega \subset \mathbb{R}$ and let $T > 0$ be the final time. The Cahn-Hilliard problem in one dimension reads as: *For any* $t \in (0, T]$, *find* $\{u(\cdot, t), w(\cdot, t)\} \in H^1(\Omega) \times H^1(\Omega)$, *such that*

$$\begin{cases} \partial_t u &= w'' & \text{in } \Omega \times (0, T], \\ w &= u^3 - u - \gamma^2 u'' & \text{in } \Omega \times (0, T], \\ \partial_n u &= \partial_n w = 0 & \text{on } \partial\Omega \times (0, T], \\ u(\cdot, 0) &= u_0(\cdot) & \text{in } \Omega. \end{cases} \tag{5.5}$$

The discontinuous Galerkin semi-discretization of problem (5.5) reads as: *For any* $t \in (0, T]$, *find* $\{u_h(\cdot, t), w_h(\cdot, t)\} \in V_h^1 \times V_h^1$, *such that*

$$\begin{cases} (\partial_t u_h, \eta_h)_{L^2(\Omega)} + \mathcal{B}_h(w_h, \eta_h) = 0 & \forall \eta_h \in V_h^1, \\ (w_h, \eta_h)_{L^2(\Omega)} = ((u_h)^3 - u_h, \eta_h)_{L^2(\Omega)} + \gamma^2 \mathcal{B}_h(u_h, \eta_h) & \forall \eta_h \in V_h^1, \\ u_h(\cdot, 0) = \Pi_h u_0(\cdot), \end{cases} \tag{5.6}$$

where the projection operator $\Pi(\cdot)$ *is the one dimensional counterpart of (4.7) and* $\mathcal{B}_h(\cdot, \cdot)$ *is defined as in* (5.2) *with* $\mathcal{E}_h^{\Gamma_D} = \emptyset$.

Let $0 = t_0 < t_1 < ... < t_N = T$ be the uniform partition of $[0, T]$ with time-step $\Delta t = T/N$. Then, we consider the fully-discretization of the problem using the one dimensional version of implicit Euler method (4.8) and convex-splitting method (4.10).

An equivalent form of the one dimensional implicit Euler discretization (4.8) of Cahn-Hilliard problem reads as: *Find* $\mathbf{v} = \left[\mathbf{u}^T, \mathbf{w}^T\right]^T \in \mathbb{R}^{2n \times 2n}$ *such that*

$$A\mathbf{v} + L(\mathbf{v}) = \mathbf{f}, \tag{5.7}$$

where

$$A = \begin{pmatrix} M/\Delta t & S \\ \gamma^2 S - M & -M \end{pmatrix},$$

$$L(\mathbf{v}) = [0, ..., 0, (u_h^3, \phi_1)_{L^2(\Omega)}, ..., (u_h^3, \phi_{2n})_{L^2(\Omega)}]^T \text{ and } \mathbf{f} = [M\mathbf{u}/\Delta t, 0, ..., 0].$$

On the other hand, the one dimensional fully discretized problem with convex-splitting method becomes: *Find* $\mathbf{v} \in \mathbb{R}^{2n\times 2n}$ *such that it satisfies (5.7) with*

$$A = \begin{pmatrix} M/\Delta t & S \\ \gamma^2 S & -M \end{pmatrix},$$

$$L(\mathbf{v}) = [0, ..., 0, (u_h^3, \phi_1)_{L^2(\Omega)}, ..., (u_h^3, \phi_{2n})_{L^2(\Omega)}]^T \text{ and } \mathbf{f} = [M\mathbf{u}/\Delta t, M\mathbf{u}].$$

Next we introduce the matrix form for the linearized Cahn-Hilliard problem. To apply the Newton linearization to the one dimensional version of (4.9) and (4.10), we define the matrix

$$\tilde{L}(\mathbf{v}) = \left[\begin{array}{c|ccc} 0_{2n\times 2n} & \multicolumn{3}{c}{0_{2n\times 2n}} \\ \hline 0_{2n\times 2n} & (3(u_h)^2\phi_1, \phi_1)_{L^2(\Omega)} & \cdots & (3(u_h)^2\phi_{2n}, \phi_1)_{L^2(\Omega)} \\ & \vdots & \ddots & \vdots \\ & (3(u_h)^2\phi_1, \phi_{2n})_{L^2(\Omega)} & \cdots & (3(u_h)^2\phi_{2n}, \phi_{2n})_{L^2(\Omega)} \end{array}\right]$$

and the vector

$$\ell(\mathbf{v})_j = (2(u_h)^3, \phi_j)_{L^2(\Omega)},$$

for $j = 1, ..., 2n$. An iteration of the linearized Cahn-Hilliard problem reads as: *Let* $\tilde{\mathbf{v}}$ *be an approximate solution of problem (5.7), find* $\mathbf{v} \in \mathbb{R}^{2n\times 2n}$ *such that*

$$\left(A + \tilde{L}(\tilde{\mathbf{v}})\right)\mathbf{v} = \mathbf{f} + \ell(\tilde{\mathbf{v}}), \tag{5.8}$$

where A and $\mathbf{f}$ are defined depending on the time-discretization scheme used.

The linear system (5.8) can be associated to the weak formulation of the following prototype problem

$$\begin{cases} v - bu'' &= f, \\ -cv'' + dv - u &= g, \end{cases} \tag{5.9}$$

where $b, c \in \mathbb{R}^+$, $d \in \mathbb{R}$ and f, g are suitable functions. In particular, we have the following correspondences: b represents the time-step Δt, c is the interface parameter γ^2 and d can be interpreted as a linearization parameter.

Assumption 5.1 *Let the solution of Cahn-Hilliard problem (4.2) belong to the interval* $[-1, 1]$.

This condition is reasonable, especially when the initial datum is random uniformly distributed with amplitude less than 1. With the Assumption 5.1, the parameter d belongs to $[-1, 2]$ when we use the implicit Euler time discretization, otherwise, in convex-splitting case, d belongs to $[0, 3]$. We remark that also the discrete solution belongs to the corresponding interval if the time-step utilized is small enough.

Next, we extend the Gauss-Seidel smoother to the linearized Cahn-Hilliard problem (5.8). The two main changes are the collective strategy and the local linearization. The collective approach handle, at the same time, all the variables referred to the block of degrees of freedom.

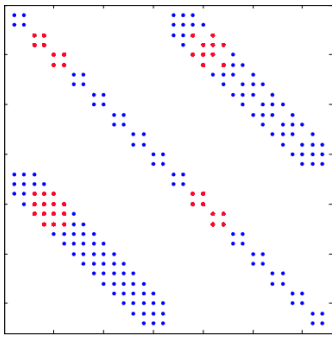

Figure 5.4: Example of components (red points) of the operator $A + \tilde{L}(\tilde{\mathbf{v}})$ that composed the local matrix of the smoother.

To simplify the notation, for $i = 1, ..., n - s + 1$, we define

$$\tilde{I}_s(K_i) = I_s(K_i) \cup (I_s(K_i) + 2n)\,,$$

i.e., $\mathbf{v}_{\tilde{I}_s(K_i)} = [\mathbf{u}^T_{I_s(K_i)}, \mathbf{w}^T_{I_s(K_i)}]$. In a similar manner, we define the set $\tilde{I}^{\pm}_s(K_i)$ and we extend all the definition for e_i, $i = 1, ..., n - s + 2$.
Since we have a non-linear problem at each iteration i we solve the local problem after the Newton linearization. The element-wise and interface-wise smoothers for Cahn-Hilliard problem (5.5) read as in Algorithm 6 and Algorithm 7, respectively.

Algorithm 6 (One iteration of the *ECGS* algorithm for Cahn-Hilliard problem) $\mathbf{v}^{new} = ECGS(\mathbf{v}, s)$

for $i = 1, \ldots, n - s + 1$ **do**
  Solve $A_{\tilde{I}_s(K_i),\tilde{I}_s(K_i)}\ \tilde{\mathbf{v}}_{\tilde{I}_s(K_i)} = \mathbf{f}_{\tilde{I}_s(K_i)} - A_{\tilde{I}_s(K_i),\tilde{I}^-_s(K_i)}\mathbf{v}_{\tilde{I}^-_s(K_i)} - A_{\tilde{I}_s(K_i),\tilde{I}^+_s(K_i)}\ \mathbf{v}_{\tilde{I}^+_s(K_i)}$;
  Update $\mathbf{v} = [\mathbf{v}^T_{\tilde{I}^-_s(K_i)}, \tilde{\mathbf{v}}^T_{\tilde{I}_s(K_i)}, \mathbf{v}^T_{\tilde{I}^+_s(K_i)}]^T$.
end for
Set $\mathbf{v}^{new} = \mathbf{v}$;

5.4 LFA approach

We want to investigate the efficiency of the proposed smoothers employing the LFA approach. For the sake of simplicity, we will consider the simplest case of non-overlapping blocks, i.e., $s = 1$. The LFA is usually employed for linear

Algorithm 7 (One iteration of the $ICGS$ algorithm for Cahn-Hilliard problem) $\mathbf{v}^{new} = ICGS(\mathbf{v}, s)$

for $i = 1, \ldots, n - s + 2$ **do**
  Solve $A_{\tilde{I}_s(e_i),\tilde{I}_s(e_i)}\ \tilde{\mathbf{v}}_{\tilde{I}_s(e_i)} = \mathbf{f}_{\tilde{I}_s(e_i)} - A_{\tilde{I}_s(e_i),\tilde{I}_s^-(e_i)}\ \mathbf{v}_{\tilde{I}_s^-(e_i)} - A_{\tilde{I}_s(e_i),\tilde{I}_s^+(e_i)}\ \mathbf{v}_{\tilde{I}_s^+(e_i)}$;
  Update $\mathbf{v} = [\mathbf{v}^T_{\tilde{I}_s^-(e_i)}, \tilde{\mathbf{v}}^T_{\tilde{I}_s(e_i)}, \mathbf{v}^T_{\tilde{I}_s^+(e_i)}]^T$.
end for
Set $\mathbf{v}^{new} = \mathbf{v}$;

system of equations, but in our case, the discretized Cahn-Hilliard equation lead to a non-linear system of equations. Nevertheless, within the FAS algorithm it is necessary to solve a linearized version of the original problem. Thus, the application of the LFA approach makes sense in this framework.

We point out that the LFA technique is performed supposing that $\Omega = \mathbb{R}$ and it has been meshed with a uniform triangulation $\mathbb{Z}_h = \{jh \ : \ j \in \mathbb{Z}\}$. Before presenting the LFA approach we have to introduce the infinite-matrix A_h known as Toeplitz matrix and some useful properties.

5.4.1 Fourier analysis for a block-Toeplitz matrix A_h

Let A_h be a infinite block-Toeplitz matrix of the form

$$A_h = \begin{bmatrix} \ddots & \ddots & \ddots & \ddots & \ddots & \ddots \\ \ddots & \mathbf{a}_0 & \mathbf{a}_{-1} & \mathbf{a}_{-2} & \mathbf{a}_{-3} & \ddots \\ \ddots & \mathbf{a}_1 & \ddots & \ddots & \ddots & \ddots \\ \ddots & \ddots & \ddots & \ddots & \mathbf{a}_{-1} & \ddots \\ \ddots & \mathbf{a}_3 & \mathbf{a}_2 & \mathbf{a}_1 & \mathbf{a}_0 & \ddots \\ \ddots & \ddots & \ddots & \ddots & \ddots & \ddots \end{bmatrix},$$

where $(A_h)_{mj} = \mathbf{a}_{m-j} \in \mathbb{R}^2 \times \mathbb{R}^2$, $m, j \in \mathbb{Z}$. We define the basis of elementary modes as $e_{h,\theta}(jh) = e^{ijh\theta}$ for all $\theta \in \mathbb{T}_h \equiv [-\pi/h, \pi/h]$ and the space of the trial and test piecewise linear functions by X_h^1. The discrete Fourier transform of a Toeplitz operator A_h is defined by

$$\widehat{A_h}(\theta) = \sum_{k \in \mathbb{Z}} \mathbf{a}_k e^{-ikh\theta} \qquad \forall \theta \in \mathbb{T}_h.$$

It has been proved in [44] that the following identity holds:

$$\sum_{j \in \mathbb{Z}} \mathbf{a}_{m,j} e_{h,\theta}(jh) = \widehat{A_h}(\theta) e_{h,\theta}(mh) \qquad \forall \theta \in \mathbb{T}_h.$$

We denote by $W_h(\theta)$ the matrix of eigenvectors $\mathbf{w}(\theta)$ of $\widehat{A_h}(\theta)$ and by $\Lambda_h(\theta)$ the diagonal matrix composed by the eigenvalues of $\widehat{A_h}(\theta)$, i.e.,

$$\widehat{A_h}(\theta)W_h(\theta) = W_h(\theta)\Lambda_h(\theta).$$

Setting $(W_h \otimes e_{h,\theta})(jh) = W_h(\theta)e^{ijh\theta}$ we have

$$A_h(W_h \otimes e_{h,\theta}) = \widehat{A_h}(\theta)(W_h \otimes e_{h,\theta}) = (W_h \otimes e_{h,\theta})\Lambda_h(\theta). \tag{5.10}$$

Therefore, the eigenvectors of A_h are the columns $\mathbf{w}(\theta)e_{h,\theta}(mh)$ of $(W_h \otimes e_{h,\theta})$ and the eigenvalues of A_h and $\widehat{A_h}(\theta)$, $\theta \in \mathbb{T}_h$, are the same.

For a linear system

$$A_h\mathbf{x} = \mathbf{f} \tag{5.11}$$

with a A_h Toeplitz matrix, we consider the iterative algorithm

$$\mathbf{x}^{k+1} = \mathbf{x}^k - B_h(A_h\mathbf{x}^k - \mathbf{f}),$$

where B_h is an approximate inverse of A_h. We define the amplification matrix by $N_h^S = I - B_hA_h$. Decomposing A_h as

$$A_h = L + D + U,$$

where L, D and U are the strictly block-lower, block-diagonal and strictly block-upper parts of A_h, respectively, the Fourier transform of the Gauss-Seidel amplification operator becomes

$$\widehat{N_h^S}(\theta) = -(\widehat{D} + \widehat{L})^{-1}\widehat{U}.$$

It easy to prove that the Fourier transform of L, D and U are given by

$$\widehat{L} = Le^{-i\theta h}, \qquad \widehat{D} = D, \qquad \widehat{U} = Ue^{i\theta h},$$

respectively.

Remark 5.2 *If A_h is a Toeplitz matrix then N_h^S is a Toeplitz matrix as well [45].*

Next, we recall the structure of the SIPG Toeplitz stiffness matrix with penalty parameter μ. From (5.3) and the definition (5.2) of the DG bilinear form $\mathcal{B}_h$ we obtain the blocks corresponding to the stencil of element-wise stiffness matrix S_h and the element-wise mass matrix M_h:

$$S_h = [\mathbf{s}_1|\mathbf{s}_0|\mathbf{s}_{-1}] = \frac{1}{h}\left[\begin{array}{cc|cc|cc} -1/2 & 1-\mu & \mu & 0 & -1/2 & 0 \\ 0 & -1/2 & 0 & \mu & 1-\mu & -1/2 \end{array}\right]$$

and

$$M_h = [\mathbf{m}_0] = h\left[\begin{array}{cc} 1/3 & 1/6 \\ 1/6 & 1/3 \end{array}\right].$$

Similarly, for the interface-wise approach the stencils for the matrices S_h and M_h are defined by

$$S_h = [\mathbf{s}_1|\mathbf{s}_0|\mathbf{s}_{-1}] = \frac{1}{h}\left[\begin{array}{cc|cc|cc} -1/2 & 0 & \mu & 1-\mu & -1/2 & 0 \\ 0 & -1/2 & 1-\mu & \mu & 0 & -1/2 \end{array}\right]$$

and

$$M_h = [\mathbf{m}_1|\mathbf{m}_0|\mathbf{m}_{-1}] = h\left[\begin{array}{cc|cc|cc} 0 & 1/6 & 1/3 & 0 & 0 & 0 \\ 0 & 0 & 0 & 1/3 & 1/6 & 0 \end{array}\right],$$

respectively.

5.4.2 Spectral analysis

In this section, our aim is to analyze the action of the proposed smoothers searching the eigenvalues of N_h^S by computing the eigenvalues of its Fourier transform $\widehat{N_h^S}(\theta)$ and using the relation (5.10). In particular, we want to verify that the spectral radius $\rho(\theta)$ of the amplification matrix $\widehat{N_h^S}(\theta)$ is always less than or equal to 1, for any $\theta \in \mathbb{T}_h$. In the classical smoothing framework, when the spectral radius of the iteration matrix is equal to 1 the method does not converge. On the other hand, the LFA allows the eigenvalue $\lambda(\theta)$ associated to the choice $\theta = 0$ to have modulus equal to 1, i.e. $|\lambda(\theta)| = 1$, because this is associated to the boundary conditions and therefore does not affect the convergence of the scheme. Finally, we want to check that the smoothing factor of $\widehat{N_h^S}(\theta)$, defined as $\max_{\pi/2h \le |\theta| \le \pi/h} |\lambda(\theta)|$, is sufficiently small. These two requirements are necessary to guarantee that the associated collective algorithms are good candidates to be employed as smoothers in multigrid methods.
In the following numerical experiments, we perform the analysis of three different problems evaluating the discrete Fourier operators with θ defined in

$$\Theta_h = \left\{ \left(-1 + \frac{2k}{10^4} \right) \frac{\pi}{h},\ k = 0, 1, \ldots, 10^4 \right\} \subset \mathbb{T}_h.$$

5.4.2.1 Example 1

In the first example we consider problem (5.1) with $a = 0$ ($A_h = S_h$) and proceed as in [45]. In Figure 5.5 we collect the spectrum of the amplification matrix N_h^S for the $ECGS$ and $ICGS$ iteration matrices varying the penalty parameter μ. In Figure 5.5 the high frequencies are denoted by '+' whereas the low frequencies by 'o'. The corresponding computed smoothing factors are reported in Table 5.1. The results are independent of the mesh-size h and $\rho(\theta) \le 1$, for any $\theta \in \Theta_h$.

5.4.2.2 Example 2

We have repeated the same set of experiments as before considering problem (5.1) with $a \neq 0$, that is $A_h = S_h + aM_h$. Figure 5.6 shows the computed spectrum

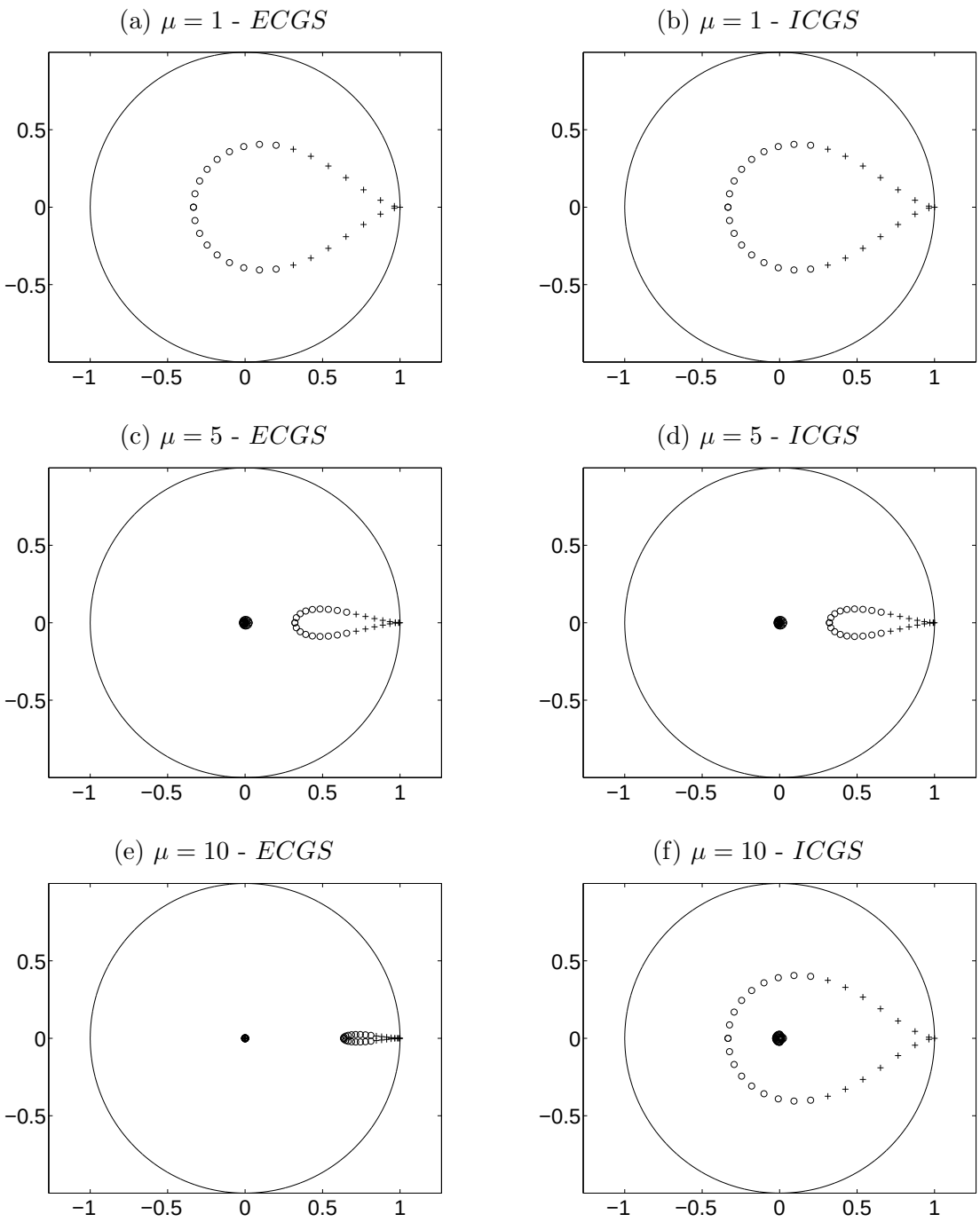

Figure 5.5: Example 1. Spectrum of $\widehat{N_h^S}(\theta)$ for the $ECGS$ (left) and $ICGS$ (right) iteration matrices employing different choices of the penalty parameter $\mu = 1, 5, 10$. High frequencies are denoted by '+' whereas lower frequencies by 'o'.

μ	$ECGS$	$ICGS$
1	0.44721	0.44721
5	0.65879	0.44721
10	0.81220	0.44721

Table 5.1: Example 1. Smoothing factor for the $ECGS$ and $ICGS$ iteration matrices as a function of $\mu = 1, 5, 10$.

for $a = 1$ and varying the mesh size $h = 10^{-k}$, $k = 1, 2, 3, 4$, and the penalty parameter $\mu = 1, 5, 10$. From these results it seems that for $h \to 0$ the spectrum of $\widehat{N_h^S}(\theta)$ tends to the corresponding one of Example 1.

The analogous results obtained by fixing $h = 0.1$ and varying both $a = 10^k$, $k = 1, \ldots, 5$ as well $\mu = 1, 5, 10$ are shown in Figure 5.7. The computed smoothing factors relative to those two sets of experiments are summarized in Table 5.2.

h	μ	$ECGS$	$ICGS$
10^{-1}	1	0.44662	0.44655
	5	0.65793	0.44543
	10	0.81166	0.44543
10^{-2}	1	0.44721	0.44721
	5	0.65878	0.44720
	10	0.81220	0.44720
10^{-3}	1	0.44721	0.44721
	5	0.65879	0.44721
	10	0.81220	0.44721
10^{-4}	1	0.44721	0.44721
	5	0.65879	0.44721
	10	0.81220	0.44721

a	μ	$ECGS$	$ICGS$
10	1	0.44132	0.43829
	5	0.65029	0.42963
	10	0.80683	0.42964
10^2	1	0.39392	0.36280
	5	0.58082	0.29595
	10	0.76085	0.29728
10^3	1	0.18429	0.15789
	5	0.24950	0.07317
	10	0.47031	0.05432
10^4	1	0.02829	0.02753
	5	0.03066	0.03414
	10	0.12396	0.10094

Table 5.2: Example 2. Smoothing factor for the $ECGS$ and $ICGS$ iteration matrices as a function of $\mu = 1, 5, 10$. We set $a = 1$ and $h = 10^{-k}$, $k = 1, 2, 3, 4$ (left), $h = 0.1$ and $a = 10^k$, $k = 1, 2, 3, 4$ (right).

5.4.2.3 Example 3

Here we consider the linearized Cahn-Hilliard problem (5.9). In this case the matrix A_h has the following form

$$A_h = \begin{pmatrix} M_h & bS_h \\ cS_h + dM_h & -M_h \end{pmatrix}.$$

We investigate how the spectrum of the resulting amplification matrix depends on both the discretization parameter h as well as the coefficient μ, b, c, d.

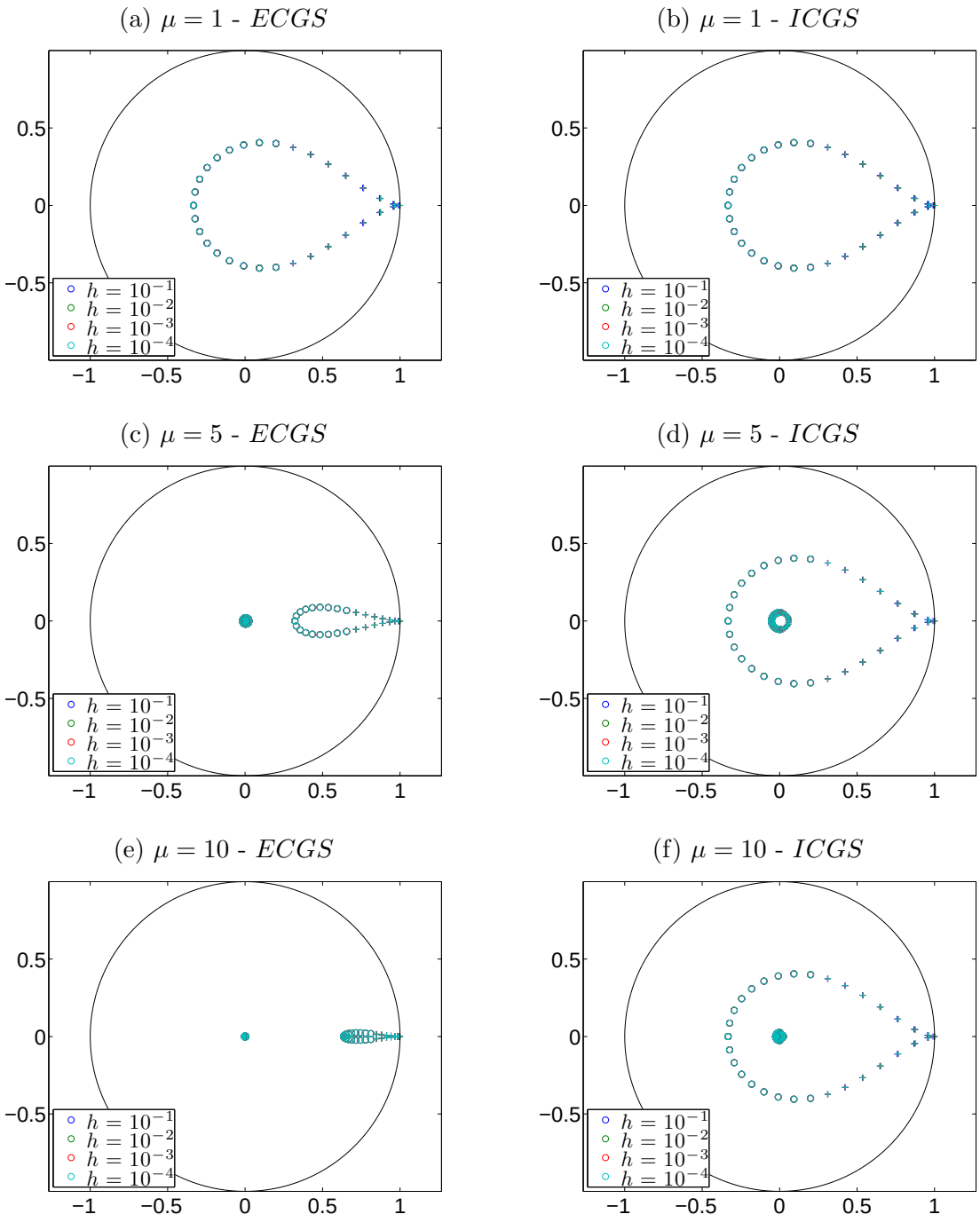

Figure 5.6: Example 2 ($a = 1$). Spectrum of $\widehat{N_h^S}(\theta)$ for the $ECGS$ (left) and $ICGS$ (right) iteration matrices employing different choices of the penalty parameter $\mu = 1, 5, 10$ and mesh size $h = 10^{-k}$, $k = 1, 2, 3, 4$. High frequencies are denoted by '+' whereas lower frequencies by 'o'.

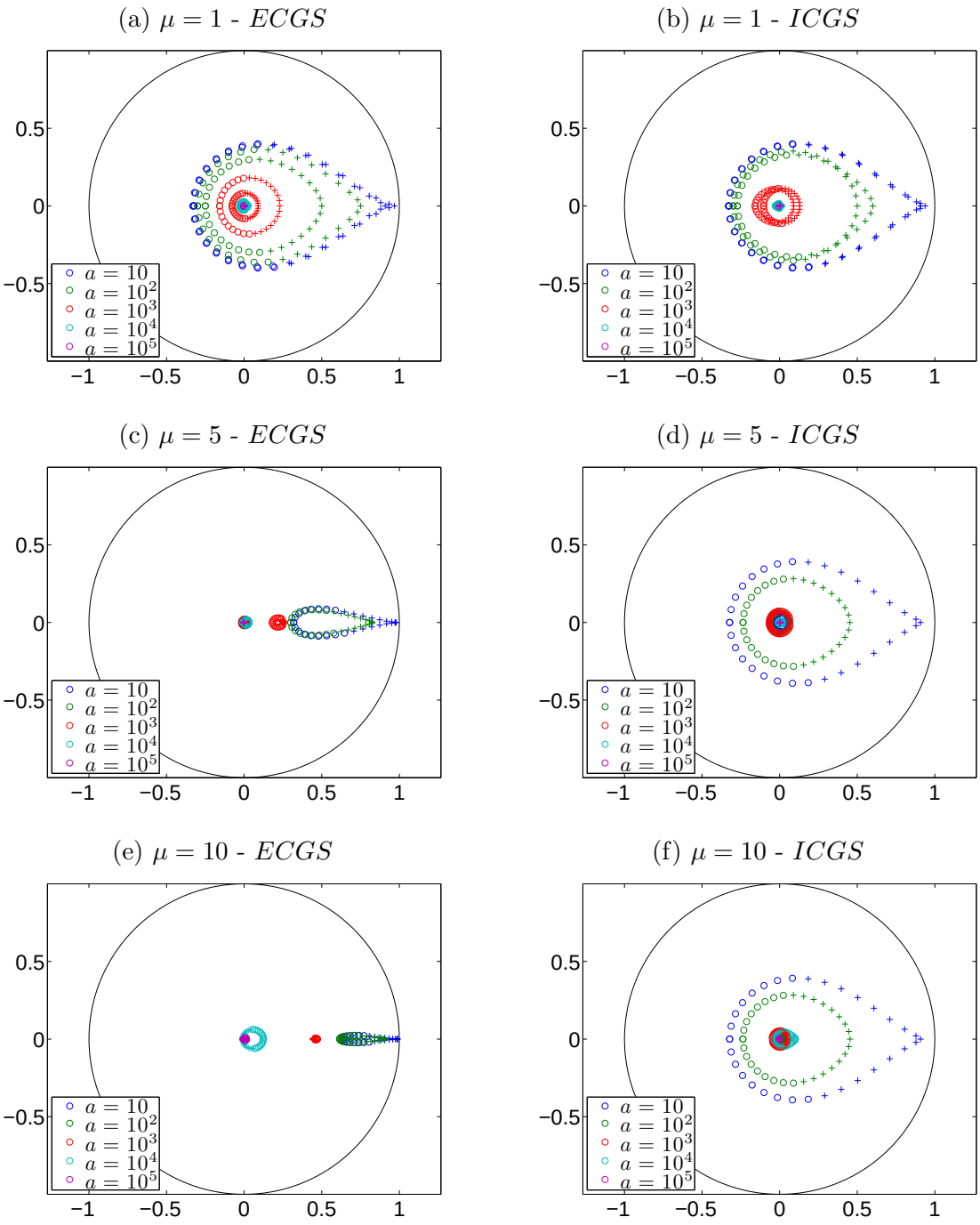

Figure 5.7: Example 2 ($h = 0.1$). Spectrum of $\widehat{N_h^S}(\theta)$ for the $ECGS$ (left) and $ICGS$ (right) iteration matrices employing different choices of the penalty parameter $\mu = 1, 5, 10$ and $a = 10^k$, $k = 1, \ldots, 5$. High frequencies are denoted by '+' whereas lower frequencies by 'o'.

Let us first consider the implicit Euler discretization for the Cahn-Hilliard problem, i.e., the parameter d belongs to $[-1, 2]$. More precisely, we consider the discrete set of values $J_{IE} = \{-1 + 3k/100,\ k = 0, 1, \ldots, 100\}$. Performing several numerical experiments, we see that negative values of $d \in J_{IE}$ can yield spectral radius values larger than one. Then, the LFA approach does not guarantee that our set of smoothers works.
Next, we analyze the eigenvalue spectra of $\widehat{N_h^S}(\theta)$ for $d \in [0, 3]$, i.e., the values corresponding to the convex-splitting choice for time discretization (see (4.10)). Also in this case, we take d in a finite set $J_{CS} = \{3k/100,\ k = 0, 1, \ldots, 100\}$. In Figure 5.8 we report the spectrum of the amplification matrix $\widehat{N_h^S}$ corresponding to the $ECGS$ and $ICGS$ smoothers varying the penalty parameter $\mu = 1, 5, 10$ and different values of $d \in J_{CS}$. Here we set $h = 0.1$, $b = 0.1$, $c = 0.01$. The analogous results obtained with $b = 0.001$ and $b = 10^{-5}$ are shown in Figure 5.9 and Figure 5.10, respectively.
In Figure 5.10-5.12 are showed the eigenvalue spectra in function of the mesh-size h and the penalization term μ setting $c = 0.01$ and $b = 10^{-5}$.
The smoothing factors of $N_h^S(\theta)$ varying both h, μ, b, c are summarized in Table 5.3. From these results we can conclude that a critical behaviour seems to

h	μ	b	c	$ECGS$	$ICGS$
0.1	1	0.1	0.01	0.45002	0.45101
0.1	5	0.1	0.01	0.65917	0.45006
0.1	10	0.1	0.01	0.81230	0.45005
0.1	1	0.001	0.01	0.44750	0.44759
0.1	5	0.001	0.01	0.65883	0.44750
0.1	10	0.001	0.01	0.81221	0.44750
0.01	1	0.1	0.01	0.44724	0.44725
0.01	5	0.1	0.01	0.65879	0.44724
0.01	10	0.1	0.01	0.81220	0.44724
0.1	1	0.1	0.0001	0.47311	0.48724
0.1	5	0.1	0.0001	0.66233	0.47680
0.1	10	0.1	0.0001	0.81311	0.47668
0.01	1	0.1	0.0001	0.44750	0.44759
0.01	5	0.1	0.0001	0.65883	0.44750
0.01	10	0.1	0.0001	0.81221	0.44750

Table 5.3: Example 3. Smoothing factor for the $ECGS$ and $ICGS$ iteration matrices as a function of $h,\ \mu,\ b,\ c$.

take place when $c \to 0$, i.e., when the interface parameter goes to zero. In this case, the smoothing factor of the amplification matrix N_h^S increases. On the other hand, when b (i.e., Δt) and h tend to zero the behaviour of the smoothing factor seems to be similar to the one observed in Example 1. Moreover, from these

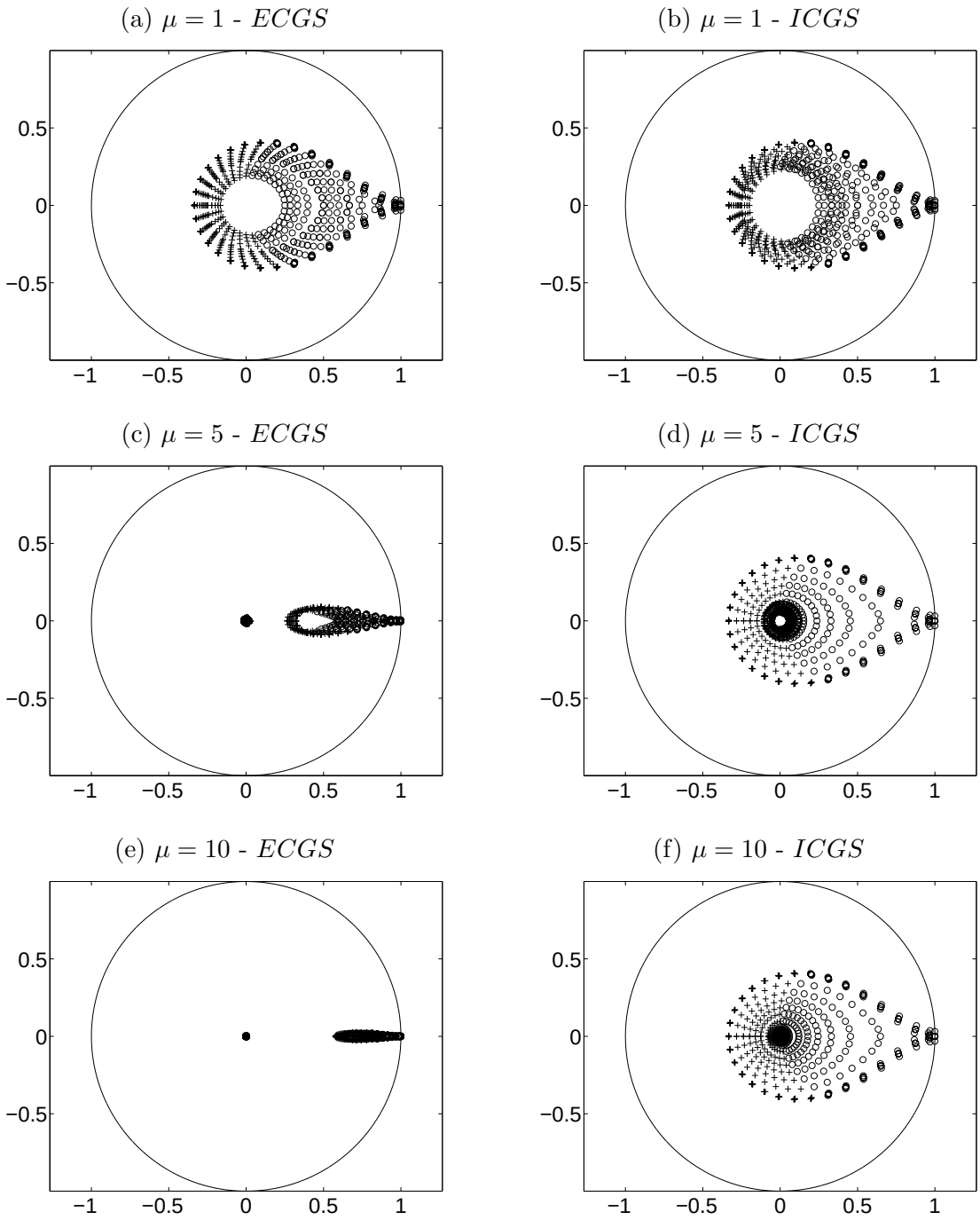

Figure 5.8: Example 3 ($h = 0.1$, $b = 0.1$ and $c = 0.01$). Spectrum of $\widehat{N_h^S}(\theta)$ for the $ECGS$ (left) and $ICGS$ (right) iteration matrices employing different choices of the penalty parameter $\mu = 1, 5, 10$. High frequencies are denoted by '+' whereas lower frequencies by 'o'.

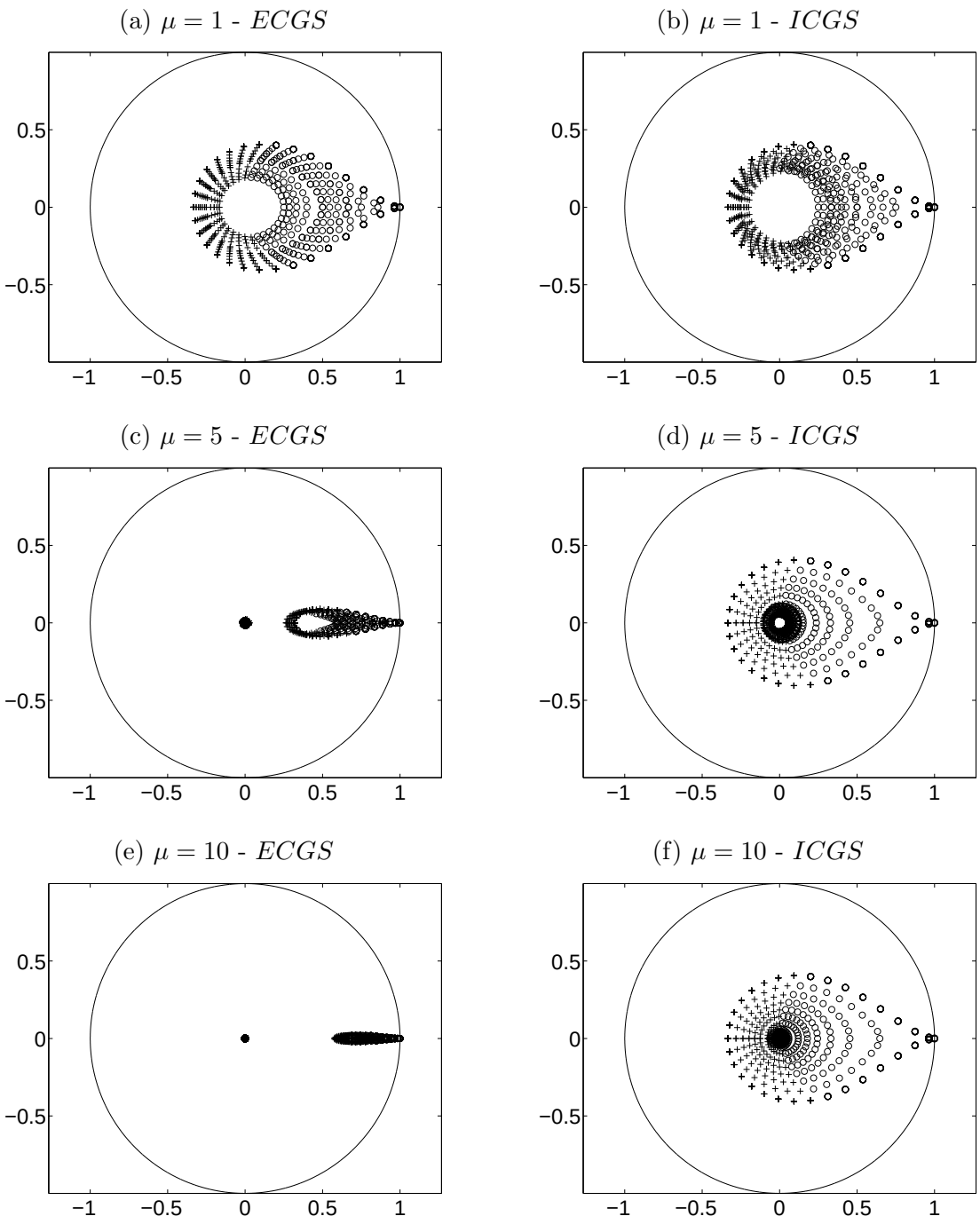

Figure 5.9: Example 3 ($h = 0.1$, $b = 0.001$ and $c = 0.01$). Spectrum of $\widehat{N_h^S}(\theta)$ for the $ECGS$ (left) and $ICGS$ (right) iteration matrices employing different choices of the penalty parameter $\mu = 1, 5, 10$. High frequencies are denoted by '+' whereas lower frequencies by 'o'.

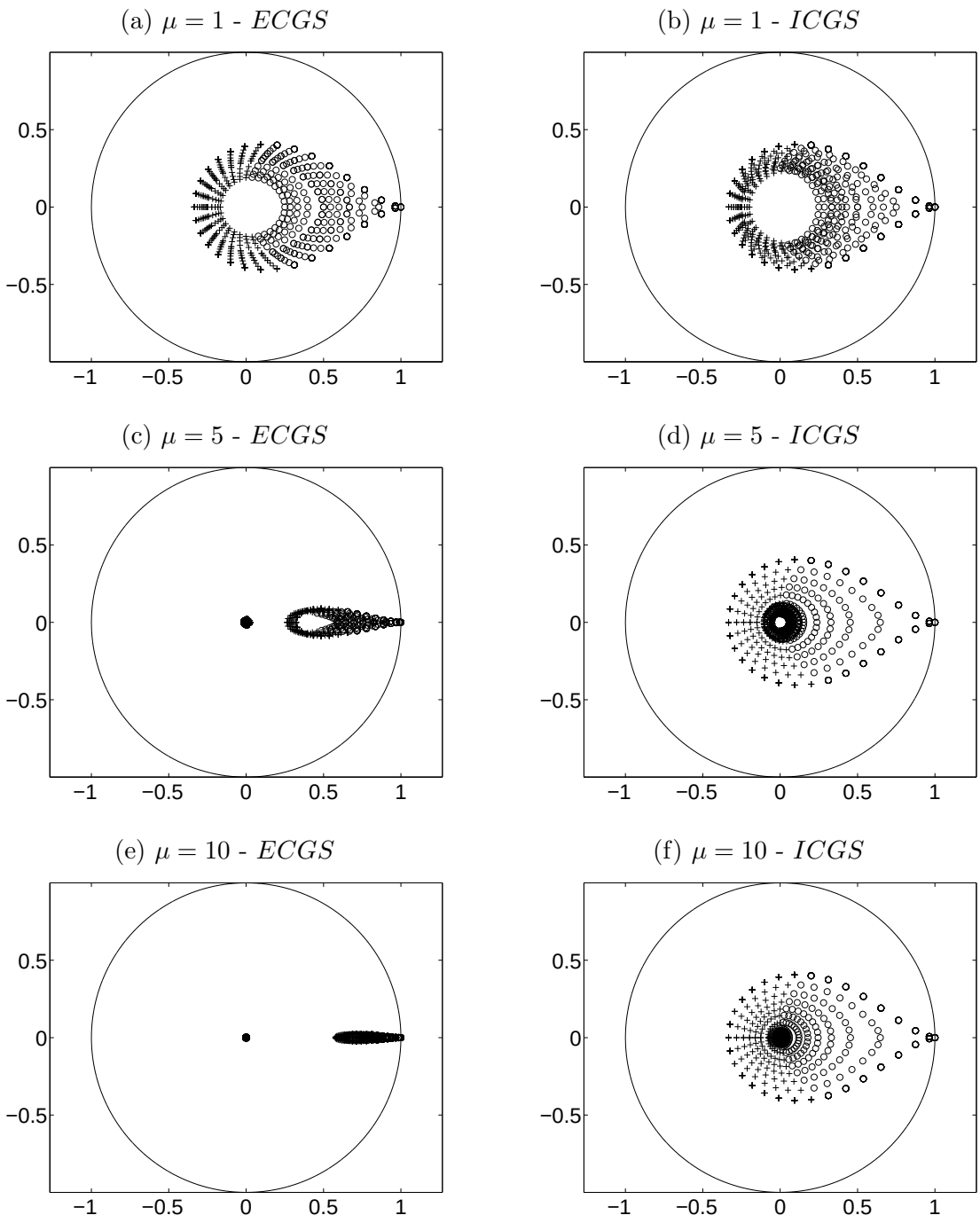

Figure 5.10: Example 3 ($h = 0.1$, $b = 10^{-5}$ and $c = 0.01$). Spectrum of $\widehat{N_h^S}(\theta)$ for the $ECGS$ (left) and $ICGS$ (right) iteration matrices employing different choices of the penalty parameter $\mu = 1, 5, 10$. High frequencies are denoted by '+' whereas lower frequencies by 'o'.

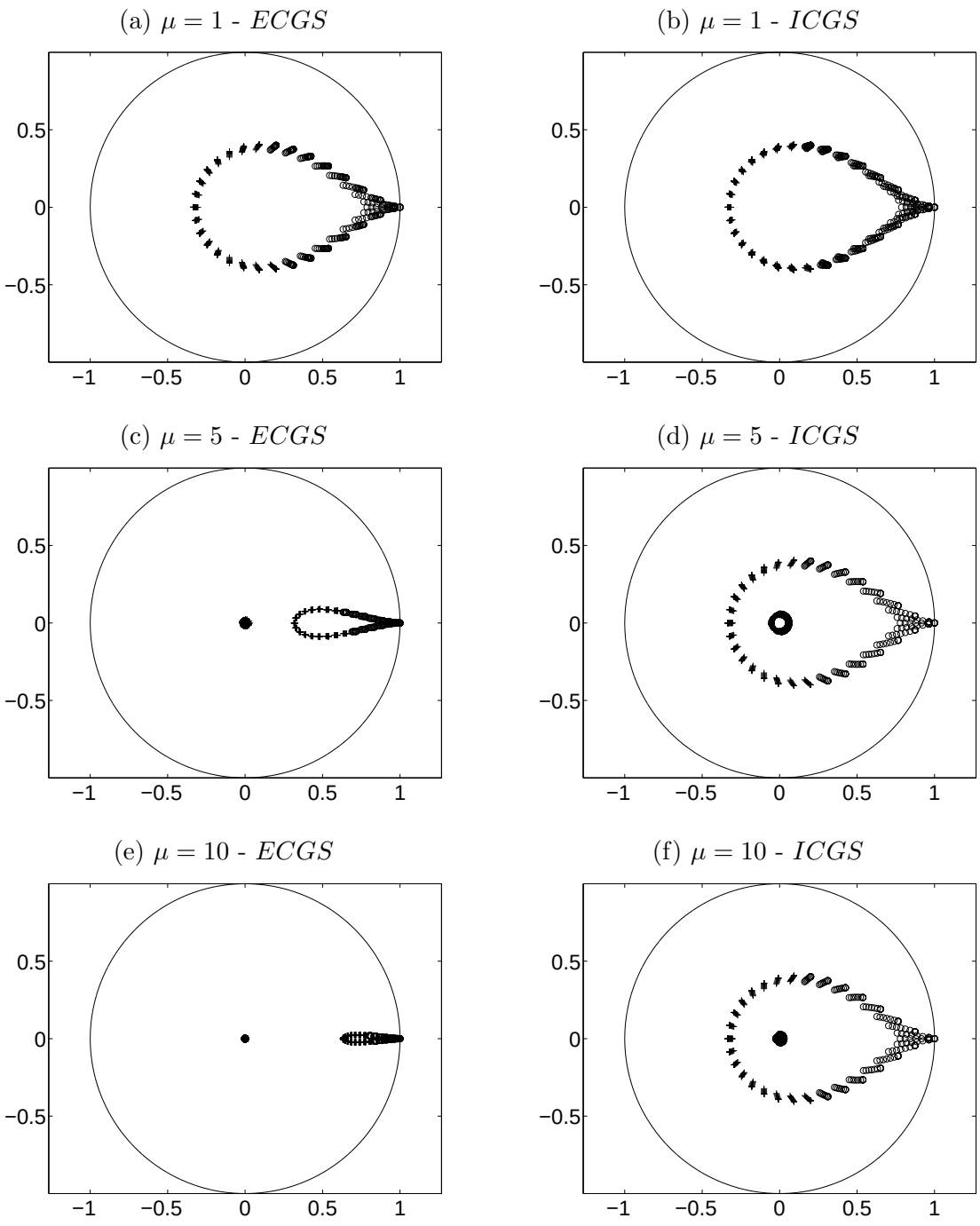

Figure 5.11: Example 3 ($h = 0.03$, $b = 10^{-5}$ and $c = 0.01$). Spectrum of $\widehat{N_h^S}(\theta)$ for the $ECGS$ (left) and $ICGS$ (right) iteration matrices employing different choices of the penalty parameter $\mu = 1, 5, 10$. High frequencies are denoted by '+' whereas lower frequencies by 'o'.

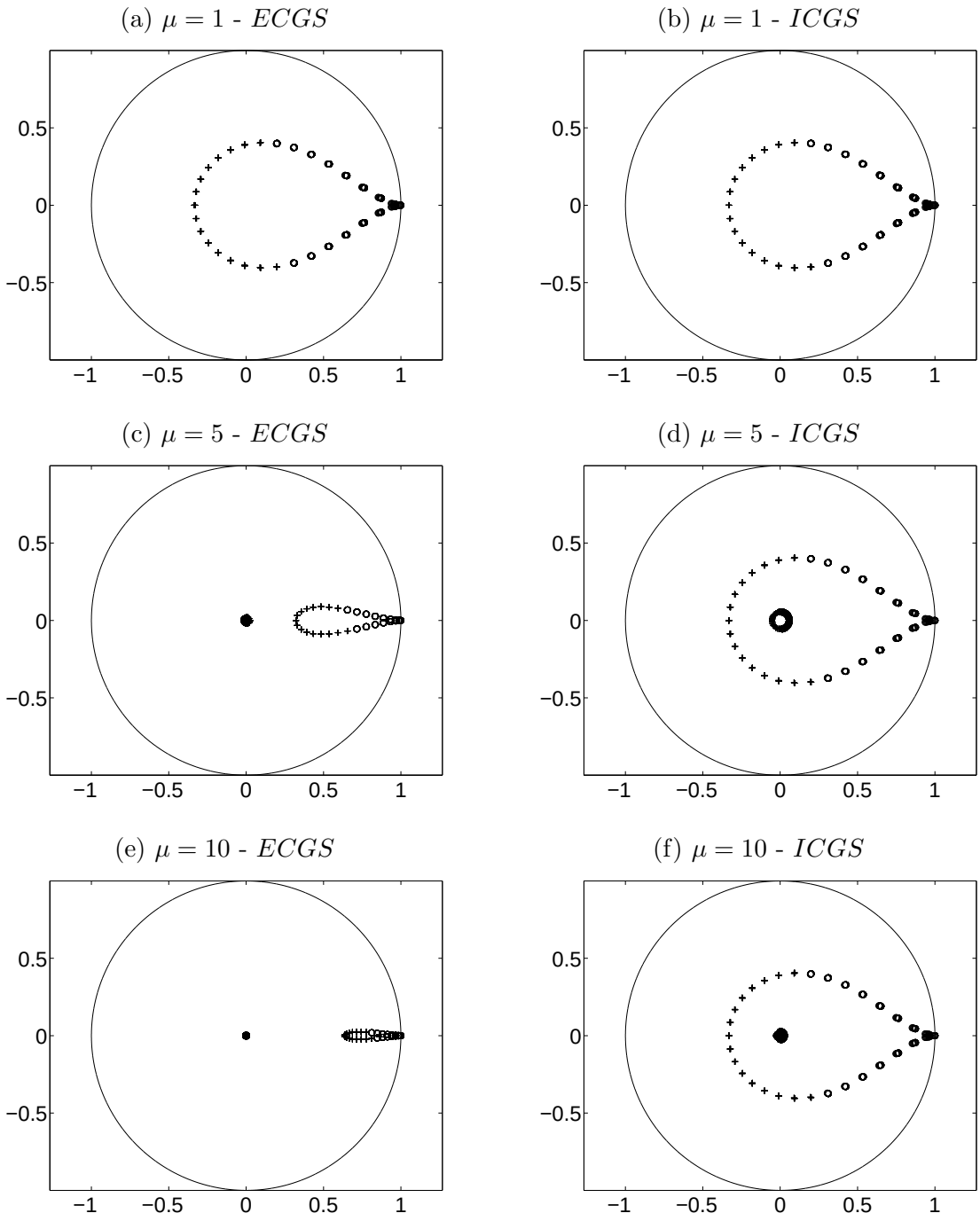

Figure 5.12: Example 3 ($h = 0.01$, $b = 10^{-5}$ and $c = 0.01$). Spectrum of $\widehat{N_h^S}(\theta)$ for the $ECGS$ (left) and $ICGS$ (right) iteration matrices employing different choices of the penalty parameter $\mu = 1, 5, 10$. High frequencies are denoted by '+' whereas lower frequencies by 'o'.

results, the $ICGS$ approach seems to preferable to the $ECGS$ one.

5.5 Two-level analysis

In this section we extend the LFA to the two-level method obtained considering also a coarse correction. To this aim we introduce the (nested) coarse triangulation $\mathcal{T}_H$ of Ω with $H = 2h$ and the corresponding DG space X_H^1. To introduce the two-level operator we require:

- The Toeplitz matrices A_h and A_H on the fine and the coarse levels, respectively;
- The prolongation operator $I_H^h : X_H^1 \longrightarrow X_h^1$ such that $(I_H^h \mathbf{v}_H)(x) = \mathbf{v}_H(x)$ for all $x \in \mathbb{R} \setminus \mathbb{Z}_h$ and for all $\mathbf{v}_H \in X_H^1$;
- The restriction operator $I_h^H : X_h^1 \to X_H^1$ defined as the transpose of the prolongation operator, i.e., $I_H^h = (I_H^h)^T$.

With the above notations, the coarse grid correction matrix is defined as

$$N_h^{CGC} = I - I_H^h A_H^{-1} I_h^H A_h.$$

Following [44], we introduce the operator $P_H^h : [\ell^2(\mathbb{Z}_H)]^2 \to [\ell^2(\mathbb{Z}_h)]^2$ and $R_h^H : [\ell^2(\mathbb{Z}_h)]^2 \to [\ell^2(\mathbb{Z}_H)]^2$ defined as

$$(P_H^h \mathbf{v}_H)(jh) = \begin{cases} \mathbf{v}_H(Hj/2), & \text{if j even,} \\ 0, & \text{otherwise,} \end{cases}$$

and

$$(R_h^H \mathbf{v}_h)(jH) = \mathbf{v}_h(2jh).$$

Then, there exist two Toeplitz operator $P_h, R_h : [\ell^2(\mathbb{Z}_h)]^2 \to [\ell^2(\mathbb{Z}_h)]^2$ such that the prolongation and restriction operators can be written as $I_H^h = P_h P_H^h$ and $I_h^H = R_h^H R_h$. Since we want to work on both the fine and coarse, we introduce a different notation for the Fourier transformation:

$$\hat{\mathbf{v}}_h(\theta), \quad \theta \in \mathbb{T}_h \text{ is equivalent to write } \begin{pmatrix} \hat{\mathbf{v}}_h(\theta) \\ \hat{\mathbf{v}}_h(\theta + \pi/h) \end{pmatrix}, \quad \theta \in \mathbb{T}_H,$$

where the space of the frequencies on the coarse level is defined as

$$\mathbb{T}_H = \left[-\frac{\pi}{H}, \frac{\pi}{H}\right] = \left[-\frac{\pi}{2h}, \frac{\pi}{2h}\right].$$

From [43], can be proven that

$$\widehat{I_H^h \mathbf{v}_H}(\theta) = (\widehat{P_h P_H^h \mathbf{v}_H})(\theta) = \frac{1}{2} \begin{bmatrix} \widehat{P_h}(\theta) \\ \widehat{P_h}(\theta + \pi/h) \end{bmatrix} \mathbf{v}_h(\theta), \qquad \theta \in \mathbb{T}_H,$$

and

$$\widehat{I_H^h \mathbf{u}_h}(\theta) = (\widehat{R_h^H R_h \mathbf{u}_h})(\theta) = \left[\widehat{R_h}(\theta), \widehat{R_h}(\theta+\pi/h)\right] \begin{bmatrix} \widehat{\mathbf{u}_h}(\theta) \\ \widehat{\mathbf{u}_h}(\theta+\pi/h) \end{bmatrix}, \ \theta \in \mathbb{T}_H.$$

Now, with the above notation, we are able to write the Fourier transform of the amplification operator of the coarse-grid correction as

$$\begin{aligned}\widehat{N_h^{CGC}}(\theta) &= \left(\widehat{I} - \widehat{I_H^h}\widehat{L_H^{-1}}\widehat{I_h^H}\widehat{L_h}\right) \\ &= \begin{pmatrix} I & 0 \\ 0 & I \end{pmatrix} - \begin{pmatrix} \widehat{P_h}(\theta) \\ \widehat{P_h}(\theta+\pi/h) \end{pmatrix} (\widehat{L_H}(\theta))^{-1} \\ &\qquad \times \begin{pmatrix} \widehat{R_h}(\theta) & \widehat{R_h}(\theta+\pi/h) \end{pmatrix} \begin{pmatrix} \widehat{L_h}(\theta) & 0 \\ 0 & \widehat{L_h}(\theta+\pi/h) \end{pmatrix},\end{aligned}$$

for $\theta \in \mathbb{T}_H$, cf. [44]. Then, the amplification error for the two-level operator reads as

$$M_h^{TL} = (N_h^S)^{\nu_2} N_h^{CGC} (N_h^S)^{\nu_1},$$

where, as before, ν_1, ν_2 denote the number of pre- and post-smoothing iterations. In the following, we study the behaviour of the spectrum of M_h^{TL} with $\nu_1 = 0$ and $\nu_2 = 1$.

5.5.1 Example 1

We consider the same test case as the one considered in Section 5.4.2.1.
In Figure 5.13 we report the computed spectrum of the operator M_h^{TL} as a function of the penalization parameter μ employing both the $ECGS$ and $ICGS$ smoothers. The corresponding spectral radius is reported in Table 5.4. We clearly observe that $ECGS$ smoother does not guarantees the convergence of the two-level schemes except for $\mu = 1$, whereas the scheme is convergent for any μ if the $ICGS$ smoother is employed.

μ	$ECGS$	$ICGS$
1	0.99999	0.99999
5	2.04100	0.33333
10	2.52247	0.33333

Table 5.4: Example 1. Spectral radius of M_h^{TL} as a function of the penalization parameter $\mu = 1, 5, 10$.

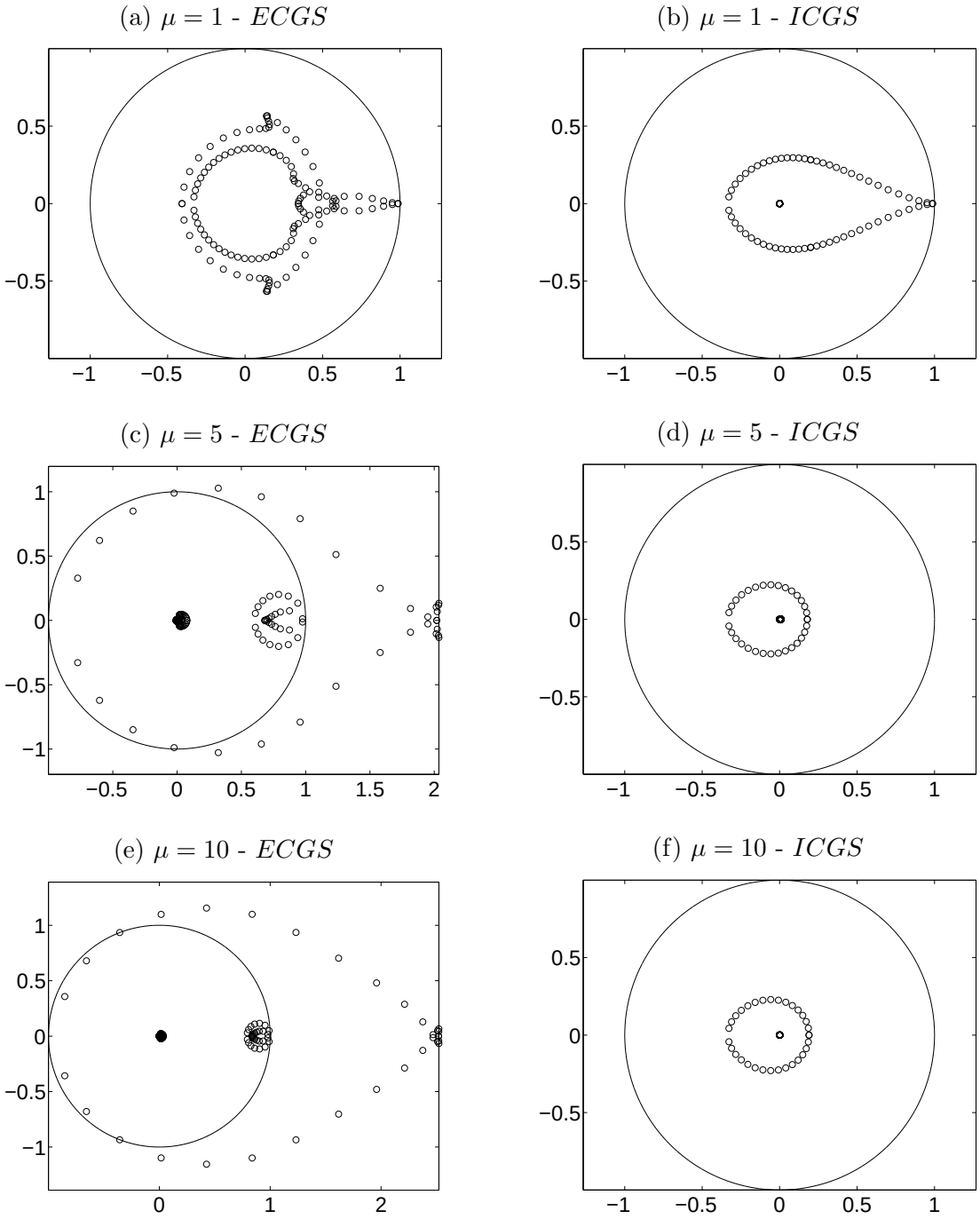

Figure 5.13: Example 1. Spectrum of $\widehat{M_h^{TL}}(\theta)$ employing both $ECGS$ (left) and $ICGS$ (right) smoothers for different values of the penalty parameter $\mu = 1, 5, 10$.

5.5.2 Example 2

Here we consider the same test case of Section 5.4.2.2. In Figure 5.14 we report the spectrum of M_h^{TL} for different mesh size $h = 10^{-k}$, $k = 1, 2, 3, 4$, an different choices of the penalization parameter $\mu = 1, 5, 10$. These results have been obtained employing both $ECGS$ and $ICGS$ smoothers. The corresponding computed spectral radii are summarized in Table 5.5.

h	μ	$ECGS$	$ICGS$
10^{-1}	1	0.99556	0.99118
	5	2.03617	0.33222
	10	2.52018	0.33223
10^{-2}	1	0.99994	0.99990
	5	2.04097	0.33332
	10	2.52244	0.33332
10^{-3}	1	0.99999	0.99999
	5	2.04100	0.33333
	10	2.52247	0.33333
10^{-4}	1	0.99999	0.99999
	5	2.04100	0.33333
	10	2.52247	0.33333

Table 5.5: Example 2. Spectral radius of M_h^{TL} as a function of the penalization parameter $\mu = 1, 5, 10$ and $h = 10^{-k}$, $k = 1, 2, 3, 4$.

From these results we can conclude that the $ECGS$ smoother does not guarantee the convergence of the two level-method, whereas the two-level algorithm is always convergent if the $ICGS$ is employed.
In Figure 5.15 we report the analogous results shown in Figure 5.14 but in this case we fix $h = 0.1$ and let vary the coefficient $a = 10^k$, $k = 1, ..., 5$. As before, the $ICGS$ smoother guarantees that all the eigenvalues of M_h^{TL} are contained in the unit circle, independently of the value of a, and larger values of a accelerate the convergence rate.

5.5.3 Example 3

Here we have repeated the experiments shown in Section 5.4.2.3 employing the two-level algorithm. In Figure 5.16 we report the computed spectrum with the following choices of parameters $h = 0.1$, $b = 0.1$ and $c = 0.01$. The analogous results obtained with $b = 10^{-5}$ are shown in Figure 5.17, whereas in Figure 5.18 are shown the computed spectra obtained with $h = 0.01$, $b = 10^{-5}$ and $c = 0.01$.

The corresponding computed spectral radii are summarized in Table 5.5. As in Example 2, the convergence of the two level-method is not guaranteed when the $ECGS$ smoother is employed (at least for $\mu > 1$). On the other hand,

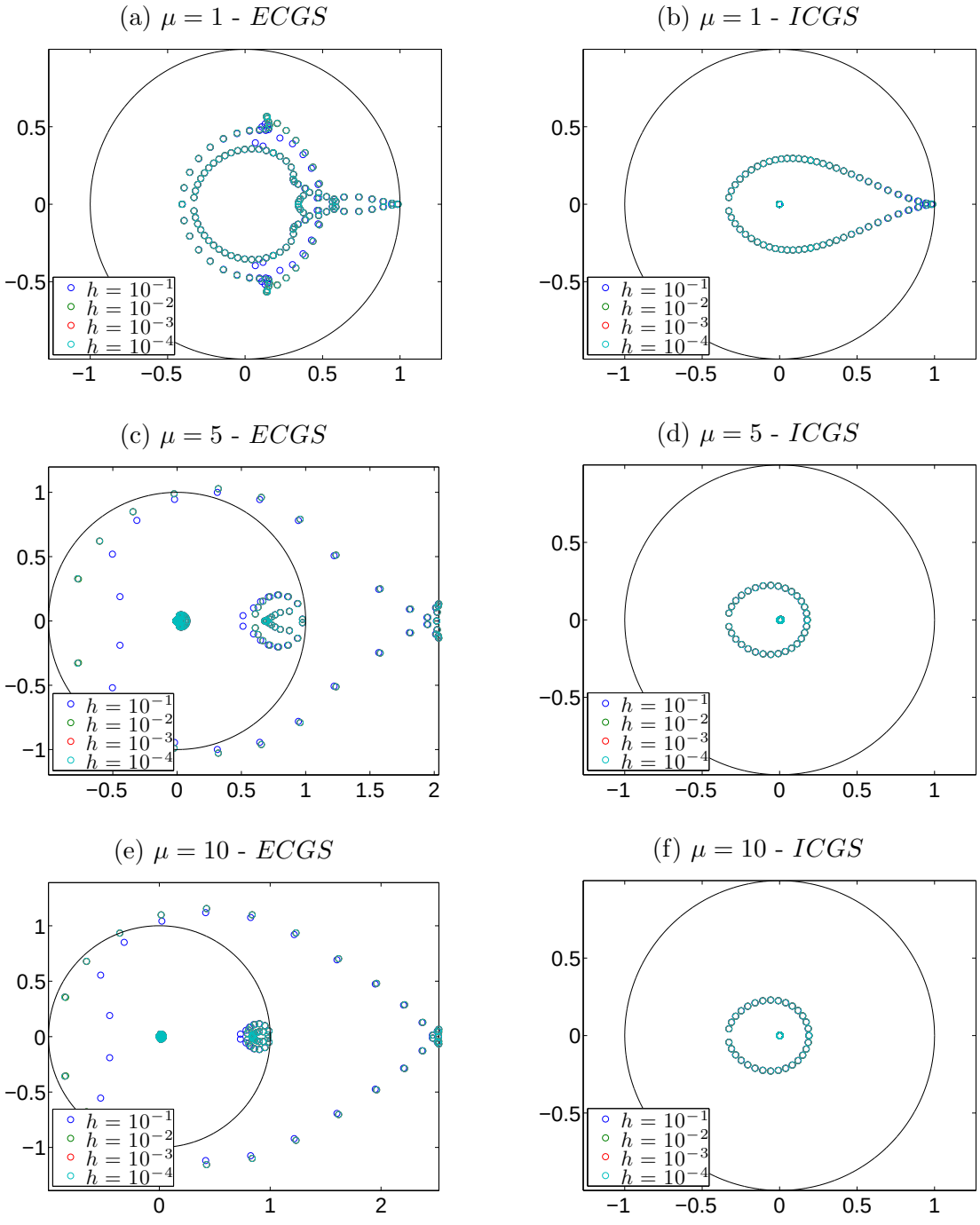

Figure 5.14: Example 2 ($a = 1$). Spectrum of $\widehat{M_h^{TL}}(\theta)$ employing both $ECGS$ (left) and $ICGS$ (right) smoothers for different values of the penalty parameter $\mu = 1, 5, 10$ and different mesh size $h = 10^{-k}$, $k = 1, 2, 3, 4$.

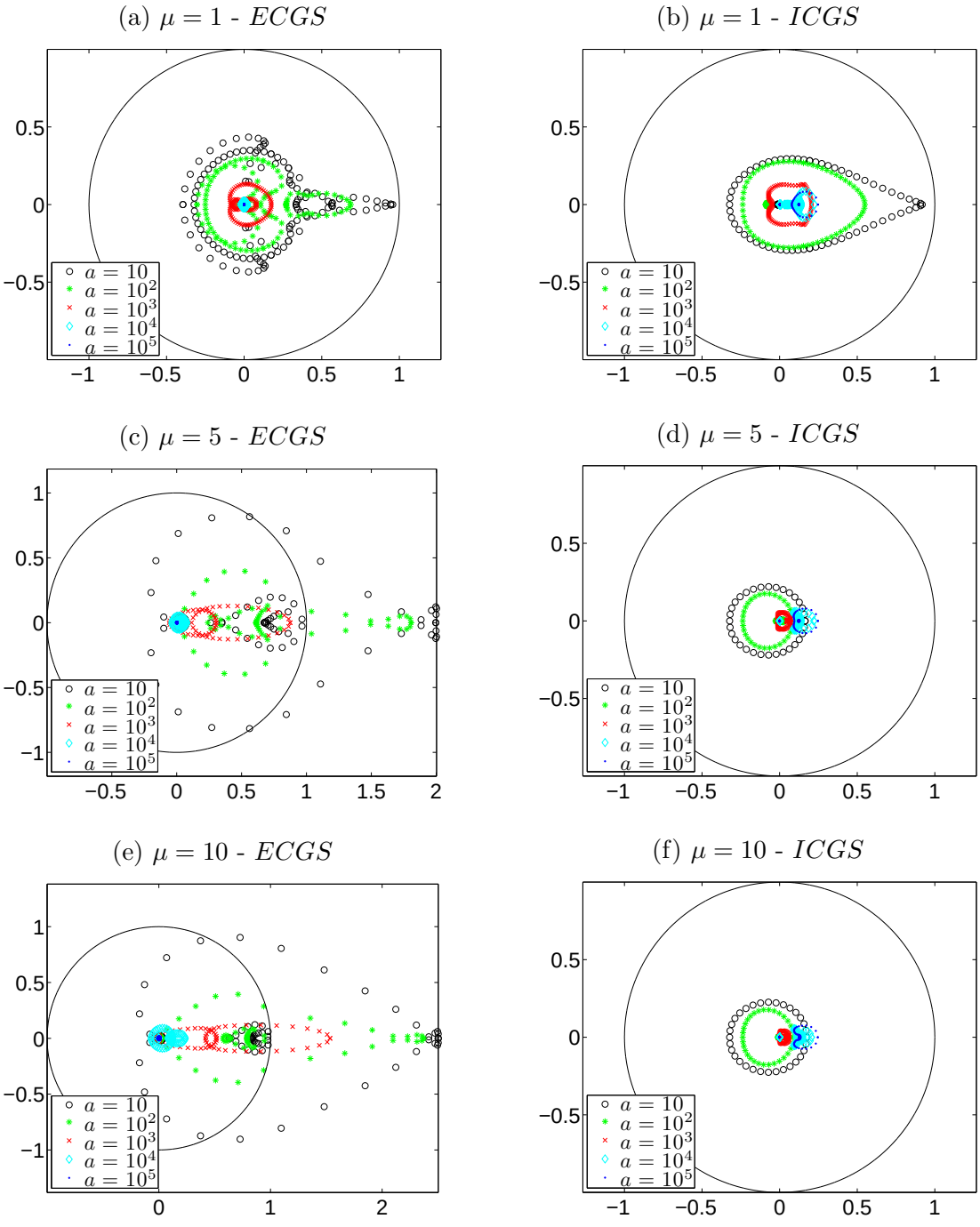

Figure 5.15: Example 2 ($h = 0.1$). Spectrum of $\widehat{M_h^{TL}}(\theta)$ employing both $ECGS$ (left) and $ICGS$ (right) smoothers for different values of the penalty parameter $\mu = 1, 5, 10$ and different $a = 10^k$, $k = 1, ..., 5$.

$ICGS$ smoother with $\mu > 1$ guarantees the convergence of the associated two level-method.

h	μ	b	c	$ECGS$	$ICGS$
0.1	1	0.1	0.01	0.99993	0.99970
0.1	5	0.1	0.01	2.04368	0.33338
0.1	10	0.1	0.01	2.52362	0.33349
0.1	1	0.001	0.01	1.00000	1.00000
0.1	5	0.001	0.01	2.04128	0.33333
0.1	10	0.001	0.01	2.52259	0.33334
0.01	1	0.1	0.01	1.00000	1.00000
0.01	5	0.1	0.01	2.04103	0.33333
0.01	10	0.1	0.01	2.52248	0.33333
0.1	1	0.1	0.0001	0.99985	0.99970
0.1	5	0.1	0.0001	2.06091	0.33670
0.1	10	0.1	0.0001	2.53075	0.33971
0.01	1	0.1	0.0001	1.00000	1.00000
0.01	5	0.1	0.0001	2.04128	0.33333
0.01	10	0.1	0.0001	2.52259	0.33334

Table 5.6: Example 3. Spectral radius of M_h^{TL} as a function of the mesh size h, the penalization parameter μ, b and c.

5.5.4 Damping parameter

In this section, we want to improve the rate of convergence of the two-level method with the $ICGS$ smoother by introducing a suitable damping parameter α. With such a modification the amplification error for the two-level operator becomes

$$M_{h,\alpha}^{TL} = (1-\alpha)I + \alpha(N_h^S)^{\nu_2} N_h^{CGC} (N_h^S)^{\nu_1}.$$

The optimal damping parameter α that minimizes the spectral radius of $M_{h,\alpha}^{TL}$ is given by

$$\alpha = \frac{2}{2 - (\lambda_{min} - \lambda_{max})},$$

where λ_{min} and λ_{max} are respectively the largest and the smallest real eigenvalues of M_h^{TL}.

Given as the numerical experiments reported in Section 5.5 highlighted a similar behaviour of the two-level method independently of the kind of problem under investigation, in the following we will consider as "optimal value" for α the one computed for the Example 1 (cf. Section 5.5.1), which is reported in Table 5.7 for two choices of the penalization parameter $\mu = 5, 10$.

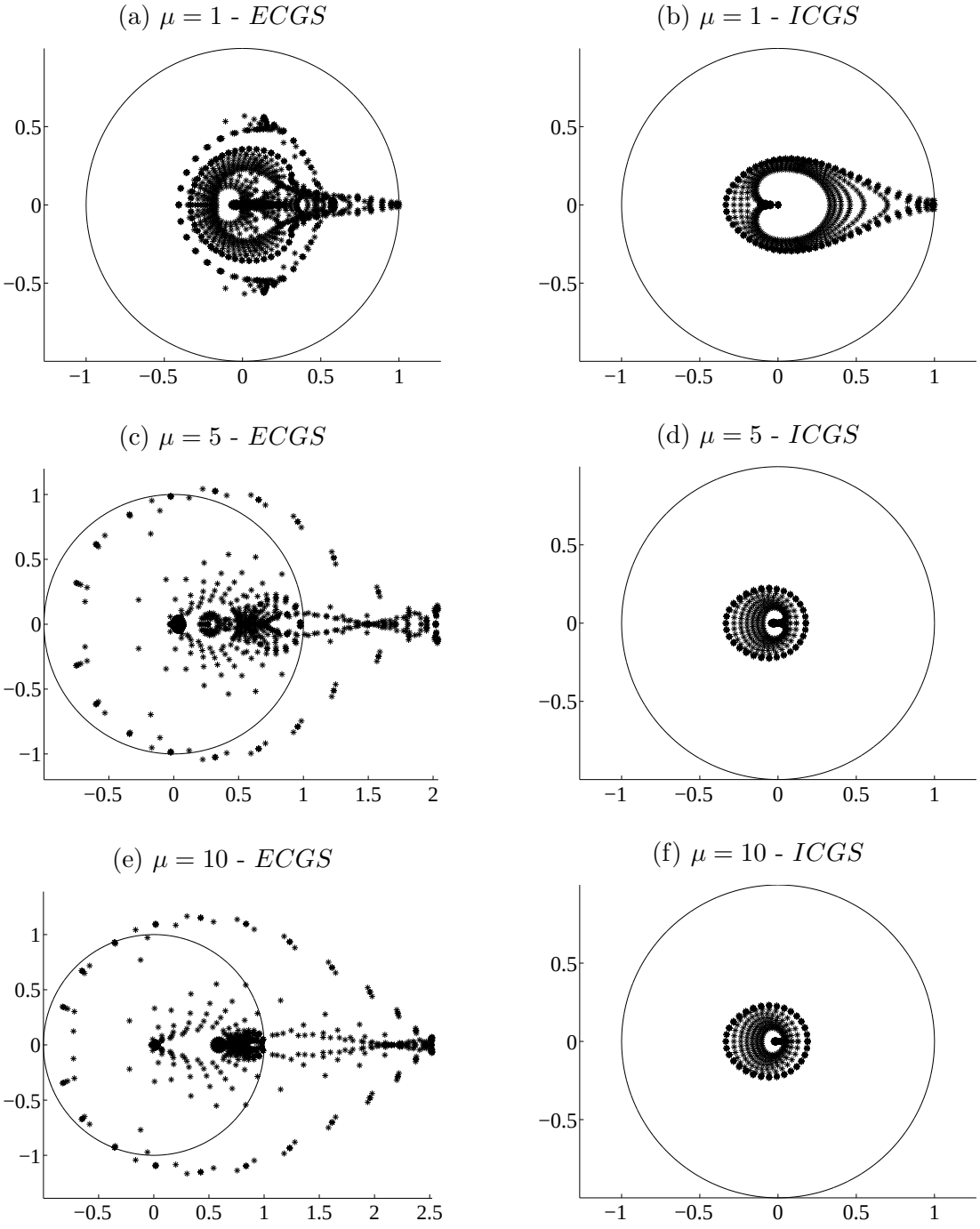

Figure 5.16: Example 3 ($h = 0.1$, $b = 0.1$ and $c = 0.01$). Spectrum of $\widehat{M_h^{TL}(\theta)}$ employing both $ECGS$ (left) and $ICGS$ (right) smoothers for different values of the penalty parameter $\mu = 1, 5, 10$.

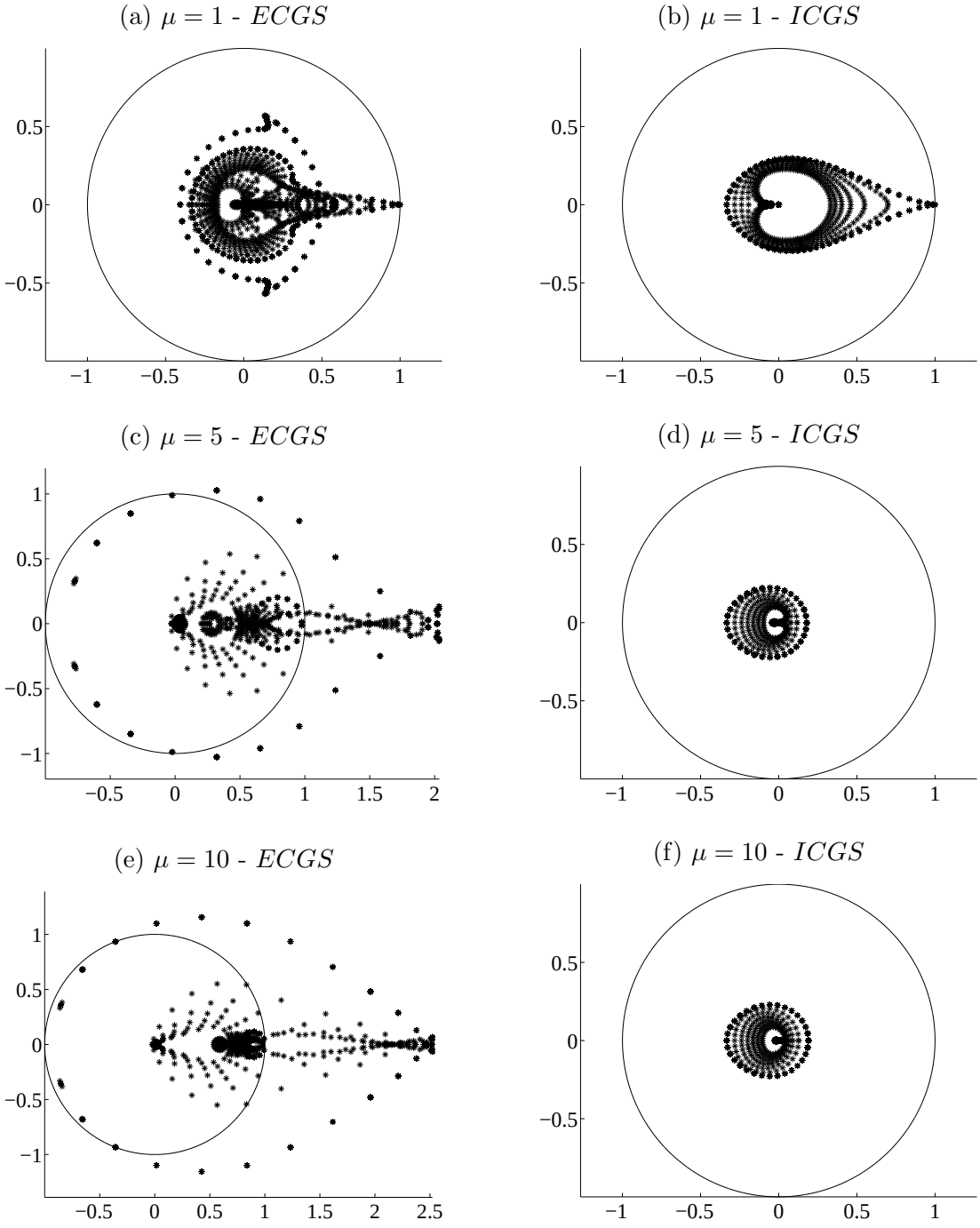

Figure 5.17: Example 3 ($h = 0.1$, $b = 10^{-5}$ and $c = 0.01$). Spectrum of $\widehat{M_h^{TL}}(\theta)$ employing both *ECGS* (left) and *ICGS* (right) smoothers for different values of the penalty parameter $\mu = 1, 5, 10$.

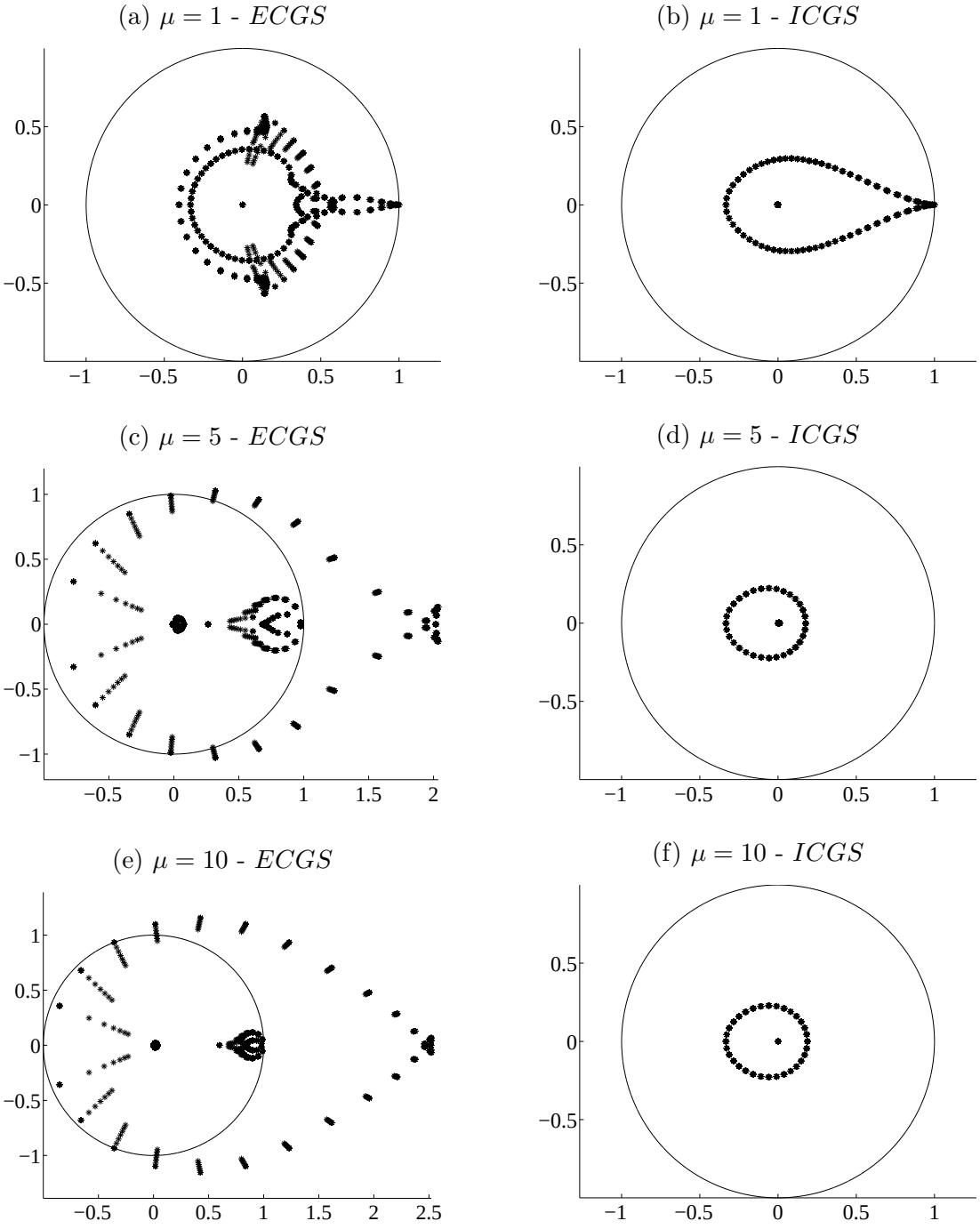

Figure 5.18: Example 3 ($h = 0.01$, $b = 10^{-5}$ and $c = 0.01$). Spectrum of $\widehat{M_h^{TL}(\theta)}$ employing both $ECGS$ (left) and $ICGS$ (right) smoothers for different values of the penalty parameter $\mu = 1, 5, 10$.

	$\mu = 5$	$\mu = 10$
α	0.9282	0.9331

Table 5.7: Example 1. Optimal damping parameter for the two-level operator $M_{h,\alpha}^{TL}$ ($ICGS$ smoother).

We have repeated the same tests that gave rise to the numerical outputs reported in Table 5.5 and Table 5.6 and we have employed as smoother the $ICGS$ method with damping parameter given in Table 5.7. The results are reported in Table 5.8 and Table 5.9, respectively. Comparing these results with the analogous ones presented in Table 5.5 and Table 5.6, we notice that the convergence rates are clearly improved.

h	$\mu = 5$	$\mu = 10$
10^{-1}	0.23663	0.24318
10^{-2}	0.23753	0.24404
10^{-3}	0.23754	0.24405
10^{-4}	0.23754	0.24405

Table 5.8: Example 2. Spectral radius of $M_{h,\alpha}^{TL}$ as a function of the penalization parameter $\mu = 5, 10$ and $h = 10^{-k},\ k = 1, 2, 3, 4$ ($ICGS$ smoother).

h	b	c	$\mu = 5$	$\mu = 10$
0.1	0.1	0.01	0.23823	0.24488
0.1	0.001	0.01	0.23760	0.24413
0.01	0.1	0.01	0.23760	0.24413
0.1	0.1	0.0001	0.25580	0.26524
0.01	0.1	0.0001	0.23760	0.24413

Table 5.9: Example 3. Spectral radius of $M_{h,\alpha}^{TL}$ as a function of the mesh size h, the penalization parameter μ, b, c ($ICGS$ smoother).

5.6 Numerical results

In this section we report some 1D numerical experiments where we applied FAS algorithm employing the smoothers presented in Section 5.2 and Section 5.3 to solve problems (5.1) and (5.5), respectively. In the case of problem (5.1) FAS algorithm reduces to the usual MG algorithm. For this set of numerical experiments, we set $\mu = 10$ and we consider a sequence of nested structured grids with $h_k = 2^{-k},\ k = 1, 2, ...$

In the following we will test only the $ICGS$ smoothers with $s = 1, 2, 3$ (cf. Figure 5.1), since it is the one that exhibits better convergence properties.

5.6.1 Test case 1

We consider problem (5.1) on $\Omega = (0, 1)$ with $a = 1$, $f(x) = 4\pi^2 \cos(2\pi x) + \cos(2\pi x)$ and homogeneous Neumann boundary conditions. The exact solution is given by $u(x) = \cos(2\pi x)$.

We explore the behaviour of the residual at each smoothing iteration using as initial guess $u_0(x) = (\cos(3\pi x) + \cos(10\pi x) + \cos(2^k 3/4\pi x))/3$ for each grid k. In Figure 5.19 we report the behaviour of the L^2-norm of the residual varying the grid ($k = 4, 6, 8$) and the classical Gauss-Seidel smoother. Comparing the two cases with the same computational cost per iteration ($ICGS$ with $s = 1$ and Gauss-Seidel) we obtain that our proposed smoother dumps the error faster, especially for the first iterations.

We now perform the same set of experiments using MG algorithm as a solver. In particular, we set $\nu_1 = \nu_2 = 3$ and we employ two-level, W-cycle (using 3 grids) and V-cycle (using $k = 2$ as the coarsest grid) schemes.

In Figure 5.20-5.22 we report the behaviour of L^2-norm of the residual for each scheme versus the work unit (WU), i.e., the computational cost of one relaxation on the fine grid. Moreover, for each scheme, we perform the same numerical experiments employing the Gauss-Seidel as a smoother.

In all the considered multigrid methods that employing $ICGS$ smoother, the algorithm converges and the number of iterations to satisfy the convergence criterion ($\|r\| \leq 10^{-7}$) seems independent on the level. Otherwise, in the Gauss-Seidel case, the convergence is very slow and it depends on the size (i.e., on the level) of the problem.

5.6.2 Test case 2

Here we consider the same set of experiments of Section 5.6.1 applied to the one dimensional version of (4.10). In particular, choosing $f = g = 0$, using different grid level $k = 4, ..., 10$ and setting $u_0(x) = (\cos(3\pi x) + \cos(10\pi x) + \cos(2^k 3/4\pi x))/3$ as initial data, we perform a single iteration in time solving the problem only for $t = t_1$. We also set $\Delta t = 10^{-3}$ and $\gamma = 0.1$.

In Figure 5.23 we report the behaviour of the L^2-norm of the residual on different grids when the $ICGS$ smoother is used as a solver with $s = 1, 2, 3$.

In Figures 5.24-5.26 are shown the results of the L^2-norm of the residual in terms of WU when FAS is employed with two-grid, V-cycle and W-cycle schemes, respectively.

Also in this case, all the algorithms converge and the number of iterations to satisfy the stopping condition seems independent of the level and similar to the

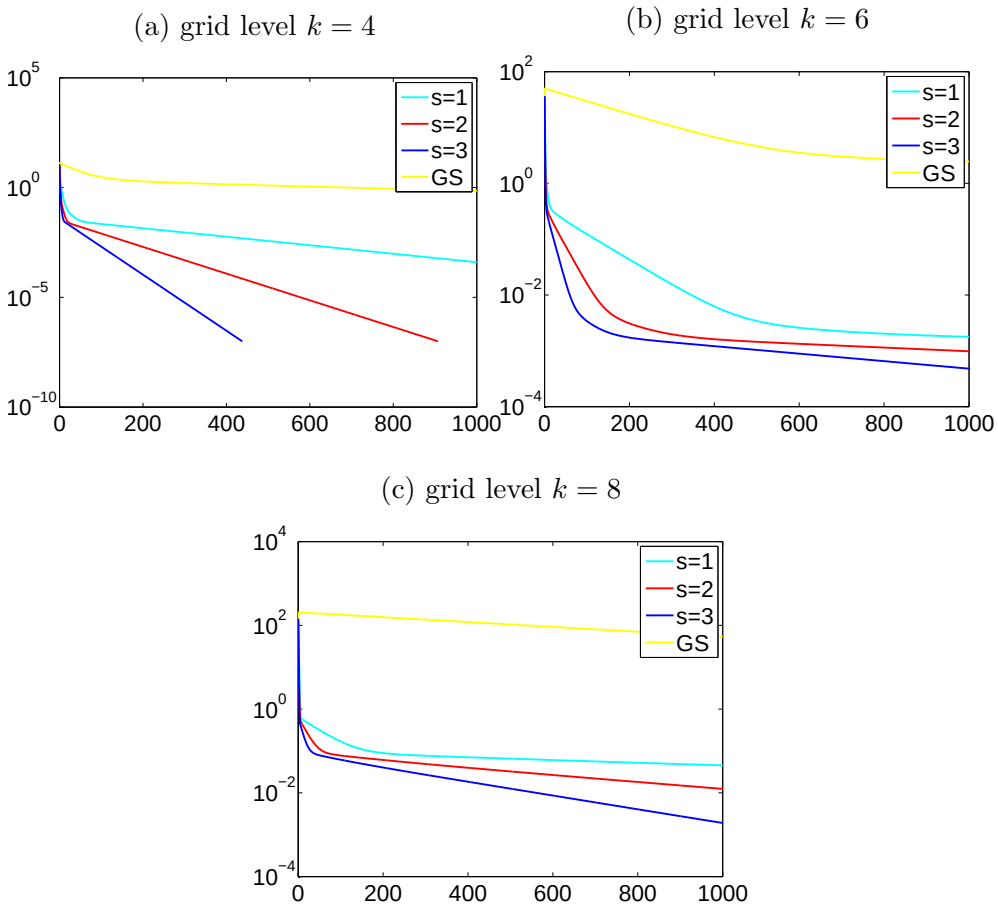

Figure 5.19: Test case 1. L^2-norm of the residual versus the number of smoothing steps for the $ICGS$ smoother with $s = 1, 2, 3$ comparing with Gauss-Seidel smoother.

ones of Section 5.6.1. The comparison between the FAS using the proposed set of smoothers and the FAS with Gauss-Seidel smoother is under investigation.

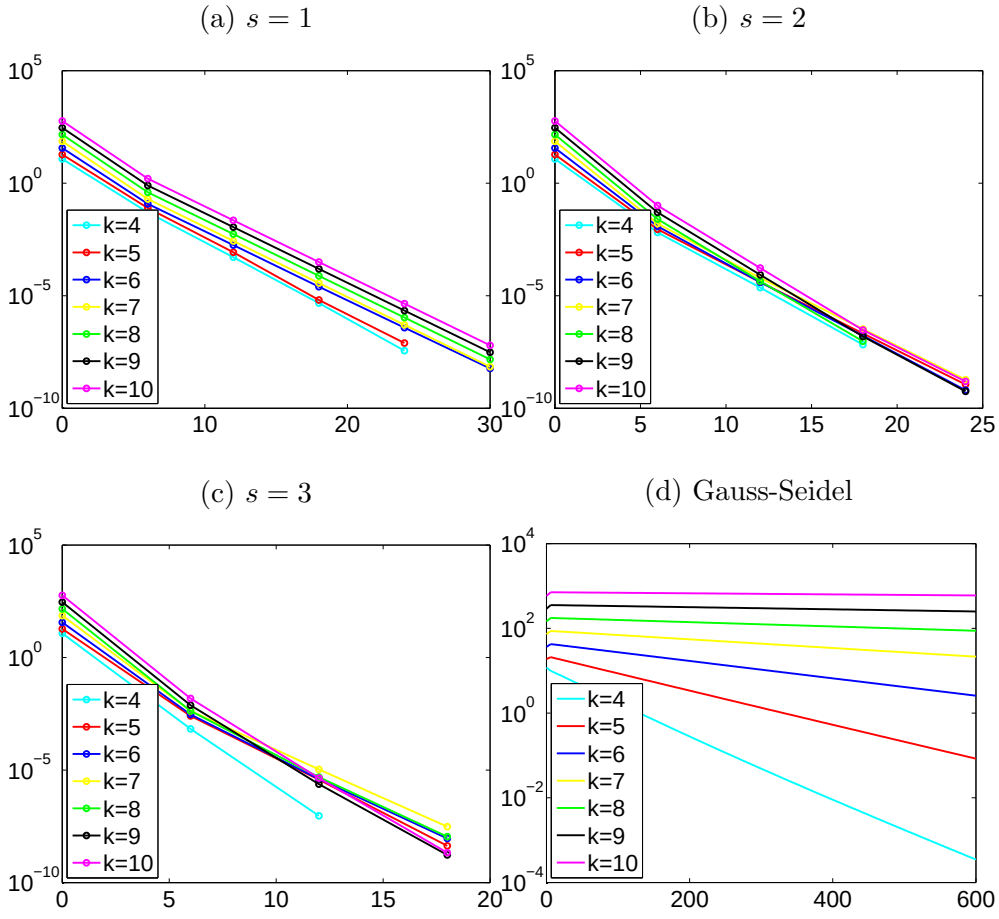

Figure 5.20: Test case 1. L^2-norm of the residual versus the WU for the two-level scheme using $ICGS$ smoother with $s = 1, 2, 3$ comparing with two-level scheme using Gauss-Seidel smoother.

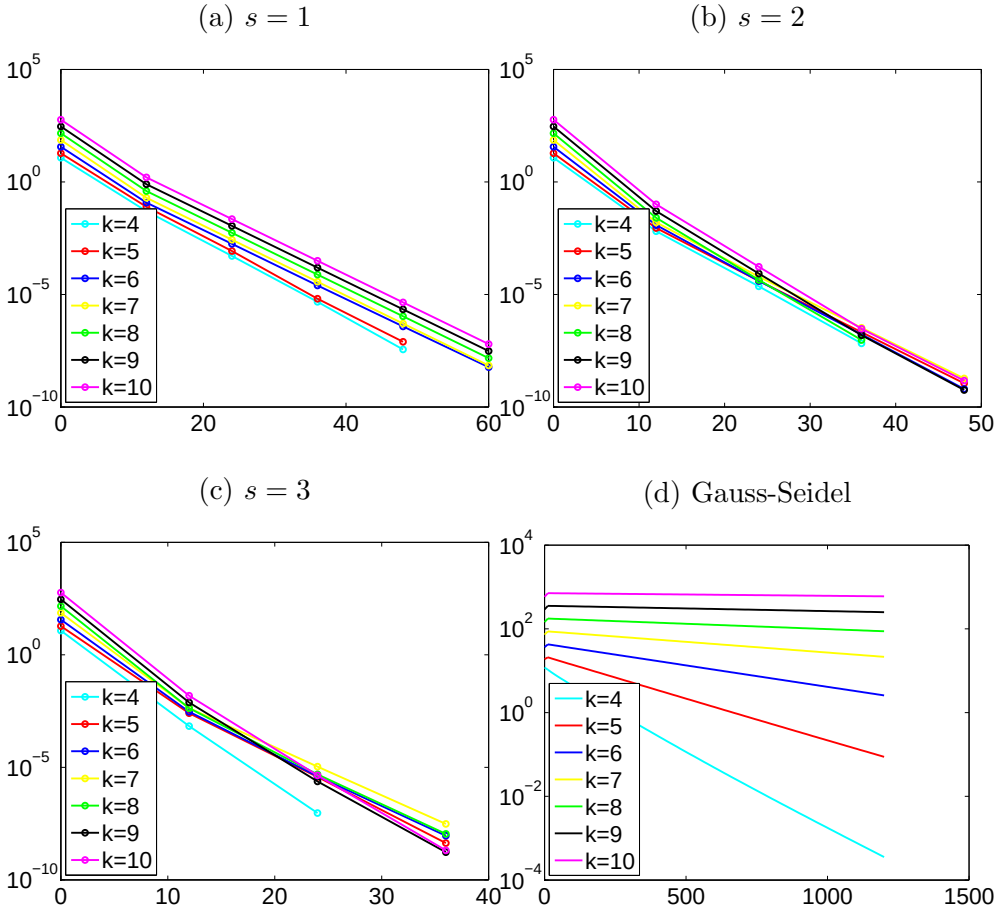

Figure 5.21: Test case 1. L^2-norm of the residual versus the WU for the W-cycle scheme using $ICGS$ smoother with $s = 1, 2, 3$ comparing with W-cycle scheme using Gauss-Seidel smoother.

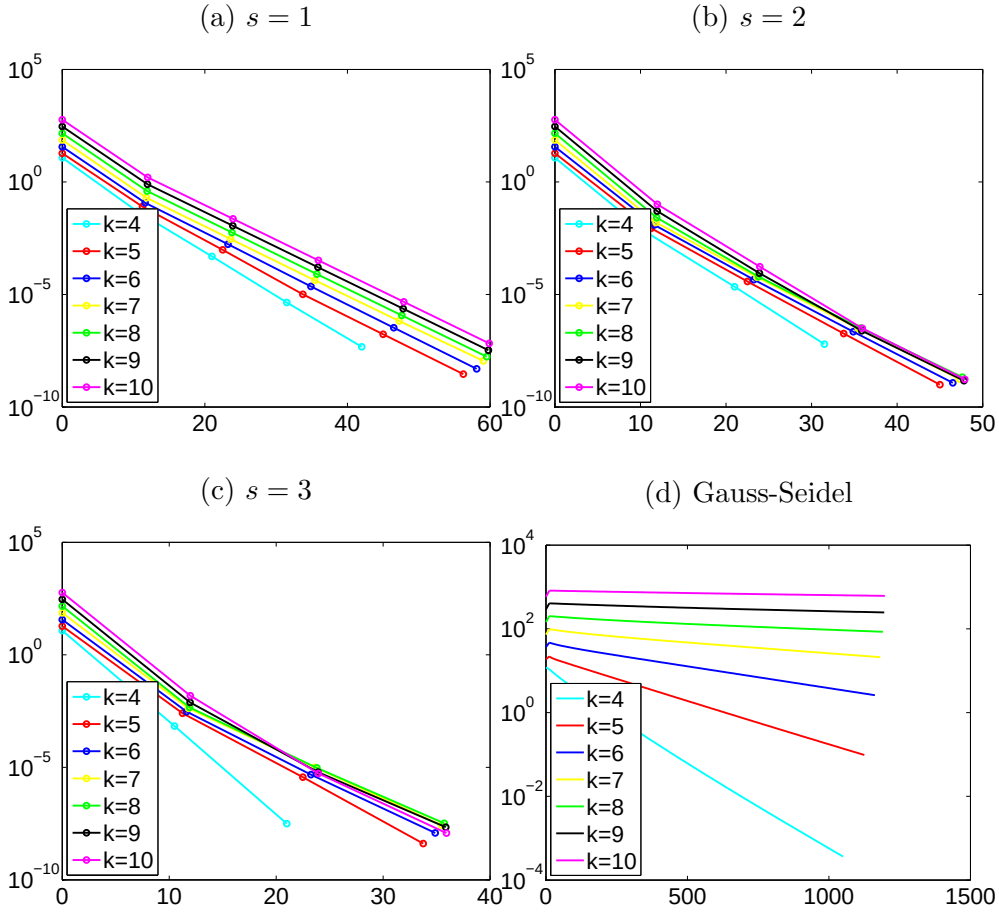

Figure 5.22: Test case 1. L^2-norm of the residual versus the WU for the V-cycle scheme using $ICGS$ smoother with $s = 1, 2, 3$ comparing with the V-cycle scheme using Gauss-Seidel smoother.

(a) grid level $k = 4$

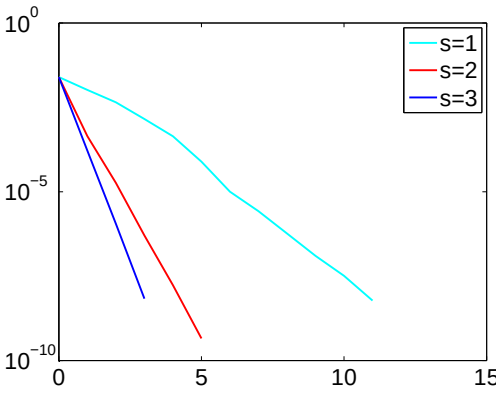

(b) grid level $k = 6$

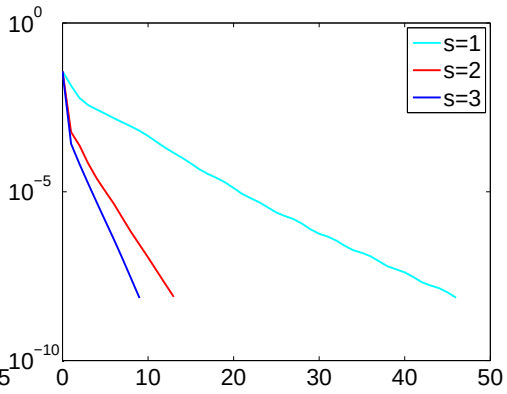

(c) grid level $k = 8$

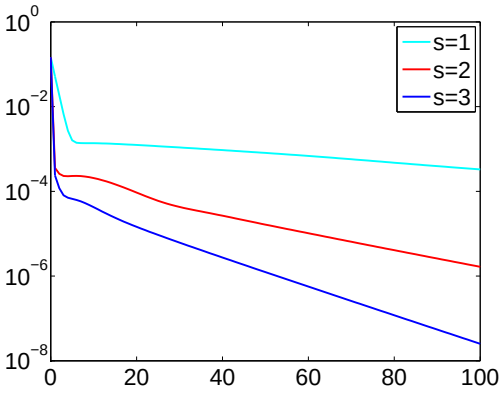

Figure 5.23: Test case 2. L^2-norm of the residual versus the number of smoothing steps for the $ICGS$ smoother with $s = 1, 2, 3$.

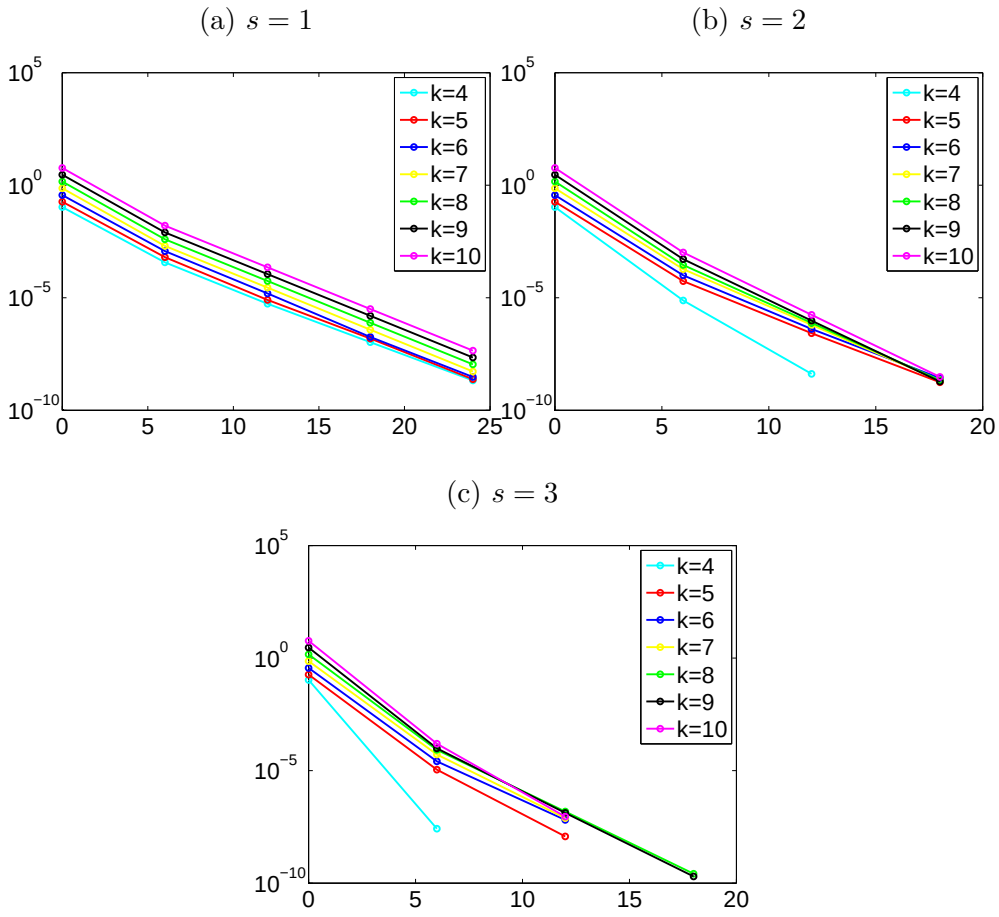

Figure 5.24: Test case 2. L^2-norm of the residual versus the WU for the two-level scheme using $ICGS$ smoother with $s = 1, 2, 3$.

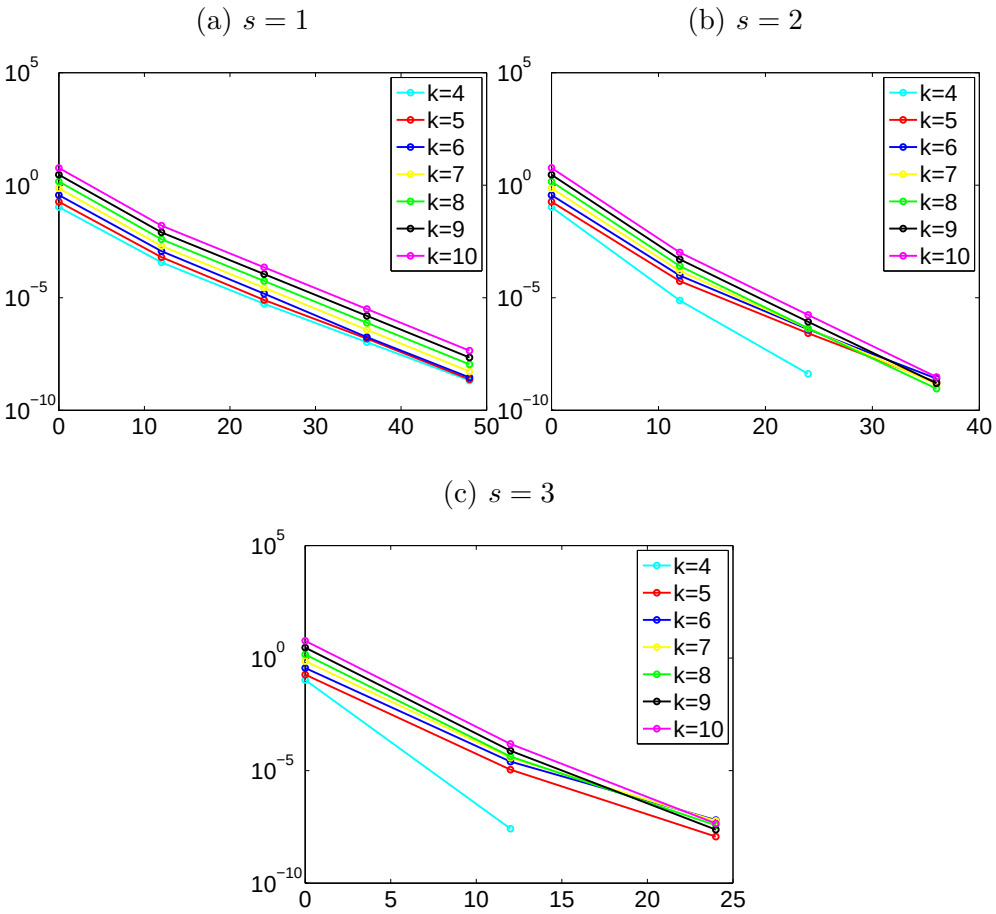

Figure 5.25: Test case 2. L^2-norm of the residual versus the WU for the w-cycle scheme using $ICGS$ smoother with $s = 1, 2, 3$.

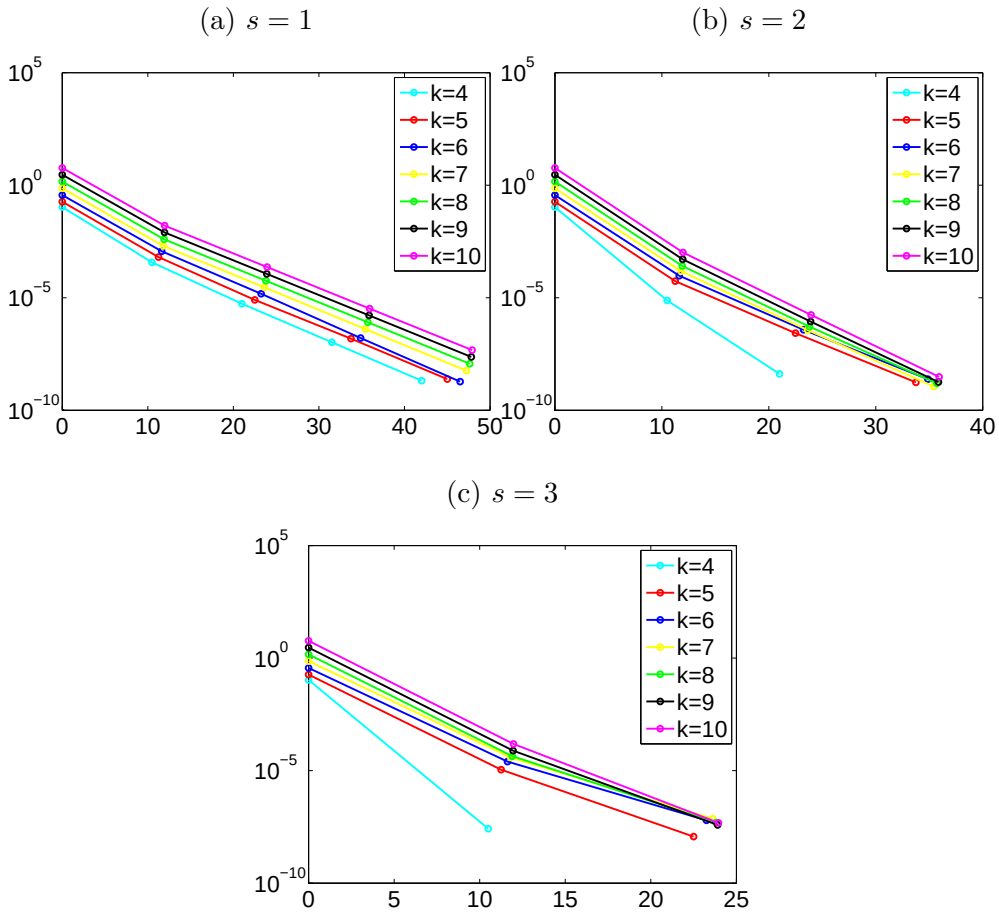

Figure 5.26: Test case 2. L^2-norm of the residual versus the WU for the V-cycle scheme using $ICGS$ smoother with $s = 1, 2, 3$.

6

Discontinuous Galerkin discretization of the Cahn-Hilliard problem with dynamic boundary conditions

This chapter is devoted to the discontinuous Galerkin discretization of the Cahn-Hilliard problem with dynamic boundary conditions. Several numerical experiments are reported to compare the behaviour of the discontinuous Galerkin solutions with the conforming results with the results present in literature [21] obtained by employing a conforming approach.

6.1 Continuous problem

Let $\Omega = (a, b) \times (c, d) \subset \mathbb{R}^2$ be a rectangular domain and let Γ be its boundary. More precisely, let Γ_1, Γ_2 be the union of the top and bottom/left and right edges, respectively (see Figure 3.1).

We consider the following Cahn-Hilliard problem with dynamic boundary conditions:

$$\begin{cases} \partial_t c - \Delta w = 0 & \text{in } \Omega \times (0, T], \\ w = \phi(c) - \gamma^2 \Delta c & \text{in } \Omega \times (0, T], \\ \partial_n c = -\alpha c + \beta \Delta_\Gamma c - g_s(c) - \lambda \partial_t c & \text{on } \Gamma_1 \times (0, T], \\ \partial_n w = 0 & \text{on } \Gamma_1 \times (0, T], \\ \text{periodic boundary conditions} & \text{on } \Gamma_2 \times (0, T], \end{cases} \tag{6.1}$$

with $\lambda, \alpha, \beta, \gamma > 0$. The functions ϕ, g_s belong to $C^2(\mathbb{R}, \mathbb{R})$ and satisfy the standard dissipativity assumptions:

$$\liminf_{|v| \to \infty} \phi'(v) > 0, \qquad \liminf_{|v| \to \infty} g_s'(v) > 0 \qquad \forall v \in \mathbb{R}. \tag{6.2}$$

The function $\phi(\cdot)$ represents the derivative of the Cahn-Hilliard free energy $\Phi(\cdot)$ and it is usually taken as $\phi(c) = c^3 - c$.

Since we deal with (classical and not isoparametric) discontinuous Galerkin elements, we set Ω as a polygonal domain. More general domains can be treated by resorting to isoparametric techniques (cf. high order methods for surfaces in Chapter 2). This aspect will be object of further investigations.

We have introduced periodic condition on some edges of $\partial\Omega$ (cf. Figure 3.1) to model an infinite slab domain as in [21]. All the following theoretical results still hold employing dynamic boundary conditions on entire $\partial\Omega$.
For a positive constant λ, we introduce the space

$$H^s_\lambda(\Omega,\Gamma) = \{v \in H^s(\Omega) : \lambda v_{|\Gamma_1} \in H^s(\Gamma)\}, \qquad s \geq 1,$$

and endow it with the norm

$$\|u\|_{H^s_\lambda(\Omega,\Gamma_1)} = \left(\|u\|^2_{H^s(\Omega)} + \lambda\|u_{|\Gamma_1}\|^2_{H^s(\Gamma)}\right)^{1/2}.$$

We also set

$$L^2_\lambda(\Omega,\Gamma) = \{v \in L^2(\Omega) : \lambda v_{|\Gamma_1} \in L^2(\Gamma)\},$$

equipped with the norm

$$\|u\|_{L^2_\lambda(\Omega,\Gamma_1)} = \sqrt{\|u\|^2_{L^2(\Omega)} + \lambda\|u_{|\Gamma_1}\|^2_{L^2(\Gamma_1)}}.$$

To ease the notation, when $\lambda = 1$, we will omit the subscript.

The weak formulation of the Cahn-Hilliard problem with dynamic boundary condition reads: *Find* $\{c, w\} \in H^1_\lambda(\Omega,\Gamma_1) \times H^1(\Omega)$ *such that*

$$\begin{cases} (\partial_t c, \eta)_{L^2(\Omega)} + (\nabla w, \nabla\eta)_{L^2(\Omega)} = 0 & \forall \eta \in H^1(\Omega), \qquad (6.3) \\ (w,\chi)_{L^2(\Omega)} = (\phi(c),\chi)_{L^2(\Omega)} + \gamma^2(\nabla c, \nabla\chi)_{L^2(\Omega)} \\ \qquad\qquad + \beta(\nabla_\Gamma c, \nabla_\Gamma\chi)_{L^2(\Gamma_1)} + \alpha(c,\chi)_{L^2(\Gamma_1)} \\ \qquad\qquad + (g_s(c),\chi)_{L^2(\Gamma_1)} + \lambda(\partial_t c,\chi)_{L^2(\Gamma_1)} & \forall \chi \in H^1_\lambda(\Omega,\Gamma_1). \quad (6.4) \end{cases}$$

6.2 DG discretization

Let $\mathcal{T}_h$ be a quasi-uniform partition of Ω into disjoint open triangles K such that $\overline{\Omega} = \cup_{K\in\mathcal{T}_h}\overline{K}$. We set $h = \max\{\mathrm{diam}(K),\ K \in \mathcal{T}_h\}$. For $s \geq 0$, we define the following broken Sobolev space

$$H^s(\mathcal{T}_h) = \{v \in L^2(\Omega) : v_{|K} \in H^s(K,\partial K),\ K \in \mathcal{T}_h\},$$

where $H^0(\mathcal{T}_h) = L^2(\mathcal{T}_h)$. For an integer $p \geq 1$, we also define the finite dimensional space

$$V^p_h = \{v \in L^2(\Omega) : v_{|K} \in \mathbb{P}^p(K),\ K \in \mathcal{T}_h\} \subset H^s(\mathcal{T}_h),$$

for any $s \geq 0$. An interior edge e is defined as the non-empty intersection of the closure of two neighbouring elements, i.e., $\overline{e} = \overline{K_1} \cap \overline{K_2}$, for $K_1, K_2 \in \mathcal{T}_h$. We collect all the interior edges in the set $\mathcal{E}_h^0$ as we did in Chapter 3. Recalling that on $\Gamma_2 \subset \partial\Omega$ we impose periodic boundary conditions, we decompose Γ_2 as $\Gamma_2 = \Gamma_2^+ \cup \Gamma_2^-$, cf. Figure 3.1 (left), and identify Γ_2^+ with Γ_2^-, cf. Figure 3.1 (right). Then we define the set $\mathcal{E}_h^{\Gamma_2}$ of the periodic boundary edges as follows. An edge $e \in \mathcal{E}_h^{\Gamma_2}$ if $\overline{e} = \partial\overline{K}^- \cap \partial\overline{K}^+$, where $K^\pm \in \mathcal{T}_h$ such that $\partial K^\pm \subseteq \Gamma_2^\pm$, cf. Figure 3.1 (right). We also define a boundary edge e as the non-empty intersection between the closure of an element in $\mathcal{T}_h$ and Γ_1 and the set of those edges by $\mathcal{E}_h^{\Gamma_1}$. Finally, we define a boundary ridge r as the subset of the mesh vertexes that lie on Γ_1, and collect all the ridges r in the set $\mathcal{R}_h^{\Gamma_1}$. Clearly, the corner ridges have to be identified according to the periodic boundary conditions, cf. Figure 3.1 (right). The set of all the edges will be denoted by $\mathcal{E}_h$, i.e., $\mathcal{E}_h = \mathcal{E}_h^0 \cup \mathcal{E}_h^{\Gamma_1} \cup \mathcal{E}_h^{\Gamma_2}$.

Using the bilinear forms $\mathcal{B}(\cdot,\cdot)$ and $\mathcal{A}(\cdot,\cdot)$ introduced in Section 3.2.1, we can state the DG approximation as: *Find* $\{c_h, w_h\} \in V_h^p \times V_h^p$ *such that*

$$\begin{cases} (\partial_t c_h, \phi)_{L^2(\Omega)} + \mathcal{B}_h(w_h, \phi) = 0, & (6.5) \\ (w_h, \chi)_{L^2(\Omega)} = \mathcal{A}_h(c_h, \chi) + (\phi(c_h), \chi)_{L^2(\Omega)} \\ \qquad\qquad + (g_s(c_h), \chi)_{L^2(\Gamma_1)} + \lambda(\partial_t c_h, \chi)_{L^2(\Gamma_1)}, & (6.6) \end{cases}$$

for all $\phi, \chi \in V_h^p$.

Remark 6.1 *If a solution* $\{c, w\}$ *of (6.3)-(6.4) belongs to* $H^2_\lambda(\Omega, \Gamma_1) \times H^2(\Omega)$ *then the pair* $\{c, w\}$ *solves the DG formulation (6.5)-(6.6).*

We also recall the results proved in Lemma 3.1:

Lemma 6.1 *There hold*

$$\begin{aligned} \mathcal{B}_h(v, w) &\lesssim |||v|||_{\mathcal{B}_h} |||w|||_{\mathcal{B}_h} \qquad \forall v, w \in H^2(\mathcal{T}_h), \\ \mathcal{A}_h(v, w) &\lesssim |||v|||_* |||w|||_* \qquad \forall v, w \in H^2(\mathcal{T}_h). \end{aligned}$$

Moreover, for μ *large enough, there hold*

$$\begin{aligned} |||v|||^2_{\mathcal{B}_h} &\lesssim \mathcal{B}_h(v, v) \qquad \forall v \in V_h^p, \\ |||v|||^2_* &\lesssim \mathcal{A}_h(v, v) \qquad \forall v \in V_h^p. \end{aligned}$$

Next we introduce the fully discretization of problem (6.1). Let $\{t_n\}_{n=0}^N$ be a partition of $[0, T]$ with step size Δt, i.e., $t_n = n\Delta t,\ n = 0, ..., N$.

The Cahn-Hilliard problem with dynamic boundary conditions discretized with implicit Euler scheme reads as follows: *For* $1 \leq n \leq N$, *find* $\{u_h^n, w_h^n\} \in V_h^p \times V_h^p$

such that

$$\begin{cases} (\delta_t u_h^n, \phi)_{L^2(\Omega)} + \mathcal{B}_h(w_h^n, \phi) = 0, \\ (w_h^n, \chi)_{L^2(\Omega)} = \mathcal{A}_h(c_h^n, \chi) + (\phi(c_h^n), \chi)_{L^2(\Omega)} \\ \qquad\qquad + (g_s(c_h^n), \chi)_{L^2(\Gamma_1)} + \lambda(\partial_t c_h^n, \chi)_{L^2(\Gamma_1)}, \end{cases} \tag{6.7}$$

for all $\phi, \chi \in V_h^p$, *where*

$$\delta_t u_h^n = \frac{u_h^n - u_h^{n-1}}{\Delta t}, \qquad 1 \le n \le N.$$

ADDDDDD

6.3 Numerical experiments

In this section we present some numerical experiments that describe the typical behaviour of the solution of the Cahn-Hilliard problem with dynamic boundary conditions using piecewise linear elements ($p = 1$). To validate our results, we compare the computed discrete solutions with the ones presented in [21] obtained with conforming linear finite elements. To this aim, we assume that $\phi(v) = v^3 - v/2$ and $g_s(v) = k_s v - h_s$, with $k_s > 0$ and $h_s \in \mathbb{R}$. The parameter $h_s \neq 0$ describes the possible preferential attraction of one of the two components by the wall, whereas the parameter k_s governs the interaction between the components at the wall. In all the following simulations, we take as initial value an uniformly distributed random datum of amplitude ± 0.01.

6.3.1 Example 1

Let us consider the problem (6.1) on the domain $\Omega = (0, 80) \times (0, 10)$. We build the triangulation $\mathcal{T}_h$ by dividing the slab into 256×50 rectangles and by dividing every rectangle along the same diagonal into two triangles. We set $\alpha + k_s = 1$, $h_s = 0$, $\lambda = 10$, $\beta = 0.1$, $\gamma = 1$ and the time step $\Delta t = 0.1$. We report some snapshots of the computed solution with linear discontinuous elements in Figure 6.1 (left). To compare the obtained results, we report in Figure 6.1 (right) the corresponding snapshots of the conforming linear finite element solution computed in [21].

The behaviour of the two computed solutions is similar: the mixture develop into bubble-like domains and, since $h_s = 0$, we do not have any preferable component attracted by the walls.

6.3.2 Example 2

Let now consider $\Omega = (0, 80) \times (0, 40)$ and the triangulation $\mathcal{T}_h$ obtained by dividing the slab into 400×200 rectangles and by dividing every rectangle along

(a) DG discretization (b) FE discretization

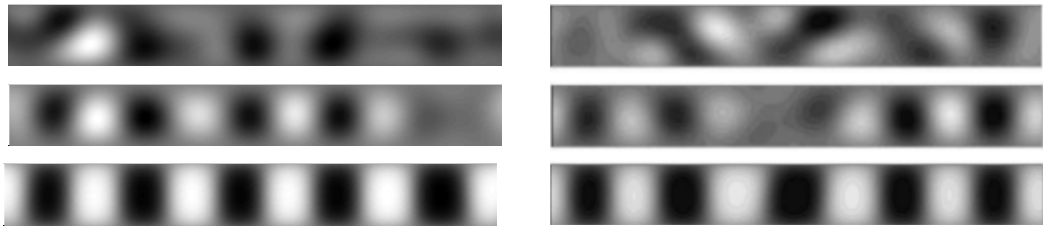

Figure 6.1: Example 1. Snapshot of the computed solutions using DG discretization (left) and FE discretization (right) taken from [21]. From top to bottom we report the computed solutions at time $t = 10, 100, 250$.

the same diagonal into two triangles. In Figure 6.2 are reported the computed results with $\alpha + k_s = -4$, $h_s = 0$, $\lambda = 10$, $\beta = 5$, $\gamma = 1$ and $\Delta t = 0.01$.

(a) DG discretization (b) FE discretization

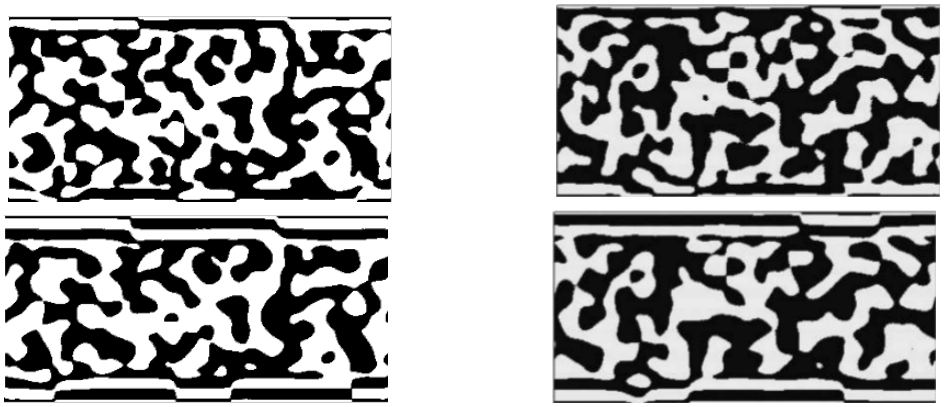

Figure 6.2: Example 2. Snapshots of the computed solutions using DG discretization (left) and FE discretization (right) taken from [21]. From top to bottom we report the solutions at time $t = 0.25$ and $t = 0.5$.

In both figures the length scale on the dynamic boundary is larger than the typical length scale in the bulk. We can also note that the surface structures develop into the bulk.

6.3.3 Example 3

In the last example, we set the domain Ω as a disk of radius 80 centered at $(0, 0)$ from which we have cut off a disk of radius 40 and centered at $(20, 0)$. The triangulation $\mathcal{T}_h$ is taken such that the exterior boundary is divided into 600 intervals and the internal boundary into 400 intervals. The above triangulation $\mathcal{T}_h$ define a discrete domain Ω_h different from Ω. In this case we imposed dynamic boundary condition on the entire $\partial\Omega$.

In Figure 6.3 and Figure 6.4 are reported the results with $\alpha+k_s = -4$, $\lambda = 10$, $\beta = 5$, $\gamma = 1$, $\Delta t = 0.01$ and $h_s = 0$ and $h_s = 0.001$, respectively.

(a) DG discretization (b) FE discretization

Figure 6.3: Example 3. Snapshot of the computed solutions at time $t = 0.5$ using DG discretization (left) FE discretization (right) taken from [21], with $h_s = 0$.

(a) DG discretization (b) FE discretization

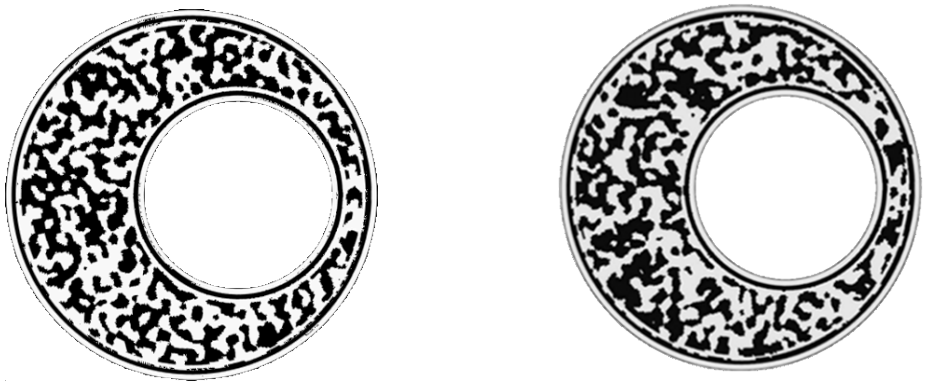

Figure 6.4: Example 3. Snapshot of the computed solutions at time $t = 0.5$ using DG discretization (left) FE discretization (right) taken from [21], with $h_s = 0.01$.

We observe, in both cases, a classical behaviour of the Cahn-Hilliard solution in the bulk. In Figure 6.3, the pattern of the solution on the boundary is similar to Example 6.2, with none preferable component attracted to the boundary. On the other hand, in Figure 6.4, when the parameter h_s is different to zero, a phase is more attract than the other to the boundary. In fact, we see that the internal and external boundary are occupied by negative (white) values that represent the first phase.

A

Appendix

In this section we recall the main ingredients of the Newton method (Appendix A.1) and of the multigrid scheme (Appendix A.2).

A.1 Newton method

The Newton method is numerical method to approximate the solution of non-linear equation of the form "*Find* $x^* \in \Omega$ *such that* $F(x^*) = 0$", where $F : \Omega \to \mathbb{R}$ is a (regular enough) function and $\Omega \subseteq \mathbb{R}^N$. The following result holds:

Theorem A.1 *Let* $F : \Omega \to \mathbb{R}$ *and let* $x^* \in \Omega$ *such that* $F(x^*) = 0$. *Moreover, we assume that the Jacobian* $J_F : \Omega \to \mathbb{R}^N \times \mathbb{R}^N$ *of* F *is Lipschitz continuous and non-singular in* x^*. *Then, there exists* δ *such that, if* $x_0 \in B_\delta(x^*)$, *the Newton sequence* $\{x_i\}_{i \geq 1}$ *with*

$$\begin{cases} J(x^{(k)})\delta x = -F(x^{(k)}), \\ x^{(k+1)} = x^{(k)} + \delta x. \end{cases}$$

converges quadratically to x^*. *Here* $B_\delta(x^*)$ *is the ball centered in* x^* *and with radius* δ.

Remark A.1 *The term* $J_F(x^{(k)})\delta x = \nabla F|_{x^{(k)}} \cdot \delta x$ *represents the directional derivative of* F *to* δx, *evaluated in* $x^{(k)}$.

Each Newton iteration requires the solution of a linear system. It is easy to see that is not necessary (nor possible in the finite arithmetic of calculators) to solve exactly the linearized system: if the solution of the non-linear system and the linearized one are quite different, we do not get any improvement to obtain an accurate solution of the latter problem.

Therefore we introduce the inexact Newton method that reads as: for each iteration find s_i such that

$$\|J_F(x_i)s_i + F(x_i)\| \leq \eta_i \|F(x_i)\|, \tag{A.1}$$

where $\eta_i > 0$.It holds the following result:

Theorem A.2 *Let $F : \Omega \to \mathbb{R}$ and let $x^* \in \Omega$ such that $F(x^*) = 0$. Moreover, we assume that the Jacobian $J_F : \Omega \to \mathbb{R}^N \times \mathbb{R}^N$ of F is Lipschitz continuous and non-singular in x^*. Then there exist δ and $\overline{\eta}$ such that if $x_0 \in B_\delta(x^*)$ and $\{\eta_i\} \subset [0, \overline{\eta}]$, then the inexact Newton sequence $\{x_i\}_{i\geq 1}$ that satisfy*

$$\begin{cases} \|J_F(x^{(i)})s_i + F(x^{(i)})\| \leq \eta_i \|F(x^{(i)}\|, \\ x_{i+1} = x_i + s_i, \end{cases}$$

converges linearly to x^*. Moreover, if $\eta_i \leq K_\eta \|F(x_i)\|$, for some $K_\eta > 0$, the convergence is quadratic.

A.2 Multigrid schemes

We now introduce the classical linear multigrid for the solution of linear system of equations $A_h \mathbf{u}_h = \mathbf{f}_h$. Algorithm 8 shows one iteration of the V-cycle algorithm.

Algorithm 8 $\mathbf{u}_h^{\text{new}}$=MG($\mathbf{f}_h$,$\mathbf{u}_h$,$h$)

Pre-smoothing: Apply ν_1 smoothing steps to obtain $\mathbf{u}_h^{pre}$ from $\mathbf{u}_h$;
Compute the defect: $\mathbf{r}_h = \mathbf{f}_h - A_h \mathbf{u}_h^{pre}$;
Restrict the defect: $\mathbf{r}_{2h} = I_h^{2h} \mathbf{r}_h$;
if $2h$ is the coarsest meshsize **then**
    Solve $A_{2h}\mathbf{e}_{2h} = \mathbf{r}_{2h}$;
else
    $\mathbf{e}_{2h}$=MG($\mathbf{f}_{2h}$,$\mathbf{u}_{2h}$,$2h$);
end if
Interpolate the correction: $\mathbf{e}_h = I_{2h}^h \mathbf{e}_{2h}$;
Correct the approximation: $\mathbf{u}_h^c = \mathbf{u}_h^{pre} + \mathbf{e}_h$;
Post-smoothing: Apply ν_2 smoothing steps to obtain $\mathbf{v}_h$ from $\mathbf{u}_h^c$.

In Algorithm 8, ν_1 and ν_2 are non negative integers and represent the number of pre- and post-smoothing iterations, respectively. The linear operators $I_h^{2h} : V_h \to V_{2h}$ and $I_{2h}^h : V_{2h} \to V_h$ are the restriction and the prolongation operators, respectively. They are essential to transfer the information between the levels within the multigrid iteration. Using nodal basis functions and nested grids, I_{2h}^h

is the matrix that represents any coarse basis functions in terms of the fine basis functions, i.e., $(I_{2h}^h)_{ij} = (\alpha_{ji})$ where

$$\phi_i^{2h} = \sum_j \alpha_{ij} \phi_j^h.$$

An equivalent definition is $\alpha_{ij} = \phi_i^{2h}(x_j^h)$, where x_j^h denote the node associated to the j-th fine basis function, i.e.,

$$\begin{cases} \phi_i^h(x_j^h) = 1 & \text{if } i = j, \\ \phi_i^h(x_j^h) = 0 & \text{otherwise.} \end{cases}$$

The full-weighted restriction operator I_h^{2h} is defined as $(I_{2h}^h)^T$. The matrix A_{2h} is the discretization of the original problem on the coarse grid.

Bibliography

[1] R. A. Adams and J. J. F. Fournier. *Sobolev spaces*, volume 140 of *Pure and Applied Mathematics (Amsterdam)*. Elsevier/Academic Press, Amsterdam, second edition, 2003.

[2] P. Antonietti, A. Dedner, P. Madhavan, B. Stinner, S. Stangalino, and M. Verani. High order discontinuous Galerkin methods on surfaces. *Submitted.*

[3] P. Antonietti, M. Grasselli, S. Stangalino, and M. Verani. Discontinuous Galerkin approximation of parabolic problems with dynamic boundary conditions. *Submitted.*

[4] P. F. Antonietti and P. Houston. A class of domain decomposition preconditioners for *hp*-discontinuous Galerkin finite element methods. *J. Sci. Comput.*, 46(1):124–149, 2011.

[5] A. C. Aristotelous, O. Karakashian, and S. M. Wise. A mixed discontinuous Galerkin, convex splitting scheme for a modified Cahn-Hilliard equation and an efficient nonlinear multigrid solver. *Discrete Contin. Dyn. Syst. Ser. B*, 18(9):2211–2238, 2013.

[6] D. N. Arnold. An interior penalty finite element method with discontinuous elements. *SIAM J. Numer. Anal.*, 19(4):742–760, 1982.

[7] D. N. Arnold, F. Brezzi, B. Cockburn, and L. D. Marini. Unified analysis of discontinuous Galerkin methods for elliptic problems. *SIAM J. Numer. Anal.*, 39(5):1749–1779, 2001/02.

[8] T. Aubin. *Nonlinear analysis on manifolds. Monge-Ampère equations*, volume 252 of *Grundlehren der Mathematischen Wissenschaften [Fundamental Principles of Mathematical Sciences]*. Springer-Verlag, New York, 1982.

[9] G. A. Baker. Finite element methods for elliptic equations using nonconforming elements. *Mathematics of Computation*, 31(137):45–59, 1977.

[10] F. Bassi and S. Rebay. A high-order accurate discontinuous finite element method for the numerical solution of the compressible Navier-Stokes equations. *J. Comput. Phys.*, 131(2):267–279, 1997.

[11] F. Bassi, S. Rebay, G. Mariotti, S. Pedinotti, and M. Savini. A high-order accurate discontinuous finite element method for inviscid and viscous turbomachinery flows. In *Proceedings of 2nd European Conference on Turbomachinery, Fluid Dynamics and Thermodynamics*, pages 99–108. Technologisch Instituut, Antwerpen, Belgium, 1997.

[12] P. Bastian, M. Blatt, A. Dedner, C. Engwer, R. Klöfkorn, R. Kornhuber, M. Ohlberger, and O. Sander. A generic grid interface for parallel and adaptive scientific computing. part II: Implementation and tests in DUNE. *Computing*, 82(2–3):121–138, 2008.

[13] C. E. Baumann and J. T. Oden. A discontinuous *hp* finite element method for the Euler and Navier-Stokes equations. *Internat. J. Numer. Methods Fluids*, 31(1):79–95, 1999. Tenth International Conference on Finite Elements in Fluids (Tucson, AZ, 1998).

[14] A. L. Bertozzi, S. Esedoglu, and A. Gillette. Inpainting of Binary Images Using the Cahn-Hilliard Equation. *IEEE Transactions on Image Processing*, 16:285–291, 2007.

[15] K. Binder, C. Billotet, and P. Mirold. On the theory of spinodal decomposition in solid and liquid binary mixtures. *Zeitschrift fr Physik B Condensed Matter*, 30(2):183–195, 1978.

[16] D. Braess. *Finite elements: Theory, fast solvers, and applications in solid mechanics*. Cambridge University Press, 2001.

[17] S. C. Brenner. Poincaré-Friedrichs inequalities for piecewise H^1 functions. *SIAM J. Numer. Anal.*, 41(1):306–324, 2003.

[18] F. Brezzi, G. Manzini, D. Marini, P. Pietra, and A. Russo. Discontinuous Galerkin approximations for elliptic problems. *Numer. Methods Partial Differential Equations*, 16(4):365–378, 2000.

[19] M. Burger, L. He, and C.-B. Schönlieb. Cahn-Hilliard inpainting and a generalization for grayvalue images. *SIAM J. Imaging Sci.*, 2(4):1129–1167, 2009.

[20] G. Caginalp. Stefan and Hele-Shaw type models as asymptotic limits of the phase-field equations. *Phys. Rev. A (3)*, 39(11):5887–5896, 1989.

[21] L. Cherfils, M. Petcu, and M. Pierre. A numerical analysis of the Cahn-Hilliard equation with dynamic boundary conditions. *Discrete Contin. Dyn. Syst.*, 27(4):1511–1533, 2010.

[22] P. G. Ciarlet. *The finite element method for elliptic problems*, volume 40 of *Classics in Applied Mathematics*. Society for Industrial and Applied Mathematics (SIAM), Philadelphia, PA, 2002. Reprint of the 1978 original [North-Holland, Amsterdam; MR0520174 (58 #25001)].

[23] B. Cockburn and C.-W. Shu. The local discontinuous Galerkin method for time-dependent convection-diffusion systems. *SIAM J. Numer. Anal.*, 35(6):2440–2463 (electronic), 1998.

[24] T. Cool, A. Bartol, M. Kasenga, K. Modi, and R. E. Garca. Gibbs: Phase equilibria and symbolic computation of thermodynamic properties. *Calphad*, 34(4):393–404, 2010.

[25] C. Dawson, S. Sun, and M. F. Wheeler. Compatible algorithms for coupled flow and transport. *Comput. Methods Appl. Mech. Engrg.*, 193(23-26):2565–2580, 2004.

[26] A. Dedner, R. Klöfkorn, M. Nolte, and M. Ohlberger. A generic interface for parallel and adaptive discretization schemes: abstraction principles and the DUNE-FEM module. *Computing*, 90(3-4):165–196, 2010.

[27] A. Dedner, P. Madhavan, and B. Stinner. Analysis of the discontinuous Galerkin method for elliptic problems on surfaces. *IMA J. Numer. Anal.*, 33(3):952–973, 2013.

[28] A. Demlow. Higher-order finite element methods and pointwise error estimates for elliptic problems on surfaces. *SIAM J. Numer. Anal.*, 47(2):805–827, 2009.

[29] A. Demlow and G. Dziuk. An adaptive finite element method for the Laplace-Beltrami operator on implicitly defined surfaces. *SIAM J. Numer. Anal.*, 45(1):421–442 (electronic), 2007.

[30] J. Douglas, Jr. and T. Dupont. Interior penalty procedures for elliptic and parabolic Galerkin methods. In *Computing methods in applied sciences (Second Internat. Sympos., Versailles, 1975)*, pages 207–216. Lecture Notes in Phys., Vol. 58. Springer, Berlin, 1976.

[31] G. Dziuk. Finite elements for the Beltrami operator on arbitrary surfaces. In *Partial differential equations and calculus of variations*, volume 1357 of *Lecture Notes in Math.*, pages 142–155. Springer, Berlin, 1988.

[32] S. C. Eisenstat and H. F. Walker. Choosing the forcing terms in an inexact Newton method. *SIAM J. Sci. Comput.*, 17(1):16–32, 1996. Special issue on iterative methods in numerical linear algebra (Breckenridge, CO, 1994).

[33] C. Elliott and A. Stuart. Global dynamics of discrete semilinear parabolic equations. *SIAM Journal on Numerical Analysis*, 30(6):1622–1663, 1993.

[34] C. M. Elliott and D. A. French. Numerical studies of the Cahn-Hilliard equation for phase separation. *IMA J. Appl. Math.*, 38(2):97–128, 1987.

[35] C. M. Elliott and D. A. French. A Nonconforming Finite-element Method for the Two-dimensional Cahn-Hilliard Equation. *SIAM J. Numer. Anal.*, 26(4):884–903, Aug. 1989.

[36] L. C. Evans. *Partial differential equations*, volume 19 of *Graduate Studies in Mathematics*. American Mathematical Society, Providence, RI, second edition, 2010.

[37] K. J. Fidkowski. A high-order discontinuous galerkin multigrid solver for aerodynamic applications. *Master's Thesis, M.I.T.*, 2004.

[38] I. Fonseca, M. Morini, and V. Slastikov. Surfactants in foam stability: A phase field model. *Arch. Ration. Mech. Anal.*, 183(3):411–456, 2007.

[39] E. Fried and M. Gurtin. Dynamic solid-solid transitions with phase characterized by an order parameter. *Physica D: Nonlinear Phenomena*, 72(4):287–308, 1994.

[40] D. Furihata. A stable and conservative finite difference scheme for the Cahn-Hilliard equation. *Numerische Mathematik*, 87(4):675–699, 2001.

[41] G. Gilardi, A. Miranville, and G. Schimperna. Long time behavior of the Cahn-Hilliard equation with irregular potentials and dynamic boundary conditions. *Chin. Ann. Math. Ser. B*, 31(5):679–712, 2010.

[42] H. Gomez and T. J. R. Hughes. Provably unconditionally stable, second-order time-accurate, mixed variational methods for phase-field models. *J. Comput. Phys.*, 230(13):5310–5327, 2011.

[43] P. W. Hemker. *Fourier analysis of gridfunctions, prolongations and restrictions*. Afdeling Numerieke Wiskunde [Department of Numerical Mathematics], 93. Mathematisch Centrum, Amsterdam, 1980.

[44] P. W. Hemker, W. Hoffmann, and M. H. van Raalte. Two-level Fourier analysis of a multigrid approach for discontinuous Galerkin discretization. *SIAM J. Sci. Comput.*, 25(3):1018–1041 (electronic), 2003.

[45] P. W. Hemker, W. Hoffmann, and M. H. van Raalte. Fourier two-level analysis for discontinuous Galerkin discretization with linear elements. *Numer. Linear Algebra Appl.*, 11(5-6):473–491, 2004.

[46] J. Hilliard and J. Cahn. On the nature of the interface between a solid metal and its melt. *Acta Metallurgica*, 6(12):772–774, 1958.

[47] J.-H. Jeong, N. Goldenfeld, and J. A. Dantzig. Phase field model for three-dimensional dendritic growth with fluid flow. *Phys. Rev. E*, 64:041602, Sep 2001.

[48] T. Kashiwabara, C. Colciago, L. Dede, and A. Quarteroni. Well-posedness, regularity, and convergence analysis of the finite element approximation of a Generalized Robin boundary value problem. *To be appear.*

[49] D. Kay, V. Styles, and E. Süli. Discontinuous Galerkin finite element approximation of the Cahn-Hilliard equation with convection. *SIAM J. Numer. Anal.*, 47(4):2660–2685, 2009.

[50] E. Khain and L. M. Sander. Generalized Cahn-Hilliard equation for biological applications. *Phys. Rev. E*, 77:051129, May 2008.

[51] Y.-T. Kim, N. Provatas, N. Goldenfeld, and J. Dantzig. Universal dynamics of phase-field models for dendritic growth. *Phys. Rev. E*, 59:R2546–R2549, Mar 1999.

[52] I. Klapper and J. Dockery. Mathematical description of microbial biofilms. *SIAM Rev.*, 52(2):221–265, 2010.

[53] J.-L. Lions and E. Magenes. *Non-homogeneous boundary value problems and applications. Vol. I.* Springer-Verlag, New York-Heidelberg, 1972. Translated from the French by P. Kenneth, Die Grundlehren der mathematischen Wissenschaften, Band 181.

[54] Q.-X. Liu, A. Doelman, V. Rottschafer, M. De Jager, P. Herman, M. Rietkerk, and J. Van De Koppel. Phase separation explains a new class of selforganized spatial patterns in ecological systems. *Proceedings of the National Academy of Sciences of the United States of America*, 110(29):11905–11910, 2013.

[55] J. Lowengrub and L. Truskinovsky. Quasi-incompressible Cahn-Hilliard fluids and topological transitions. *R. Soc. Lond. Proc. Ser. A Math. Phys. Eng. Sci.*, 454(1978):2617–2654, 1998.

[56] A. Miranville. Asymptotic behavior of the Cahn-Hilliard-Oono equation. *Journal of Applied Analysis and Computation*, 1:523–536, 2011.

[57] F. Nabet. Convergence of a finite-volume scheme for the Cahn-Hilliard equation with dynamic boundary conditions. *HAL preprint - hal-00872690*, 2014.

[58] O. Penrose and P. C. Fife. Thermodynamically consistent models of phase-field type for the kinetics of phase transitions. *Phys. D*, 43(1):44–62, 1990.

[59] I. Perugia and D. Schötzau. An *hp*-analysis of the local discontinuous Galerkin method for diffusion problems. In *Proceedings of the Fifth International Conference on Spectral and High Order Methods (ICOSAHOM-01) (Uppsala)*, volume 17, pages 561–571, 2002.

[60] W. H. Reed and T. R. Hill. Triangular mesh methods for the neutron transport equation. 1973.

[61] L. Rineau and M. Yvinec. 3D surface mesh generation. *CGAL Editorial Board, editor, CGAL User and Reference Manual*, 3:53, 2009.

[62] B. Rivière. *Discontinuous Galerkin methods for solving elliptic and parabolic equations*, volume 35 of *Frontiers in Applied Mathematics*. Society for Industrial and Applied Mathematics (SIAM), Philadelphia, PA, 2008. Theory and implementation.

[63] B. Rivière, M. F. Wheeler, and V. Girault. Improved energy estimates for interior penalty, constrained and discontinuous Galerkin methods for elliptic problems. I. *Comput. Geosci.*, 3(3-4):337–360 (2000), 1999.

[64] A. Sharma and E. Ruckenstein. An analytical nonlinear theory of thin film rupture and its application to wetting films. *Journal of Colloid And Interface Science*, 113(2):456–479, 1986.

[65] J. Shen and X. Yang. Numerical approximations of Allen-Cahn and Cahn-Hilliard equations. *Discrete Contin. Dyn. Syst.*, 28(4):1669–1691, 2010.

[66] S. Tremaine. On the origin of irregular structure in saturn's rings. *Astronomical Journal*, 125(2 1766):894–901, 2003.

[67] U. Trottenberg, C. W. Oosterlee, and A. Schüller. *Multigrid*. Academic Press, Inc., San Diego, CA, 2001. With contributions by A. Brandt, P. Oswald and K. Stüben.

[68] G. N. Wells, E. Kuhl, and K. Garikipati. A discontinuous Galerkin formulation for the Cahn–Hilliard equation. *J Comput Phys*, 218(2):860–877, 2006.

[69] J. Wloka. *Partial differential equations*. Cambridge University Press, Cambridge, 1987. Translated from the German by C. B. Thomas and M. J. Thomas.